UNIVERSITY OF CALIFORNIA,
IRVINE

Physically Informed Estimation of Spatial Precipitation Extremes

DISSERTATION

submitted in partial satisfaction of the requirements
for the degree of

DOCTOR OF PHILOSOPHY

in Civil and Environmental Engineering

by

Charlotte A. Love

Dissertation Committee:
Professor Amir AghaKouchak, Chair
Distinguished Professor Efi Foufoula-Georgiou
Assistant Adjunct Professor Phu Nguyen

2022

TABLE OF CONTENTS

LIST OF FIGURES

LIST OF TABLES

ACKNOWLEDGMENTS

I would like to thank Professor Amir AghaKouchak for being my advisor and mentor all these years. Thank you for your enthusiasm in encouraging me to switch from a Masters to a PhD student when I first applied. Thank you for always being supportive of my goals and ideas from the very beginning, and for pushing me to succeed. Thank you also for the many opportunities to network and improve my teaching skills. Thank you also for creating such a welcoming environment for all of the students and researchers in your group and helping us to feel like we are part of one big family.

Thank you to my committee members, Professor Efi Foufoula-Georgiou and Professor Phu Nguyen, for taking the time to provide thoughtful feedback on my work. Thank you also to Professor Foufoula-Georgiou for teaching stochastic hydrology and sharing your extensive knowledge with us. Thank you to Professor Phu Nguyen for happily agreeing to serve on all my exams and committees over the course of my doctoral work here as a student at UCI.

Thank you to my collaborator, Dr. Brian E. Skahill, for inspiring the direction of my doctoral research. Thank you for being available to brainstorm ideas and discuss results. Without your guidance I would have become lost down even more rabbit holes while trekking this far into the realm of spatial MEV analysis.

Thank you to my labmates and friends here at UCI who have encouraged me, cried with me, and celebrated with me through all these years, including the lockdown of 2020. Without your friendship I would have gone a little crazy. But seriously, you have been an inspiring and uplifting force, whether in-person or from afar, even if you did not realize it in the moment.

Thank you to my family that have always loved and patiently supported me through all the twists, turns, and adventures of my life. Thank you for always being my home.

Lastly, thank you to the following agencies that funded my research work: US Army Corps of Engineers Contract Number W912HZ-16-A-0080; the National Science Foundation, Award No. CMMI-1635797; and the National Oceanic and Atmospheric Administration, Award No. NA19OAR4310294.

VITA

Charlotte A. Love

EDUCATION

Doctor of Philosophy in Civil and Environmental Engineering **2022**
University of California, Irvine *Irvine, CA*

Master of Science in Environmental Engineering **2019**
University of California, Irvine *Irvine, CA*

Bachelor of Science in Earth Sciences **2014**
University of California, San Diego *La Jolla, CA*

RESEARCH EXPERIENCE

Graduate Student Researcher **2015–2022**
University of California, Irvine *Irvine, California*

Contract Student **2016–2020**
U.S. Army Corps of Engineers

Staff Research Associate I **2014–2015**
Scripps Institution of Oceanography, UCSD *La Jolla, California*

TEACHING EXPERIENCE

Teaching Assistant, Engr 190W **Spring Qtr. 2021**
Communications in the Professional World *University of California, Irvine*

Teaching Assistant, EngrCEE 81B **Winter Qtrs. 2018–2021**
Civil Engineering Practicum II *University of California, Irvine*

UCI Global Connect Presenter **Fall Qtrs. 2017–2020**
Climate Change *University of California, Irvine*

Teaching Assistant, SIO 110 **Winter Qtr. 2014**
Introduction to GIS and GPS for Scientists *University of California, San Diego*

JOURNAL PUBLICATIONS

Love, C. A., Skahill, B. E., England, J. F., Karlovits, G., Duren, A., & AghaKouchak, A. (2020). Integrating Climatic and Physical Information in a Bayesian Hierarchical Model of Extreme Daily Precipitation. *Water*, 12(8), 2211.

Wu, J., Chen, X., **Love, C. A.**, Yao, H., Chen, X., & AghaKouchak, A. (2020). Determination of water required to recover from hydrological drought: Perspective from drought propagation and non-standardized indices. *Journal of Hydrology*, 590, 125227.

AghaKouchak, A., Chiang, F., Huning, L. S., **Love, C. A.**, Mallakpour, I., Mazdiyasni, O., et al. (2020). Climate Extremes and Compound Hazards in a Warming World. *Annual Review of Earth and Planetary Sciences*, 48(1), 519–548.

Ragno, E., A. AghaKouchak, **C. A. Love**, L. Cheng, F. Vahedifard, & C. H. R. Lima. (2018). Quantifying Changes in Future Intensity-Duration-Frequency Curves Using Multimodel Ensemble Simulations. *Water Resources Research*, 54(3), 1751–1764.

Sadegh, M., **Love, C. A.**, Farahmand, A., Mehran, A., Tourian, M. J., & AghaKouchak, A. (2017). Multi-Sensor Remote Sensing of Drought from Space. Chapter In *Remote Sensing of Hydrological Extremes* (pp. 219–247). Springer, Cham.

Publications In Review

Love, C. A., Skahill, B. E., Russell, B., Baggett, J., & AghaKouchak, A. (in review) An Effective Trend Surface Fitting Framework for Spatial Analysis of Extreme Events. *Geophysical Research Letters*.

Hallerbäck, S., Huning, L. S., **Love, C. A.**, Persson, M., Stensen, K., Gustafsson, D., & AghaKouchak, A. (in review). Warming Climate Shortens Ice Durations and Alters Freeze and Breakup Patterns in Swedish Water Bodies. *The Cryosphere*.

Publications Under Preparation

Love, C. A., Skahill, B. E., & AghaKouchak, A. Areal Estimation of Extreme Precipitation Using Max-Stable Processes Across Climatically Different Regions. Submission planned for 2022.

Love, C. A., AghaKouchak, A., et al. Methods for Detecting, Modeling, and Assessing the Risk of Compound Extreme Events. Submission planned for 2022.

CONFERENCE PRESENTATIONS

Love, C. A., B.E. Skahill, A. AghaKouchak, Quantifying Future Changes in Extreme Precipitation Using a Max-Stable Process Model, Poster, *AGU Fall Meeting 2019*, San Francisco, CA

Love, C. A., B.E. Skahill, A. AghaKouchak, Quantifying the Cost of Assuming Spatial Independence Among Observations Using a Max-Stable Spatial Process, Poster, *27th IUGG General Assembly 2019*, Montreal, Quebec, Canada

Love, C. A., B.E. Skahill, A. AghaKouchak, Analysis of Annual Maxima Daily Precipitation Data Using a Max-Stable Spatial Process: Quantifying the Cost of Assuming Spatial Independence Among Extreme Data, Poster, *AGU Fall Meeting 2018*, Washington, D.C.

Love, C. A., B.E. Skahill, A. AghaKouchak, J.F. England, G.S. Karlovits, A.M. Duren, Comparison of extreme precipitation return levels using spatial Bayesian hierarchical modeling versus regional frequency analysis, Poster, *8th GEWEX Open Science Conference: Extremes and Water on the Edge 2018*, Canmore, Alberta, Canada

Love, C. A., B.E. Skahill, A. AghaKouchak, J.F. England, G.S. Karlovits, A.M. Duren, Comparison of extreme precipitation return levels using spatial Bayesian hierarchical modeling versus regional frequency analysis, Poster, *AGU Fall Meeting 2017*, New Orleans, LA

Love, C. A., B.E. Skahill, A. AghaKouchak, J.F. England, G.S. Karlovits, A.M. Duren, Extreme Rainfall Analysis using Bayesian Hierarchical Modeling in the Willamette River Basin, Poster, *AGU Fall Meeting 2016, San Francisco*, CA

Love, C. A., S. Madadgar, M.J. Tourian, A. Mehran, A. AghaKouchak, California Drought Recovery Assessment Using GRACE Gravimetry Information, Poster, *AGU Fall Meeting 2015*, San Francisco, CA

Love, C. A., L. Salmi, and J.S. Haase, Measuring Site Response for Seismic Hazard in the Ohio River Valley, Poster, *Scripps Student Symposium 2014*, La Jolla, CA

HONORS AND AWARDS

AGS Travel Grant **2016, 2019**
University of California, Irvine

Honorable Mention **2016**
NSF Graduate Research Fellowships Program

UCI Competitive Edge Summer Research Program **2015**
University of California, Irvine

ABSTRACT OF THE DISSERTATION

Physically Informed Estimation of Spatial Precipitation Extremes

By

Charlotte A. Love

Doctor of Philosophy in Civil and Environmental Engineering

University of California, Irvine, 2022

Professor Amir AghaKouchak, Chair

Improving the analysis of the intensity and frequency of spatial extreme precipitation is essential for regional hazard preparedness and infrastructure design. Extreme precipitation events are highly variable across space and time, and current methods for analyzing extremes are often based on simplifying assumptions. For example, the commonly used assumption of spatial independence among extreme precipitation observations may be unrealistic for non-localized events (e.g., hurricane precipitation, large stratiform rainfall events). This can result in the misestimation of risk. Given the additional challenges of data records that are relatively too short for adequately estimating the rarest of events, sparse sensor networks, highly localized events, and integrating spatial data and their drivers across regions, methods for estimating exceedance probabilities that enable the proper modeling of spatially varying extreme marginal parameters and account for spatial dependence between sites need to be explored and refined.

The overarching goal of this thesis is to improve the estimation of spatial extreme precipitation by including information based on the physical processes that influence the generation of storms. Here I outline the need for the inclusion of additional physically informed covariates and improved methods for covariate selection that not only improve computation time, but also automate the process to reduce the bias of a manual selection approach. Consideration

should be given to incorporating assessments of relevant covariates and the spatial dependence of extreme events within the methods used by practitioners to ensure the selection of conservative estimates for infrastructure design.

Applying a latent variable modeling approach for analysis of annual maximum (AM) precipitation, I explore the benefits of including additional climatic covariates on regional model performance across two climatically different regions and a region of overlap. These covariates include temperature and dew point temperature, extending beyond what is classically used in practice (geographic only) and within the literature (geographic and mean precipitation). The results indicate that including additional physically informed covariates improves estimates within relatively heterogeneous regions.

I introduce a framework for the selection of relevant geographic and climatic covariates for spatially distributing marginal parameters using elastic-net regularization. Using two climatically different regions, I demonstrate the application of elastic-net regularization for trend surface development. This approach aids in automating the selection of relevant covariates in a way that is less biased than manual selection, and that is computationally more efficient than cross-validation using full model simulations for a large set of physically relevant covariates.

To quantify the impact of assuming spatial independence, a max-stable process model that accounts for inter-site dependence of the observed AM precipitation will be explored in two climatically different regions. Estimation of areal-based exceedance probabilities is of critical importance, and their calculation depends on properly modeling the spatial dependence structure and the spatially varying generalized extreme value (GEV) marginal distributions. A results comparison between the max-stable process model and a regional frequency analysis is conducted. This comparison indicates that assessing the spatial dependence and the characterization of the spatially varying marginal parameters are worth including to insure conservative estimates.

Chapter 1

Introduction

Climate extremes can profoundly impact society, natural systems, and infrastructure [Easterling et al., 2000, Rocklöv and Forsberg, 2009, Handmer et al., 2012]. In many cases, extreme events are interconnected and can have a multiplier effect that intensifies the risk to society and the environment. Extreme events are rare and often the length of data collected is insufficient for estimating the rarest of these rare events since their interval of recurrence extends beyond the data record. Therefore, statistical methods for estimating these rare events are under ongoing scrutiny as studies attempt to improve upon past work. Understanding the risks associated with spatial extremes at present and estimating their future occurrences, requires more complicated, rigorous, and robust methods. Such methods must be able to account for the spatial variability of distribution parameters, systematically take the correlation structures between variables into account, and sufficiently deal with the inherently small number of extremes. The incorporation of information into models that accounts for the underlying processes that drive extreme events and/or events that collectively result in extreme impacts is the main focus of recent climate extremes research.

Classically, univariate extreme value analysis (EVA) methods have been extensively used to

study the magnitude of extreme events and the frequency of their occurrence [Lang et al., 1999, Katz et al., 2002, Katz, 2010]. Current indices use univariate methods to detect extreme events and can be categorized into three main types: (1) daily, monthly, and/or annual maxima/minima of a certain climate variable (e.g., temperature or precipitation); (2) duration of an extreme event (e.g., number of consecutive days in a year above a relative extreme threshold, such as temperatures above the 90_{th} percentile of the long-term climatology), and (3) duration and/or frequency of an absolute extreme exceedance threshold (e.g., annual number of frost days (minimum temperature below 0 °C) or number of consecutive frost days per year)[Lang et al., 1999, Katz et al., 2002, Katz, 2010]. However, the modeling of extreme events with multiple physical and geographic drivers that vary spatially is not as straightforward.

Extending univariate EVA to the multivariate and spatial case requires appropriately modeling the dependence among extreme observations and is an active and evolving area of research [Coles et al., 1999, Schlather and Tawn, 2003, Heffernan and Tawn, 2004]. Multivariate extreme value (MEV) theory accounts for the tail dependence of multiple random variables. Given that natural processes like rainfall or wind are climatological in nature, capturing the spatial variability of their distribution parameters is essential when estimating the statistics of their extreme occurrences [Cooley et al., 2007]. Several MEV methods can be extended to this spatial case by including both the latent spatial process and the spatial dependence [Cooley, 2009, Davison et al., 2012].

In the following sections both empirical and parametric multivariate methods that are used for the EVA are presented. I then review the current methods used in practice and within the literature for the spatial EVA in hydrology. I then identify areas that need further investigation. While there are MEV methods reviewed herein that can be formulated to incorporate non-stationary random variables, where the parameters of the joint distribution vary as a function of time, the following discussion will focus primarily on the MEV methods

based on a stationary assumption.

1.1 Defining Extremes

In order to model extreme events, first we need to define what is meant by "extreme". In extreme value theory (EVT), determing the shape of the upper (or lower) tail of a probability distribution is focused on for determining the probability of rare, extremely large (or small) values [Coles, 2001]. The extreme events that fall within the upper tail, or maxima, of the distribution receive the most attention for modeling climate hazards since risk mitigation, infrastructure design, and resources management all rely on the quantile estimates of large climate events.

In the field of hydrology (and other climate sciences), risk assessments and infrastructure design criteria are often centered around estimates of the frequency and intensity of extreme events. In hydrology, these correspond to the return period and return level of, for example, either a flood or extreme precipitation event. The return level is the quantile of the annual maxima associated with the exceedance probability $1 - F(x)$. Here $F(x)$ is the cumulative distribution function (CDF) of the random variable X (e.g., annual maxima) and $F_x(x)$ is the non-exceedance probability of a single $x \in X$, which can be represented using the notation of Stedinger et al. [1993] as

$$F_x(x) = Pr(X \leq x). \tag{1.1}$$

In turn, the return period T is the inverse of the exceedance probability. Given the relationship $T = [1 - F_x(x)]^{-1}$, the return level associated with a specific return period of interest (e.g., 100-year return period) can be calculated if $F(x)$ has been estimated [Stedinger et al., 1993]. Therein lies the challenge that extreme value analysis tries to address, the deter-

mination of which extreme value distribution using which methods can best estimate $F(x)$ for a given extreme event type to reach the most appropriate quantile estimates for a given region. As you will hear echoed throughout these review sections, some of the confounding factors when estimating the distribution function of maxima revolve around the best way to select truly extreme values, the ever-present lack of data for rare events, regional heterogeneity, variability of the dependence between data, variability of the distribution parameters spatially or temporally, and computational limitations.

1.1.1 Block Maxima

The block maxima approach for characterizing extreme observations is a commonly used method in extreme value analysis. The approach defines the series of maxima, $max(X_1, \ldots, X_n)$, as the single largest event during each block of time (e.g., annual maximum) where $X_1, \ldots, X_n$ are independent and identically distributed (i.i.d.) random variables. This is also pointed out as a caveat of the block maxima method given that the maxima are restricted to only one event per block of time whether or not the event is truly extreme, and that selecting only one maxima throws out other potentially useful extreme events.

The statistical modeling of these extremes is then based on the extremal types theorem, which describes the limiting distribution of a series of maxima $max(X_1, \ldots, X_n)$ that satisfies the property of max-stability. Given that their marginal distribution function F has the upper terminus $x_F = \sup\{x : F(x) < 1\}$ and normalizing parameters $a_n > 0$ and b_n as $n \to \infty$ exist, then the distribution of the rescaled maxima converges to a non-degenerate limiting distribution G [Coles, 2001], where

$$Pr\left(\frac{max(X_1, \ldots, X_n) - b_n}{a_n} \leq x\right) = F^n\left(a_n x + b_n\right) \to G(x). \tag{1.2}$$

If the non-degenerate limiting distribution G for the block maxima exists and satisfies

$$G^n(b'_n + a'_n x) = G(x) \tag{1.3}$$

for $x \in \mathbb{R}$, $n \in \mathbb{N}$, and the sequences $a'_n > 0$ and b'_n then it is max-stable and falls within the Generalized Extreme Value (GEV) family of distributions of the form [Coles, 2001]

$$G(x) = \begin{cases} exp\left[-\left(1 + \frac{\xi(x-\mu)}{\sigma}\right)^{-\frac{1}{\xi}}\right], & \xi \neq 0 \\ exp\left[-exp\left\{-\left(\frac{x-\mu}{\sigma}\right)\right\}\right], & \xi \to 0. \end{cases} \tag{1.4}$$

where μ, σ, and ξ are the location, scale, and shape parameters, respectively, with $\sigma > 0$. The GEV family is made up of three distributions that vary by tail behavior, namely the Gumbel ($\xi \to 0$), the Fréchet ($\xi > 0$), and the Weibull ($\xi < 0$) distributions. The goal then is to determine the best fitting parameters of G so that inferences can be made about the maxima. Common methods used for parameter fitting for the GEV and other extreme value distributions include maximum likelihood (ML) [Prescott and Walden, 1980], probability weighted moments (PWM) [Greenwood et al., 1979], and L-moments [Hosking, 1990].

1.1.2 Threshold Exceedances

The threshold exceedance method, also known as peaks over threshold (POT) or partial duration series, for modeling extremes defines the series of independent maxima as the events that exceed a certain threshold (u). The POT approach has the advantage of being able to capture all events that are extreme based on a selected threshold [Shane and Lynn, 1964, Todorovic and Zelenhasic, 1970]. This means that years without events that are considered extreme may not have any usable data points, while other years with many $x > u$ will have multiple maxima. Although this can result in a set of random variables that are no longer i.i.d., Juncosa [1949] extended the limiting distribution results to the dependent case.

The unique limiting distribution G' of the random variable x exceeding the sufficiently large threshold u is the Generalized Pareto Distribution (GPD) which was introduced by Pickands [1981]. For $x > u$ and $\{x : 1 + \xi(x - \mu)/\sigma > 0\}$

$$G'(x) = 1 - \xi \left[1 + \frac{\xi(x-\mu)}{\sigma}\right]_{x>u}^{-\frac{1}{\xi}}. \tag{1.5}$$

where μ, $\sigma > 0$, and ξ are the location, scale (positive value), and shape parameters, respectively [Coles, 2001]. Similar to the GEV distribution, the GPD shape parameter determines the tail type where $\xi < 0$ is a bounded tail, $\xi = 0$ is a light tail, and $\xi > 0$ is a heavy tail.

Caveats to the POT method is that "extreme" depends upon the chosen threshold, which can be challenging to define within a multivariate scenario [Zheng et al., 2014]. If the threshold is too low bias will be introduced since the model will no longer be following its asymptotic basis. Conversely, if the threshold is too high the data will be too sparse leading to high variance [Coles, 2001]. If the series of maxima are dependent, the POT method can allow for the modeling of clusters of events that occur in succession that may have a larger impact than a single extreme event through use of a compound Poisson process [Davison and Huser, 2015, Leadbetter, 1991]. Otherwise, the POT method may require extra analysis to confirm that extreme events are not serially correlated, namely, that selected extremes are from separate events in time [Coles, 2001].

1.2 Multivariate Extreme Value Theory

Multivariate extreme value (MEV) theory is used to model the probability of extreme events due to multiple drivers across space and/or time. Statistical modeling methods are needed that account for multiple variables with spatial and temporal dependence. Examples of events that would require MEV methods include the associated flooding due to a hurricane

or other large-scale storm (e.g., Katrina 2005, Sandy 2012, and Harvey 2017) during which intense rainfall hits a large spatial region covering gauges at multiple sites. Another example could be the combination of extreme high temperatures and low precipitation at a location over time that led to the recent extreme events in Californian (2014), the central United States (2012), Russia (2010), and Europe (2003). However, extension of univariate extreme value theory to multivariate extreme values (MEV) is not immediately straightforward since there is no natural ordering in higher dimension [Barnett, 1976, Tawn, 1988]. In the following general overview, the discussion is restricted to the bivariate case where the variable of interest is a vector.

1.2.1 Asymptotic Dependence

A joint density function describes the probability of a multivariate random variable given the influence of its components, which involves characterizing their marginal distributions and their dependence. In other words, a multivariate random variable is composed of a vector of random variables [Coles, 2001]

$$\mathbf{X} = [X_1, \ldots, X_n]^T \tag{1.6}$$

wherein information about how the components X_i influence each other helps with the specification of $\mathbf{X}$. In the general case where the components X_i influence each other (aka, dependence), the joint distribution function for $\mathbf{X}$ is [Coles, 2001]

$$F(\mathbf{x}) = Pr\left\{X_1 \leq x_1, \ldots, X_n \leq x_n\right\} \tag{1.7}$$

where $\{\mathbf{x} : x_1, \ldots, x_n\}$ with the joint density function

$$f(\mathbf{x}) = \frac{\partial^n F}{\partial x_1 \ldots \partial x_n}. \tag{1.8}$$

Then the joint marginal density function for a dependent (X_1, X_2) could then be obtained by integrating out the other components

$$f_{X_1,X_2}(x_1, x_2) = \int \cdots \int_{-\infty}^{\infty} f(x_1, x_2, u_3, \ldots, u_n) du_n \ldots du_3. \tag{1.9}$$

Translating these concepts to a bivariate MEV context, the multivariate random variable composed of an i.i.d. vector of random variables $Z_i(X_i, Y_i)(1 \leq i \leq n)$ and

$$maxZ_i(1 \leq i \leq n) = (M_{1n}, M_{2n}), \tag{1.10}$$

where the dependent $M_{1n} = maxX_i$ and $M_{2n} = maxY_i$ provide information to help with the specification of $maxZ_i(1 \leq i \leq n)$. The limiting multivariate distribution G can be derived using the joint distribution F of the random vector (X, Y) and for suitable choices of the constraints $a_{n,1}$, $b_{n,1}$, $a_{n,2}$ and $b_{n,2}$ []

$$Pr\left(\frac{M_{x,n} - b_{n,1}}{a_{n,1}} \leq x, \frac{M_{y,n} - b_{n,2}}{a_{n,2}} \leq y\right) = F_n(a_{n,1} + b_{n,1}, a_{n,2} + b_{n,2}) \to G(x_1, x_2). \tag{1.11}$$

To isolate the dependence from the marginal distributions and for technical convenience, the marginal distributions are transformed to the unit Fréchet distribution, which is classically denoted as Φ where []

$$\Phi(y) = exp\left(-y^{-1}\right) fory > 0. \tag{1.12}$$

Then in the general case, G can be expressed as

$$G(x) = exp\left\{-l\left[-logG_1(z_1), \ldots, -logG_n(x_n)\right]\right\} \tag{1.13}$$

where l is the stable tail dependence function.

The Pickands dependence function [Pickands, 1981] has been commonly used to describe the dependence structure in the bivariate case, which can be defined as [Coles, 2001]

$$A(t) = l(1-t,t) \text{ or } l(t,1-t) = A(1-t) \tag{1.14}$$

and can be viewed as the stable tail dependence function restricted to the unit simplex. The Pickands dependence function uniquely determines the stable tail dependence function as

$$l(v_1, v_2) = (v_1 + v_2)A\left(\frac{v_1}{v_1 + v_2}\right). \tag{1.15}$$

Then the max-stable multivariate distribution G can be characterized by the marginals G_1 and G_2 and the Pickands dependence function A as [Beirlant et al., 2006]

$$G(x_1, x_2) = exp\left[log(G_1(x_1)G_2(x_2)A\left(\frac{log(G_1(x_1))}{log(G_1(x_1)G_2(x_2))}\right)\right]. \tag{1.16}$$

1.2.2 Asymptotic Independence

In the general case of Eq. 1.7, if the components X_i are fully independent, meaning that their behavior does not influence the others, then their joint density function factorizes as [Coles, 2001]

$$f_{X_1,\ldots,X_n}(x_1,\ldots,x_n) = \prod_{i=1}^{n} f_{X_i}(x_i). \tag{1.17}$$

This formulation for the joint density function is computationally more simple than Eq. 1.9, which is a key reason why the assumption that the components are independent is often made in MEV models.

However, the relationship between variables can vary at more extreme levels. When depen-

dence between variables gradually disappears resulting in an increasing drift toward independence it is called asymptotic independence [Beirlant et al., 2006, Bortot and Gaetan, 2014]. Standard MEV methods assume either asymptotic dependence or full independence (like the above Eq. 1.17), which leads to the over-estimation of joint probabilities for asymptotically independent variables [Coles et al., 1999]. Therefore, the development of extreme distributions that are capable of modeling both asymptotic dependence and asymptotic independence is important for avoiding miscalculations of risk.

One of the earlier methods for describing asymptotic independence within a GPD framework was introduced by Ledford and Tawn [1996] wherein they define the joint survival function of two Fréchet random variables X and Y as

$$\mathbb{P}(X > r, Y > r) \sim L(r) r^{-1/\eta} \text{ as } r \to \infty \tag{1.18}$$

where L is a slowly varying function that provides the relative strength of the coefficient of tail dependence, η, with a range $0 < \eta \leq 1$. The value of η is related to the following four classes of extremal dependence for a d-dimensional variable: 1) asymptotically dependent when $\eta = 1$, 2) near extremal independence $\eta = \frac{1}{d}$, 3) asymptotically independent with positive extremal dependence when $\frac{1}{d} < \eta < 1$, and 4) asymptotically independent with negative extremal dependence when $0 < \eta < \frac{1}{d}$ [Ledford and Tawn, 1996]. This model is extended in a more flexible form by Ledford and Tawn [1997] in their later work. However, the extremal dependence model is subject to limitations, such as difficulty in identifying a suitable parameterization for L. Furthermore, under asymptotic independence, the simultaneously large, observed components become increasingly unlikely as the dimension increases [Bortot and Gaetan, 2014].

Coles et al. [1999] also presented a measure of dependence within a copula framework using the χ coefficient. For the random variables X and Y with the transformed marginal U and

V, the dependence between the extremes can be expressed as [Coles et al., 1999]

$$\chi = \lim_{u \to 1} P\left(X > u | Y > u\right) \tag{1.19}$$

After mathematical manipulation

$$\chi(u) = 2 - \frac{logP(U < u, V < v)}{logP(U < u)}, \text{ and } \chi = \lim_{u \to 1} \chi(u) \tag{1.20}$$

where $\chi(u)$ is 0 for independent and is 1 for full dependence with $0 \leq \chi(u) \leq 1$.

When $\chi = 0$, it means that the measure is not able to provide the relative dependence information. To overcome this limitation, a second dependence measure of extremes is defined as [Coles et al., 1999]

$$\bar{\chi}(u) = \frac{2logP(U < u, V < v)}{logP(U < u)} - 1 = \frac{2log(1-u)}{log\bar{C}(u,u)}, \text{ and } \bar{\chi} = \lim_{u \to 1} \bar{\chi}(u) \tag{1.21}$$

where $-1 \leq \bar{\chi}(u) \leq 1$ and $-1 \leq \bar{\chi} \leq 1$.

To summarize, the pair (χ, $\bar{\chi}$) provides the summary of the extremal dependence. Asymptotic dependence is signified by ($\chi > 0$, $\bar{\chi} = 1$) and asymptotic independence by ($\chi = 0$, $\bar{\chi} < 1$). In the case of asymptotic independence, as $\bar{\chi} \to 1$ it gives a measure of the strength of dependence [Coles et al., 1999].

Several other studies have investigated methods for describing or testing for asymptotic independence. Coles and Pauli [2002] developed parametric copula models. Draisma et al. [2004] extended the model by Ledford and Tawn [1997] with a bivariate second order regular variation condition. Ramos and Ledford [2009] developed a new joint tail modeling approach that yields proper joint probability distributions and also encompasses the asymptotic dependence and independence within a single framework. Other efforts to accommodate the modeling of asymptotic independence are the hidden regular variation and multivariate sec-

ond order regular variation [Resnick, 2002, Maulik and Resnick, 2004, Heffernan and Resnick, 2005], which address the defect of the multivariate regular variation method in describing the asymptotic dependence [Heffernan and Resnick, 2007].

1.2.3 Conditional Dependence

It often occurs that all the components of a multi-dimensional random variable are not equally dependent or simultaneously extreme, thereby restricting the limit approach to only a few dimensions for estimating the joint distribution [Heffernan and Tawn, 2004, Heffernan and Resnick, 2007]. Heffernan and Tawn [2004] introduced a semi-parametric conditional MEV approach that can be applied to many dimensions and is based on a POT approach. They arrived at the limiting distribution G of the multi-dimensional random variable given the $Pr(X|Y > u)$ of the i.i.d. random variables X and Y with the condition that Y is extreme [Heffernan and Resnick, 2007]. In more detail, given the transformed random variables X' and Y' and assuming that the normalizaing functions $a(Y')$ and $b(Y')$ exist, the non-degenerate distribution G is attained by

$$Pr\left\{Y' - u, \frac{X' - a(Y')}{b(Y')} \leq z | Y' > u\right\} \rightarrow exp(-y)G(z) \text{ for} y > 0 \text{ as } u \rightarrow \infty \qquad (1.22)$$

For positively associated X' and Y', the normalizing functions take the form of $a(Y') = \alpha Y'$ and $b(Y') = Y^{\beta}$ for which $\alpha \in [0, 1]$ and $\beta \in (-\infty 0, 1)$ [Cheng and AghaKouchak, 2014]. The more complicated form for a negative association can be altogether avoided if a Laplace transformation is used for X' and Y' [Keef et al., 2013]. The Laplace transformation results in $\alpha \in [-1, 1]$ where $\alpha > 0$ indicates positive association and $\alpha < 0$ indicates negative association. Meanwhile, β indicates the variability of the dependence with increasingly negative values representing decreasing variability [Cheng et al., 2014b]. While the advantage of a conditional extreme model is that it provides flexibility whether the variables are asymp-

totically dependent or asymptotically independent, the downside of the approach is that it relies on semi-parametric methods since a simple closed-form distribution does not exist due to the lack of a specific dependence structure [Cheng et al., 2014b].

1.3 Empirical Methods

Empirical (aka, non-parametric) methods, are methods that are based on observed data and they have been widely implemented in univariate extreme value analysis to determine and identify data behavior. Most of these empirical univariate methods can be extended for multivariate analysis and for studying compound events. In the following sections, I review several methods that can be used for extremes in hydrology and climate.

1.3.1 Counting Method

The counting method involves empirically counting the simultaneous occurrence of two or more events at different periods. This approach requires an empirical threshold for defining the extremes of each variable. The exceedances (or non-exceedances) above (or below) the predefined threshold can then be used for studying compound extremes. However, defining the term "extreme" and characterizing a multivariate threshold above (or below) which events are considered to be extreme is not a straightforward task [Zheng et al., 2014].

For extreme thresholds, the reliability of the analysis can be impacted if the sample of compound extreme events is not large enough. Therefore, it is important to check the sample size for different thresholds to ensure the data is adequate for reliable statistical analysis [Beniston, 2009, Hao et al., 2013, Mazdiyasni and AghaKouchak, 2015]. Studies that have utilized this method include investigation by Beniston [2009] of joint extremes in precipitation and temperature within Europe, the study by Fischer and Knutti [2013] provided future

projections of combined humidity and temperature extremes using global wet-bulb temperatures during the hottest (top 1%) of days, Hao et al. [2013] examined global concurrent precipitation and temperature extremes, and Mazdiyasni and AghaKouchak [2015] studied changes in concurrent droughts and heatwaves from 1960-2010 within the U.S.

Another approach for empirical counting establishes multiple thresholds to define the varying severity of a given variable and quantify the magnitude of the simultaneous occurrence of the associated variables in question. Using this method, Chiang et al. [2018] quantified shifts in temperatures associated with different extremes in drought severity.

1.3.2 Multivariate Index

A multivariate index is developed to communicate various metrics relevant for characteristics and monitoring multiple and compound extremes. For example, the degree of clustering of extremes, the average of multiple extremes (e.g., drought, precipitation, and temperature), or the concurrence of extremes (e.g., temperature and relative humidity). These indices are often used to assess the severity, onset, and recovery of compound extreme events. Indeces that are in current use include the U.S. Climate Extremes Index (CEI) [Karl et al., 1996, Gleason et al., 2008], the Heat Index defined by Steadman [1979, 1984], the Multivariate Standardized Drought Index (MSDI) [Hao et al., 2013].

1.3.3 Structure Variable Method

The structure variable method is similar to the multivariate index method, but it focuses on the system response/behavior to a certain combination of underlying variables of interest.

The structure variable can be defined as [Coles, 2001]

$$Z = \Phi\left(M_x, M_y\right) \tag{1.23}$$

where Φ is the response/behavior function (e.g., minimum, maximum, sum, product) and M_x and M_y are extremes (minima or maxima) of variables X and Y. The variable Z can then be modeled with the standard univariate extreme value distribution for inferences (e.g., estimating return levels).

However, with this method, the justification for the GEV distribution is not strong, since other combinations of the variables X and Y may generate larger values from the function Φ than that from the component maxima [Coles, 2001]. Coles [2001] compared the structure variable method with bivariate/multivariate extremes using annual maxima sea-level data. Further limitations of this method are discussed by Hawkes [2008].

1.3.4 Empirical Bayesian Methods

Bayesian analysis assumes that it is possible to infer information about the parameters of the probability distribution of a random variable without using the data directly [Coles, 2001]. The probability distribution of the parameters (θ) is called the prior distribution (herein termed "prior" for purposes of brevity) where the parameters are treated as random variables. This is one of the benefits for application of Bayesian methods to extreme value analysis since the distribution of the parameters provides an estimate of their uncertainty leading to more robust uncertainty estimates for the maxima quantiles.

Bayes theorem describes the relationship of the prior $f(\theta)$ and the likelihood $f(\mathbf{x}|\theta)$ for the purpose of inferring the posterior distribution $f(\theta|\mathbf{x})$. Assuming that the elements x_i of $\mathbf{x}$ are independent allowing for the simplification $f(\mathbf{x}|\theta) = \prod_{i=1}^{n} f(x_i;\theta)$, Bayes' Theorem states

[Coles, 2001]

$$f(\theta|\mathbf{x}) = \frac{f(\theta)f(\mathbf{x}|\theta)}{\int_{\Theta} f(\theta)f(\mathbf{x}|\theta)d\theta}. \tag{1.24}$$

The main computational hurdle for implementing Bayesian techniques is computing the denominator of Eq. 1.24 when the likelihood is intractable. The two popular methods to overcome this include approximate Bayesian computation (ABC) that avoids estimating $f(\mathbf{x}|\theta)$ using pseudosample simulation methods, and a modified version of ABC that incorporates an empirical likelihood Mengersen et al. [2013]. Mengersen et al. [2013] compared the ABC method with their empirical Bayesian via empirical likelihood approach and noted that using the empirical likelihood often resulted in reduced computation times. They also note that the method may be suitable for models with more complex likelihoods.

Cheng et al. [2014b] applied this empirical Bayes via empirical likelihood approach for an analysis of precipitation conditional on extreme temperatures with favorable results that were consistent with results semi-empirical approaches.

1.3.5 Graphical Dependency Models

Graphical dependency models were introduced to represent a complex dependence structure in high dimension [Hanea et al., 2015]. These models have recently gained popularity after the generalization of the simple Markov trees to belief networks (Bayesian learning) and influence diagrams (decision problems) [Bedford and Cooke, 2002].

Bayesian Networks

Bayesian Networks (BN) model a high dimensional joint distribution via a directed acyclic graph (DAG). In the DAG, each node represents a variable, while each arc connecting two

nodes represents their dependence relationship. The absence of an arc between nodes guaranties their (conditional) independence. The direct predecessors (successors) of a node is called parents (children) [Hanea et al., 2015]. A marginal distribution is representative of a node without parents. Otherwise, a conditional distribution is associated with each child node, and it is a quantitative indication of the dependence between the variables involved. Quantitative information can be retrieved from data or from an expert [Hanea et al., 2015].

Following the notation in Hanea et al. [2015], the joint density $f_{i,...,n}(x_i, ..., x_n)$ of the n-variables modeled as a BN on n-nodes is

$$f_{i,...,n}(x_i, ..., x_n) = \prod_{i=1}^{n} f_{i|Pa(i)} \left(x_i \mid x_{Pa(i)} \right) \tag{1.25}$$

where $f_{i|Pa(i)}(x_i \mid x_{Pa(i)})$ is the conditional probability of the variable x_i given its parents $x_{Pa(i)}$. If a node is without parents, then this simplifies to $f_i(x_i)$.

BNs have been mostly applied to nodes representing discrete random variables. Non-Parametric Bayesian Networks (NPBNs) have been developed for continuous random variables. The nodes of a NPBN do not require the assumption of a marginal distribution and the arcs are modeled through one-parameter conditional copulas. The copulas on the arcs are assigned based on the ordering of parent nodes. However, this ordering is not unique [Hanea et al., 2015]. Studies that made use of NPBNs in order to incorporate multiple contributing factors include the dam safety assessment by Morales-Nápoles et al. [2014] in Mexico and the compound flooding assessment by Couasnon et al. [2018a] that included riverine and coastal interactions in Texas.

Influence Diagram

An influence diagram is a generalization of the BN Bayesian framework that addresses both probabilistic inference and decision-making process. Leonard et al. Leonard et al. [2014] used extreme impacts to define a compound event and proposed the influence diagram as a general framework to define, map, analyze, model, and communicate the risk of such events. This approach formalizes the process of identifying the impact-dependence variables (and events) as well as the dependence structure between variables. It also describes the model structure necessary for risk evaluation.

Vine Copula

For analysis of bivariate variables, a rich variety of copula families are available and well-investigated [Joe, 1997]. However, the use of copulas is challenging in higher dimensions, where dependency patterns become more complex and standard multivariate copulas suffer from their rather inflexible structures [Dey and Yan, 2016]. To overcome such limitations, Joe [1996] proposed vine copulas, which were further developed by Bedford and Cooke [2001, 2002] and Kurowicka and Cooke [2007]. Vines are a graphical model that describe multivariate copulas built using a cascade of (conditional) bivariate copulas, so-called pair-copula constructions (PCCs) [Kurowicka and Cooke, 2007, Aas et al., 2009, Brechmann and Schepsmeier, 2013]. Liu et al. [2018] highlight the application of vine copulas for evaluating conditional relationships between variables and underlying physical factors involved in compound extreme events.

The basic idea of PCCs is to decompose the d-dimensional multivariate density into $d(d-1)/2$ pair-copulas and conditional pair-copula densities or building blocks, which represents the exact number in which d elements can be coupled where each pair-copula or conditional pair-copula can be chosen independently from the others and are not restricted to any specific

copula type [Joe, 1996, 1997, Bedford and Cooke, 2002, Schirmacher and Schirmacher, 2008, Jäger and Nápoles, 2017]. Bedford and Cooke [2001, 2002] systemized PCCs using a tree representation, called Regular vines (R-vines). Two subsets of R-vines are commonly applied, Canonical vines (C-vines) and Drawable vines (D-vines). The decomposition of PCCs is identified by choosing a specific non-unique order of variables (nodes) and consists of $n-1$ linked trees $T_i, i = 1, ..., n-1$. The order defines the sequence of conditioning in the PCCs: first variable 1 is conditioned, then variable 2 and so on [Brechmann and Schepsmeier, 2013]. Each edge is labeled and modeled with the pair-copula of the variables that it represents. The edges in level i become nodes for the next level $i+1$. An n-dimensional density of the C-vine copula is given by [Czado et al., 2012]

$$f(x_1, ..., x_n) = \prod_{k=1}^{n} f_k(x_k) \times \prod_{i=1}^{n-1} \prod_{j=1}^{n-i} c_{i,i+j|1:(i-1)} \left(F(x_i|x_1, ..., x_{i-1}), F(x_{i+j}|x_1, ..., x_{i-1})\right) \quad (1.26)$$

where $f(x_1, ..., x_n)$ is the joint density function of n-dimensional random variables, f_k for $k = 1, ..., n$ denotes the n marginal densities, and $c_{i,i+j|1:(i-1)}$ represents the bivariate copula densities. The vine copula's use of product expressions makes the density numerically tractable by reducing the number of dimensions that require integration, even for $d > 2$ [Dey and Yan, 2016].

1.4 Parametric Methods

Parametric methods are used to model the behavior of variables, allowing for inference of values not observed within the data. Many types of parametric subfamilies have been proposed to provide a simpler representation of the MEV distribution and cover a wide range of dependence at the same time [Bortot and Gaetan, 2014]. Some of the parametric models for extremes include the logistic distribution [Tawn, 1988], Gaussian [Smith, 1990], bilogistic [Joe et al., 1992], polynomial [Nadarajah, 1999] and Dirichlet models [Coles and

Tawn, 1991]. A variety of parametric models for bivariate and multivariate extreme value distributions have been reviewed by Kotz et al. Kotz et al. [2004], Beirlant et al. [2006], Banerjee et al. [2014], Dey and Yan [2016], and others.

1.4.1 Bayesian Methods

Bayesian methods, as introduced earlier in Section 1.3.4, allow for the incorporation of prior information for estimating parameters of the marginal (posterior) distribution. The priors of the individual parameters θ_i are sampled using MCMC methods [Gilks, 1996], often using a Gibbs or Metropolis-Hastings style sampler [Banerjee et al., 2014]. The specification of priors (e.g. uniform, Gaussian) used to sample each parameter's distribution differs based on various information and assumptions. The mean value of the prior densities allows for estimation of the posterior distribution $f(\theta|\mathbf{x})$ given Eq. 1.24. The inference based on the posterior distribution afterward is relatively straightforward and estimates of the uncertainty are easily acquired from the prior densities [Banerjee et al., 2014].

A couple of examples of the application of parametric Bayesian methods in extreme value analysis include the approach by Tsionas [2001] for estimation of a MEV Poisson regression model and by O'Brien and Dunson [2004] for a MEV logistic regression. Coles and Tawn [1996] introduced using Bayesian methods for direct prior elicitation in terms of the annual maximum rainfall quantiles, q_p, based on the GEV distribution of the form

$$q_p = \mu + \sigma \left\{ [-log\,(1-p)]^{-\xi} \right\} \xi^{-1}. \tag{1.27}$$

Translation of parametric Bayesian methods to spatial extreme value analysis follows a Bayesian hierarchical modeling (BHM) approach similar to the one introduced in the following Chapter 2, the benefits of this approach for analysis of spatial extremes in hydrology

application are covered in following Section 1.5.1. In short, the spatial BHM expands upon the parametric Bayesian approach to include a second model layer that utilizes a regression model to distribute the spatial variability of the model parameters.

1.4.2 Max-Stable Process Model

A max-stable process is the spatial analogue of the GEV distribution that takes into account the spatial dependence between pairs of observation sites. A max-stable process Z is the limit process of point-wise maxima taken over an infinite number of independent replicates $\{X_i : i \in \mathbb{N}\}$ of a continuous stochastic process X defined on index set $\mathfrak{X}$. For suitable normalizing sequences $\{a_n(x) > 0\}$ and $\{b_n(x) \in \mathbb{R}\}$,

$$Z(x) = \lim_{n\to\infty} \frac{\max_{i=1,\ldots,n} X_i(x) - b_n(x)}{a_n(x)}, x \in \mathfrak{X} \tag{1.28}$$

where the limiting process Z is either degenerate or it is a max-stable process [De Haan, 1984, Ribatet and Sedki, 2013b]. De Haan [1984] simplified characterization of a max-stable process by using a spectral representation wherein a family of non-negative continuous functions $\{f(x, y) : x, y \in \mathbb{R}^d\}$ exist such that

$$\int_{\mathbb{R}^d} f(x, y)dy = 1, \ \forall x \in \mathbb{R}^d, \ K \subset \mathfrak{X} \tag{1.29}$$

where $\int_{\mathbb{R}^d} \sup_{x\in K} f(x, y)dy < \infty$ and the max-stable process Z, with unit Fréchet margins, has the same distribution as

$$Z(x) = \max_{i=1,2,\ldots} \zeta_i f(x, U_i), \ x \in \mathbb{X}, \tag{1.30}$$

where $\{\zeta_i, U_i) : i \in \mathbb{N}\}$ are the points of a Poisson process on $(0, \infty) \times \mathbb{R}^d$ with intensity measure $d\Lambda(\zeta, u) = \zeta^{-2}d\zeta du$. Schlather [2002] later adjusted this characterization of Z to

enable the use of random functions. Incorporating functions with various characterization of spatial dependence into Z leads to the current set of max-stable process families. These models include the Smith process (aka, the Gaussian extreme value process) [Smith, 1990], the Brown-Resnick process [Brown and Resnick, 1977], the Schlather process (aka, the extremal Gaussian process)[Schlather, 2002], and the extremal-t process [Opitz, 2013]. Ribatet et al. [2016] visually illustrate the differences in the spatial patterns of these various MSP families, while noting that the inflexibility of the Smith process produces artificial surfaces within the MSP realizations.

Max-stable process models make use of an extremal coefficient function $\theta(h)$ as a measure of the strength of dependence between the marginals over all spatial separations, where in the bivariate case this would be the distance between pairs of gauged sites (covered in more detail in Chapter 4) [Schlather and Tawn, 2003]. The value of $\theta(h)$ ranges in value from $[1, d]$, where 1 is full dependence and d is the number of sites and indicates near independence (e.g., for a pairwise comparison $d = 2$). However, values greater than d can occur and indicate a negative dependence between sites [Smith, 1990]. Evaluating $\theta(h)$ explicitly is difficult with $d > 2$, thereby limiting MSP to the bivariate case [Ribatet et al., 2016].

Since the MSP models require the use of a pairwise composite log-likelihood function [Padoan et al., 2010] to keep the likelihood formulation tractable, computation can be cumbersome. However, a main benefit of the method is that it produces continuous estimates, not point-based, which allows for directly averaging over regions to produce areal estimates of return levels.

Although max-stable processes are the asymptotic distribution of block maxima (i.e., GEV distribution), Huser and Davison [2014] and Raillard et al. [2014] introduced threshold exceedance approaches that can incorporate max-stable processes. Reich et al. [2014] presented a hybrid approach that uses a copula model for maintaining GPD margins, while also accounting for temporal dependence using a transformed max-stable process.

1.4.3 Copula

Copulas have the advantage of describing the correlation structure of multiple variables independently of the marginal distribution. Based on Sklar's theorem, the d-dimensional joint cumulative distribution function F of the random variable vector $\mathbf{x} = (x_1, \ldots, x_d)$ can be expressed with copula $\mathbf{C}$ as [Sklar, 1959, Joe, 1997]

$$F(x_1, \ldots, x_d) = \mathbf{C}\left(F_1(x_1), \ldots, F_d(x_d)\right) \tag{1.31}$$

where $F_1(x_1), \ldots, F_d(x_d$ are the marginal distributions.

A variety of copula families, such as the Archimedean copula, have been commonly used in hydrology and water resources for frequency analysis [Kao and Govindaraju, 2008, Vandenberghe et al., 2011], precipitation simulation [Bardossy and Pegram, 2009, AghaKouchak et al., 2010], and geo-statistical interpolation [Bárdossy, 2006]. Although there are a variety of parametric copula models, using a non-extreme value distribution can lead to underestimation of spatial dependence [Ribatet and Sedki, 2013a] making extreme distributions more appropriate for the modeling of extreme events (e.g., extreme value copula) [Salvadori et al., 2007, Salvadori and Michele, 2010]. The extreme copula satisfies the condition [Galambos, 1987] [Joe, 1997, Gudendorf and Segers, 2010, Davison et al., 2012]

$$C(u_1^m, \ldots, u_d^m) \rightarrow C^m(u_1, \ldots, u_d). \tag{1.32}$$

In the bivariate case, the extreme value copula can be represented by the Pickands dependence function [Pickands, 1981]. The bivariate copula $\mathbf{C}$ is an extreme value copula if there exists a Pickands function A such that

$$C(u, v) = exp\left\{log(uv)A\left(\frac{log(v)}{log(uv)}\right)\right\} \tag{1.33}$$

where u and v are the marginal probabilities.

1.5 Spatial Analysis of Extremes in Hydrology

While many of the above MEV models can be used for modeling the joint distribution of multiple variables at a single location, the modeling of the distribution over space is of interest for risk assessment since natural hazards are often recorded across multiple sites due to physical processes that are spatial. In spatial statistics, data is pooled within a region allowing for better estimates of the marginal parameters. This is commonly referred to as trading space for time. However, the challenge is identifying the best way to capture the spatial variability of the extreme distribution parameters in a high-dimensional space while also accounting for the spatial dependence, the miscalculation of which can lead to under- or over-estimates of the associated risk [Davison et al., 2012, Ribatet et al., 2016].

Simplifying assumptions are often made to restrict the number of dimensions in MEV models so that they can be used practically and with minimal computational burden. For example, several models assume spatial independence between sites to simplify the formulation of the likelihood and keep it tractable [Coles et al., 1999]. However, which simplifying assumptions are acceptable and which ones negatively impact the estimation of risk is an ongoing area of investigation. Moreover, with the ever increasing computational power of computers, there is an increasing ability to include more covariables that help describe drivers of extreme events within models and perhaps aid in improving estimates of the marginal parameter's spatial variability. Calls have been made by for updating the standard methods used in practice, as outlined by Stedinger and Griffis [2008] in their call for updates to flood frequency analysis guidelines in the U.S.

1.5.1 Point-Based Methods

Point-based methods commonly discussed in flood frequency and extreme precipitation analysis include Regional Frequency Analysis (RFA) and Latent Variable Models (LVM). These types of methods assume spatial independence between at-site observations to simplify estimation of the spatial joint probability distribution [Renard, 2011].

The goal of point-based methods, as with any MEV analysis, is to characterize the distribution of extreme values. In the case of spatial MEV analysis for extreme precipitation, the goal is to evaluate the largest point-wise rainfall depths over a region $\mathfrak{X} \subset \mathbb{R}^2$ by evaluating the probability of the precipitation field $Y(x)$

$$Pr\left\{\sup_{x\in\mathfrak{X}} Y(x) > z\right\} \tag{1.34}$$

where $z > 0$ is a given critical quantity [Ribatet et al., 2016].

Regional Frequency Analysis

Of the various RFA methods, the most popular method involves across-region averaging since it minimizes potential bias due to correlation between stations [Cunnane, 1988]. This method is based on an index flood approach [Dalrymple, 1960] that pools the data within homogeneous subregions so that a single frequency distribuion curve (aka, growth curve) can be fit for the region under an assumption of spatial independence [Hosking and Wallis, 1988]. A scaling factor is then applied to the fitted distribution to attain estimates for individual sites. The four main steps to RFA are 1) checking the data for errors (although not unique to RFA), 2) selection and validation of homogenious subregions, 2) determination of the best fitting distribution for the subregion, and 3) estimation of the region's distribution parameters [Hosking and Wallis, 1993].

By pooling the data of relatively homogeneous sites, better quantile estimates of the frequency distribution are attained than would be possible using a single station's data [Burn, 1990, Hosking and Wallis, 1993, 2005]. Several studies have focused on improving methods for delineating these homogeneous subregions (aka, regionalization) since there are several statistical methods and choices of regional characteristics that can be employed with varying results [Ilorme and Griffis, 2013]. Hosking and Wallis [1993] outlined the use of L-moment statistics [Hosking, 1990] within the RFA framework to aid in confirming both homogeneity and fit for small to medium sample sizes, which have been applied in many precipitation frequency studies since their introduction [e.g., NOAA Atlas 14, Fowler and Kilsby, 2003, Ilorme and Griffis, 2013, Schaefer, 1990, Schaefer et al., 2008]. These methods are also applied in practice for the National Oceanic and Atmospheric Administration (NOAA) Precipitation Frequency Atlas, no. 14 (aka, NOAA Atlas 14) [NOAA Atlas 14], and are combined with a region of influence approach [Burn, 1990] to regionalization wherein each gauge site has its own region along with a potentially unique set of nearby sites. While the region of influence method does allow for smooth transitions across region boundaries, there are subjective choices that must be made during the selection process [NOAA Atlas 14]. Although covariates are not used within a RFA, Schaefer et al. [2008] used regression methods to improve the spatial mapping of L-moment statistics that included latitude and mean annual precipitation within their regional predictor equations in an effort to account for the spatial nature of marginal distributions when selecting subregions.

In contrast to the spatial methods that I will discuss in the following sections, RFA has a homogeneity requirement that can limit the benefit of pooling data when faced with a highly heterogenous region since the resulting subregions may only include a small number of sites, especially in regions with sparse sensor networks. For example, Schaefer et al. [2008] note that in the highly heterogeneous Willamette River Basin of Oregon, some of the subregions in their study only contained 7 sites despite the relatively dense sensor network. Such a limited number of sites can be seen as problematic when the desire is to estimate the 100-year return

level and beyond for infrastructure design. Additionally, the NOAA Atlas 14 documentation notes that there are several stations where the regional approach do not perform well for fitting the observed data requiring individual at-site fits for those sites [NOAA Atlas 14]. Renard [2011] points out many of these flaws of RFA and more, while also promoting the use of a BHM framework.

RFA methods rely on regression models to interpolate at-site results to ungauged sites. Grover et al. [2002] compared various regression methods including linear, nonlinear, and nonparametric. While, NOAA Atlas 14 and Schaefer et al. [2008] used the Parameter-elevation Regressions on Independent Slopes Model (PRISM) approach developed by Daly et al. [1997] to spatially interpolate each site's data series means as a base for estimating their quantile grids.

Latent Variable Models

To account for the spatial nature of extreme precipitation, Latent Variable Models (LVM) (e.g., Bayesian Hierarchical Models) have been developed that allow for the incorporation of spatially varying geographic and climatic covariates for distributing extremal model parameters in space (i.e., trend surfaces) [Cooley et al., 2007, Renard, 2011, Banerjee et al., 2014, Davison et al., 2012, Ribatet et al., 2012, Wikle et al., 1998].

Using LVM methods, the random variable $Y(s)$ with spatially varying GEV paramters at each gauged site $s \in S$ represented as

$$Y(s) \sim GEV\mu(s), \sigma(s), \xi(s). \tag{1.35}$$

The distribution parameters are estimated using a Gaussian process with a mean function and a parametric covariance function Dyrrdal et al. [2014], Ribatet et al. [2016]. The mean

function is based on physically relevant geographic or climatic covariates for the region. For example, the spatially varying parameters $\mu(s), \sigma(s), \xi(s)$ within the BHM model that I use in Chapter 2 take the form

$$\begin{aligned}
\mu_s &= x_s^\top \theta^\mu + \tau_s^\mu \\
\kappa_s &= x_s^\top \theta^\kappa + \tau_s^\kappa \\
\xi_s &= x_s^\top \theta^\xi + \tau_s^\xi \\
\tau_s^\nu &\sim GP(\alpha^\nu, \lambda^\nu)
\end{aligned} \tag{1.36}$$

where $\kappa_s = 1/\sigma_s$ to ensure that the scale parameter remains positive. The covariates are represented by x_s, the regression parameters are θ^ν, and the spatial random effects terms is denoted by τ_s^ν with hyper-parameters α^ν and λ^ν related to its covariance function, and where $\nu \in \{\mu, \sigma, \xi\}$. In this way, LVMs are able to handle some heterogeneity, which reduces the need to define homogeneous subregions [Cunnane, 1988].

In order to improve spatial estimates of extreme precipitation, it is important to account for the processes that influence its generation [Maraun et al., 2010]. As detailed above, latent variable models are able to address this through the inclusion of relevant covariates. However, a common challenge is identifying the optimal covariates to include [Blanchet and Davison, 2011, Davison et al., 2012, Ribatet, 2017]. Steinschneider and Lall [2015], developed and incorporated an atmospheric river index as a variable within their latent variable model. Cooley et al. [2007] performed a BHM analysis of extreme precipitation along the Front Range in Colorado, wherein they determined that including covariates related to the climate of the region (i.e., elevation and mean seasonal precipitation) provided improved representations of the spatial variability of rainfall intensity compared with the traditionally used latitude and longitude only. However, the majority of studies rely on using either geographic covariates only (i.e., latitude and longitude) or at most will also include mean annual precipitation or mean seasonal precipitation. However, as noted by Ribatet [2013], applying tend surfaces

that are too simple can result in bias due to mischaracterization of the dependence structure.

BHM can be seen as an improvement over RFA methods due to the robust uncertainty estimates and ease of including covariate information within the model. Additionally, by incorporating stochastic processes, the prediction of quantiles at ungauged sites is simpler [Davison et al., 2012]. However, while promoting the use of BHM over the classic RFA methods, Renard [2011] notes that the assumption of spatial independence is still a flaw of both methods. The covariates are related to the spatial dependence of the parameters, not the spatial dependence in the data; these are two different processes.

Areal Reduction Factors

Since point-based methods are only capable of producing point-based estimates, the additional step of using Areal Reduction Factors (ARFs) is required to transform their quantile estimates to an areal averaged depth estimate most often used for modeling rainfall-runoff relationships and design storm estimates. In practice, the ARFs utilized are based on the Technical Paper No. 29 (TP-29) guidelines [U.S. Weather Bureau, 1958] and are a function of the area of the watershed and the precipitation duration, and assume that the ratio does not vary with frequency. Therefore, the TP-29 ARFs are solely meant to serve as a ratio of the average depth to the point depth of the annual maxima over a region (i.e., watershed) with a maximum area of 1100 mi^2 as follows

$$P_a = ARF \times P_p \tag{1.37}$$

where, for a given watershed and duration, P_a is the areal average precipitation depth, P_p is the mean of the point precipitation depth, and ARF is the areal reduction factor [U.S. Weather Bureau, 1958]. Leclerc and Schaake [1972] present a simplified approach for

calculating the above ARF term as follows

$$ARF = 1 - exp(-1.1t^{0.25}) + exp(-1.1t^{0.25} - 0.01A) \tag{1.38}$$

where t is the duration in hours and A is the area of the watershed in square miles.

Arguments against the above fixed area approach often point out that it does not account for the frequency of the quantiles, the shape of the watershed, or the individual storm event characteristics (e.g., how the size of the storm impacts correlation) [Asquith and Famiglietti, 2000, Olivera et al., 2008].

1.5.2 Areal Methods

Max-stable process models are the spatial analog of MEV analysis and incorporate a spatial dependence component. By including spatial dependence, they are capable of producing estimates that are continuous surfaces versus the point-based results of the previous section. The ability to directly estimate areal exceedances without having to use ARFs is one of the benefits from a design and planning perspective. Additionally, these models are also capable of incorporating physically relevant covariates within their modeling frameworks for describing the spatial variability of parameters.

The main impediment to the application of MSP models in practice is the computational burden. While some of the MSP models have been around for a while, application of the framework to spatial extreme value analysis was not popular until recently due to the lack of a closed form likelihood, which resulted in heavy computational burdens [Ribatet et al., 2016]. However, the introduction of a pairwise composite log-likelihood function [Padoan et al., 2010], as mentioned earlier in Section 1.4.2, has allowed for the development of computationally usable models.

Fitting spatial series of maxima with a MSP model is usually broken into two stages wherein the spatial dependence and the trend surfaces are fit separately. After which, the fitted spatial dependence and trend surfaces are used together to produce realizations of the max-stable process. This two staged modeling approach is demonstrated in Chapter 4 for this dissertation.

MSP models have been applied in the literature by Coles and Tawn [1996] for areal rainfall in southwest England, by Reich and Shaby [2011] for analysis of temperature maxima in the southeast U.S., by Stephenson et al. [2016] for extreme rainfall for developing IDF curves, by Westra and Sisson [2011] for detecting non-stationarity in extreme precipitation, and a few others. The majority of the MSP literature (including most listed here) is based on demonstrating improvements in methodology. Extensive use for applications based assessments has not yet been established.

Copula have been adapted in several studies for the modeling of joint extremes [e.g. AghaKouchak et al., 2010, Madadgar and Moradkhani, 2014, Mazdiyasni et al., 2017, Couasnon et al., 2018b], and have been gaining in popularity over the years. Application of copula methods have been made more accessible through the introduction of analysis tools like MvCAT [Sadegh et al., 2017] and copula do not suffer from the same intractable likelihood issues that slowed the adoption of MSP models.

Several copula can be extended to the spatial case given Kolmogorov's extension theorem [Kolmogorov], which defines how a collection of finite-dimensional distributions can define a stochastic process. As noted by [Ribatet and Sedki, 2013a], Gaussian and Student copulas are popular for the spatial case given the ease of replacing the Gaussian and Student random vectors with processes. However, an extreme value copula should be used for modeling spatial extremes to avoid improper characterizations of the tail dependence [Renard and Lang, 2007]. As an example of this, Renard and Lang [2007] demonstrated the underestimation of risk that can occur when using copula that assume asymptotic independence (i.e. Gaussian copula)

for extreme data that are dependent. Therefore, it is important to use a diagnostic measures for determining the extremal dependence of the data for choosing the correct copula families [Coles et al., 1999, Tootoonchi et al., 2021].

1.6 Improving Extreme Precipitation Estimation with Physical Information

Due to the spatial nature of extreme climate events, the estimation of exceedance probabilities for infrastructure design and hazard mitigation depends on properly modeling the spatially varying marginal parameters and appropriately characterizing dependence. Recognizing that simplifying assumptions can introduce under- or over-estimation of exceedance probabilities, the goal of this dissertation is to challenge some of these assumptions using recent methods in spatial extremes analysis.

In the following Chapter 2, I use a spatial Bayesian Hierarchical Model (BHM) framework that includes a Bayesian Model Averaging (BMA) component to compare the spatial modeling of daily precipitation annual maxima for two climatically different regions, along with a region of overlap between the two Love et al. [2020]. I compare posterior inclusion probability (PIP) results produced via BMA for the individual parameters of the GEV distribution for various models by region. I compare a wide range of models from relatively simple (location covariates only) to rather complex (location, elevation, and monthly and seasonal mean precipitation, temperature, and dew point temperature). My results indicate that the inclusion of dew point temperature and mean daily temperature is important for improving predictive performance within a highly heterogeneous region. The results within the region of overlap indicate that storm type should be considered in the regionalization of observed spatial precipitation data since the dominant storm type of the pooled data the regional models were

based on impacted the predictive performance across all of the models, regardless of climatic covariates employed. I outline which covariates were most influential across several models for estimation of the GEV parameters based on each region's PIP results.

In Chapter 3, I introduce a framework for the selection of proper geographic and climatic covariates for the spatial analysis of extremes using elastic-net regularization. The elastic-net regression allows for the exploration of relatively large sets of physically-based covariates relevant to spatial extremes. I demonstrate the application of elastic-net regularization within a block maxima approach and the Generalized Extreme Value (GEV) distribution for spatial modeling. However, the approach is general and can be applied using other probability distributions. I used two climatically different regions, northeastern Colorado and the Texas-Louisiana Gulf Coast, with different dominant storm generating mechanisms. My results show a good fit for the spatially varying location and scale parameters of the GEV distribution in both regions when comparing calibration and validation data sets. The fit for the spatially varying GEV shape parameter within the Gulf Coast region shows promise since this parameter is known for being difficult to fit and, as a result, is often set to a fixed value. The results have significant implications for the analysis of the recurrence intervals of extreme events.

In Chapter 4, I present a comparison between max-stable process model results for two climatically different regions within the coterminous United States and their NOAA Atlas 14 counterparts that are based on RFA methods. RFA assumes independence between sites allowing for quicker computation times, this assumption is not reasonable in regions with either dense station networks or large-scale dominant storm mechanisms (e.g., mesoscale thunderstorms, tropical cyclones). Since we know that extreme events are often shared across sites, ignoring inter-site dependence can lead to miscalculations in return levels with the potential for devastating impacts on urban and agricultural areas that depend on infrastructure designed using such assumptions (e.g. Louisiana flooding, Boulder Colorado

floods). The exception to this would be regions with a sparse number of sites and/or with extreme precipitation events that are highly localized - but then you have a completely different model accuracy issue. My results provide insights into the impact of the inclusion of spatial dependence within regions dominated by large-scale storms.

Chapter 2

Integrating Climatic and Physical Information in a Bayesian Hierarchical Model of Extreme Daily Precipitation

This chapter is based on the following published work:

Love, C. A., Skahill, B. E., England, J. F., Karlovits, G., Duren, A., & AghaKouchak, A. (2020). Integrating Climatic and Physical Information in a Bayesian Hierarchical Model of Extreme Daily Precipitation. Water, 12(8), 2211. https://doi.org/10.3390/w12082211

2.1 Introduction

The ability to estimate the magnitude and frequency of extreme precipitation events is an essential part of infrastructure planning and flood prediction [Gumbel, 1958, Luke et al., 2017,

Stedinger and Griffis, 2008]. Extreme events directly affect infrastructure and residents of a region, while also having an economic effect [Cheng and AghaKouchak, 2014, **?**, Stedinger and Griffis, 2008]. They are often localized and difficult to predict. Extreme precipitation estimates are often required in regions where gauge data is sparse [Cooley et al., 2007]. In regions that do have relatively dense observational networks integrating spatial information (i.e., multiple extremes across space) for frequency is not straightforward [Cooley et al., 2007].

Following the early contributions by Gumbel [1941], which expanded upon the work of Fisher and Tippett [1928], frequency analysis became widely used for estimating rainfall or streamflow corresponding to different return periods [Bonnin et al., 2006, Davison and Smith, 1990, England Jr. et al., 2015, Fowler and Kilsby, 2003]. The process generally involves fitting a representative parametric distribution function (e.g., generalized extreme value distribution, Log-Pearson, exponential) to extreme values (e.g., exceeding 95^{th} percentile) [Fisher and Tippett, 1928, Gumbel, 1958, Hosking and Wallis, 1993, Jenkinson, 1955]. The fitted distribution is then used to estimate the probability of occurrence of different events (e.g., precipitation and/or streamflow) [Coles, 2001]. The further out on the tail of the distribution inference is made, the greater the uncertainty [Coles, 2001, Davison et al., 2012, Papalexiou et al., 2018].

Precipitation is a spatial process and several methods have been developed to integrate spatial information into frequency analysis [Cooley, 2009]. One approach for spatial extreme precipitation analysis is spatial Bayesian Hierarchical Modeling (BHM)[Cooley et al., 2007, Renard, 2011]. BHM distributes extremal model parameters in space using covariate information pertaining to geographical and climatological factors that influence regional precipitation extremes [Banerjee et al., 2014, Davison et al., 2012, Ribatet et al., 2012, Wikle et al., 1998]. The advantages of a BHM-based spatial analysis of extremes include (a) that BHM does not require the decomposition of the study region into homogeneous subregions

[Cooley et al., 2007]; (b) it is robust in the treatment of uncertainty [Banerjee et al., 2014, Cooley et al., 2007]; (c) BHM can be easily adapted to accommodate treatments of non-stationarity [Banerjee et al., 2014, Cheng et al., 2014a, Economou et al., 2014]; and (d) it allows the inclusion of physical features (e.g., elevation) of the region and other relevant climatic variables (e.g., temperature, moisture transport) [Cooley et al., 2007, Ahn et al., 2017]. Moreover, the Bayesian inference methodological framework readily supports the inclusion of additional data types relevant to the analysis; for example, information derived via elicitation and climate indices [Coles and Tawn, 1996, Economou et al., 2014, Kwon et al., 2008, Steinschneider and Lall, 2015]. A potential challenge with applying spatial BHM however, is either locating or developing relevant covariate data to support its deployment. Past spatial BHM extreme value studies incorporate covariate information from gridded model outputs or interpolated data sets (i.e. ERA-Interim reanalysis data, VIC, ECHAM4.5, interpolated data sets from the Spatial Climate Analysis Service, and the Hulme data set) [Cooley et al., 2007, Ghosh and Mallick, 2011, Kwon et al., 2008, Najafi and Moradkhani, 2013, 2014, Sang and Gelfand, 2008, Steinschneider and Lall, 2015].

In this study, we incorporate the Parameter-elevation Relationships on Independent Slopes Model (PRISM) data set [Daly et al., 1994, 1997, 2008] as a source of covariate information within a BHM framework that includes Bayesian model averaging (BMA) for each parameter's general linear model. We consider a wide range of models from relatively simple (location covariates only) to rather complex (location, elevation, and monthly mean climatic variables). The climatic variables used include mean daily temperature and dewpoint temperature, which goes beyond the inclusion of precipitation of previous studies in the western U.S. [Bracken et al., 2016]. We compare model choice, complexity, and covariates in two distinct regions in Oregon with different dominating rainfall generation mechanisms, and a region of overlap. We apply BMA to account for model uncertainty and to access covariate selection across models and domains. We analyze the posterior inclusion probabilities (PIP) generated using BMA for the model covariates, model performance, and the contribution of

the spatial random effects term to the parameter estimates. The overarching goal of this paper is to determine the effectiveness of including BMA within a spatial BHM framework across climatically varying regions.

2.2 Methods

In this study, I model annual maxima (AM) daily precipitation data from Oregon using the generalized extreme value (GEV) family of distribution functions. The GEV family of distribution functions are of the form [Coles, 2001]

$$G(x) = \Big\{ - \Big[1 + \xi\Big(\frac{x-\mu}{\sigma}\Big)^{-\frac{1}{\xi}}\Big]\Big\} \tag{2.1}$$

defined on $\{x : 1+\xi(x-\mu)/\sigma > 0\}$ where $\{(\mu, \sigma, \xi) : \mu \in \mathbb{R}, \sigma > 0, \xi \in \mathbb{R}\}$. The location ($\mu$), scale ($\sigma$), and shape ($\xi$) parameters of the distribution specify the center of the distribution, the size of the deviation around μ, and the tail behavior of the distribution, respectively. The GEV family incorporates the three possible extreme value distributions which correspond to $\xi < 0$ (Weibull), $\xi = 0$ interpreted as the limit as $\xi \to 0$ (Gumbel), and $\xi > 0$ (Fréchet).

My spatial BHM extreme rainfall analysis was performed using the R software package 'spatial.gev.bma' [Lenkoski, 2014]. The framework implements a Markov Chain Monte Carlo (MCMC) sampling methodology to estimate the spatially dependent parameters of the GEV distribution [Dyrrdal et al., 2014]. Additionally, the framework uses BMA to assess model uncertainty related to the covariates employed [Dyrrdal et al., 2014]. The framework developed by Lenkoski [2014] assumes stationarity with time [Dyrrdal et al., 2014].

A mathematical overview of the framework is presented below, and it follows the exposi-

tion detailed by Dyrrdal et al. [2014]. Each GEV spatially dependent parameter is defined by a general linear model (GLM) of the covariates plus a spatial random effects term (τ) that accounts for residual spatial association not captured by the covariates. Ideally, if the covariates sufficiently capture the latent processes, the τ term should be minimal. The precipitation AM for a specific location s is represented as y_{ts} (within the spatial region of study S) and for a year t, where [Dyrrdal et al., 2014]

$$y_{ts} \sim GEV(\mu_s, \sigma_s, \xi_s), \tag{2.2}$$

and

$$\begin{aligned} \mu_s &= x_s^\top \theta^\mu + \tau_s^\mu \\ \kappa_s &= x_s^\top \theta^\kappa + \tau_s^\kappa \\ \xi_s &= x_s^\top \theta^\xi + \tau_s^\xi \\ \tau_s^\nu &\sim GP(\alpha^\nu, \lambda^\nu) \end{aligned} \tag{2.3}$$

where $\kappa_s = 1/\sigma_s$ to ensure that the scale parameter remains positive. The covariates, regression parameters, spatial random effects terms are denoted by x_s, θ^ν, and τ_s^ν, respectively, where $\nu \in \{\mu, \sigma, \xi\}$. The spatial random effects term is assumed to be a zero-centered Gaussian spatial process defined by an isotropic exponential covariance function with a sill (α^ν) and range (λ^ν) [Dyrrdal et al., 2014]. In particular,

$$E(\tau_{st}^\nu) = 0 \tag{2.4}$$

$$cov(\tau_{st}^\nu, \tau_{sr}^\nu) = \frac{1}{\alpha^\nu} exp\Big(- \frac{d_{s_t s_r}}{\lambda^\nu} \Big), s_t, s_r \in S, \tag{2.5}$$

where $d_{s_t s_r}$ is the Euclidean distance between locations s_t and s_r. The likelihood is given by

$$Pr(y_o|\{\mu_s, \sigma_s, \xi_s\}_{s\in S_o}) = \prod_{\in S_o}\prod_{t=1}^{T_s} pr(y_{ts}|\mu_s, \sigma_s, \xi_s), \tag{2.6}$$

where y_o denotes the entire set of block maxima observations. The likelihood definition does imply that y_{ts} and $y_{ts'}$ are conditionally independent for anywhere $s \neq s'$ [Dyrrdal et al., 2014]. This independence assumption may influence our results, particularly in the denser network of stations within the Willamette River Basin (WRB) where larger-scale winter storms off the Pacific Ocean dominate the AM events. However, for the sparser network of stations within the eastern Oregon region (EOR) where more localized thunderstorms dominate several sites, this is less likely to influence performance.

Model inference is performed using Markov Chain Monte Carlo (MCMC) methods, wherein the algorithm returns a chain of length N, where the n^{th} iteration contains the set of elements

$$\left\{\theta^{\nu}, \tau^{\nu}_{s\ s\in S_o}, \alpha^{\nu}, \lambda^{\nu}\right\}^{[n]}, \tag{2.7}$$

for each $\nu \in \{\mu, \kappa, \xi\}$ from which the joint posterior distribution is estimated after discarding the initial burn-in period. The Gaussian proposal distributions are tuned using second-order Taylor expansions of Eq. 7 [Dyrrdal et al., 2014]. The BMA feature within the framework makes use of conditional Bayes factors and an MC3-within-Gibbs style of sampling to account for model uncertainty (for a detailed formulation, please see [Dyrrdal et al., 2014]). For each iteration a subset of model covariates is randomly sampled, let's call this model subset M. A conditional Bayes factor evaluation is used, where the full conditional probability of M is compared with that of the proposal M'. If the proposal M' is accepted, then the regression parameters corresponding to each of the covariates used in M' are updated. If rejected, the

previous M is used. Each time M is accepted, the covariates it contains are assigned a one; conversely, each is assigned zero when rejected or not used within M. After all iterations have completed, the posterior inclusion probability (PIP) can be calculated using the number of times a covariate received a one out of the total post-burnin iterations.

The covariate information we employed for our models pertains to the geographical and climatological factors that we assume influence regional precipitation extremes within the study regions. To improve inference, as suggested by Dyrrdal et al. [2014], all covariates were standardized prior to model simulation. We evaluated the predictive performance of each model through application of leave-one-out cross validation (LOO-CV) and minimization of the continuous ranked probability score (CRPS) and root mean squared error (RMSE). RMSE was applied as

$$RMSE = \sqrt{\frac{1}{N}\sum_{j=1}^{N}\Big(F(p_j)_{obs} - F(p_j)_{pred}\Big)^2} \tag{2.8}$$

where N is the site-specific number of AM events, and p is precipitation in inches. The CRPS compares the predicted and observed cumulative distribution functions, and can be defined as

$$CRPS = \int_{-\infty}^{\infty}\big[F(p) - H(p - p_j)\big]^2 dp \tag{2.9}$$

where p represents the predicted precipitation, and p_j the observed precipitation [Gneiting and Raftery, 2007]. For $F(p)$, we used the median of the predicted GEV cumulative distributions (Eq. 2) across all iterations (post burn-in). $H(p)$ is the Heaviside step function where

$$H(p) = \begin{cases} 0, & p < 0 \\ 1, & p \geq 0. \end{cases} \tag{2.10}$$

As the distributions become increasingly similar, the CRPS approaches zero [Hersbach, 2000]. As noted by Dyrrdal et al. [2014], a small (hundredths) change in CRPS corresponds with a substantial difference in performance, which is why we chose to also use RMSE. For this study, we used a derivation of CRPS, which can be written as

$$CRPS = \frac{1}{JK} \sum_{j=1}^{J} \sum_{k=1}^{K} \left[F(p_k) - H(p_k - p_j) \right]^2 \tag{2.11}$$

where k is the number of predicted values, and j is the number of observed values.

2.3 Data

The Willamette River Basin (WRB) is located along the western part of Oregon (Figure 2.1). The region is bounded by the Coastal Range to the west, the Columbia River to the north, and the Cascade Range to the east. Extreme precipitation in the WRB primarily is a result of winter storms that occur between October and March, and which typically account for 75-80% of the region's annual precipitation [Lee and Risley, 2002, Redmond and Koch, 1991]. Temperature fluctuations are relatively small due to the basin's proximity to the Pacific Ocean; however, elevation plays a major role in its variability [Lee and Risley, 2002, Melack et al., 1997]. Elevations within the WRB range from near sea level along the Columbia River to over 3,048 m in the Cascade Range [Daly et al., 1994]. The orographic effect of the Cascade Range results in relatively high amounts of precipitation along the Columbia River Gorge [Daly et al., 1994]. Overall, the Pacific northwest region experiences warm, dry summers due to intensification of the Pacific subtropical high, and cool, wet winters as the polar jet stream dips southward bringing storms from the Gulf of Alaska [Mock, 1996]. We also focus on eastern Oregon (EOR), which encompasses the region east of the Cascade Range crest-line, the high desert of southeastern Oregon, north-central Deschutes–Umatilla Plateau, and the Blue Mountains in the northeast. We chose this additional region since

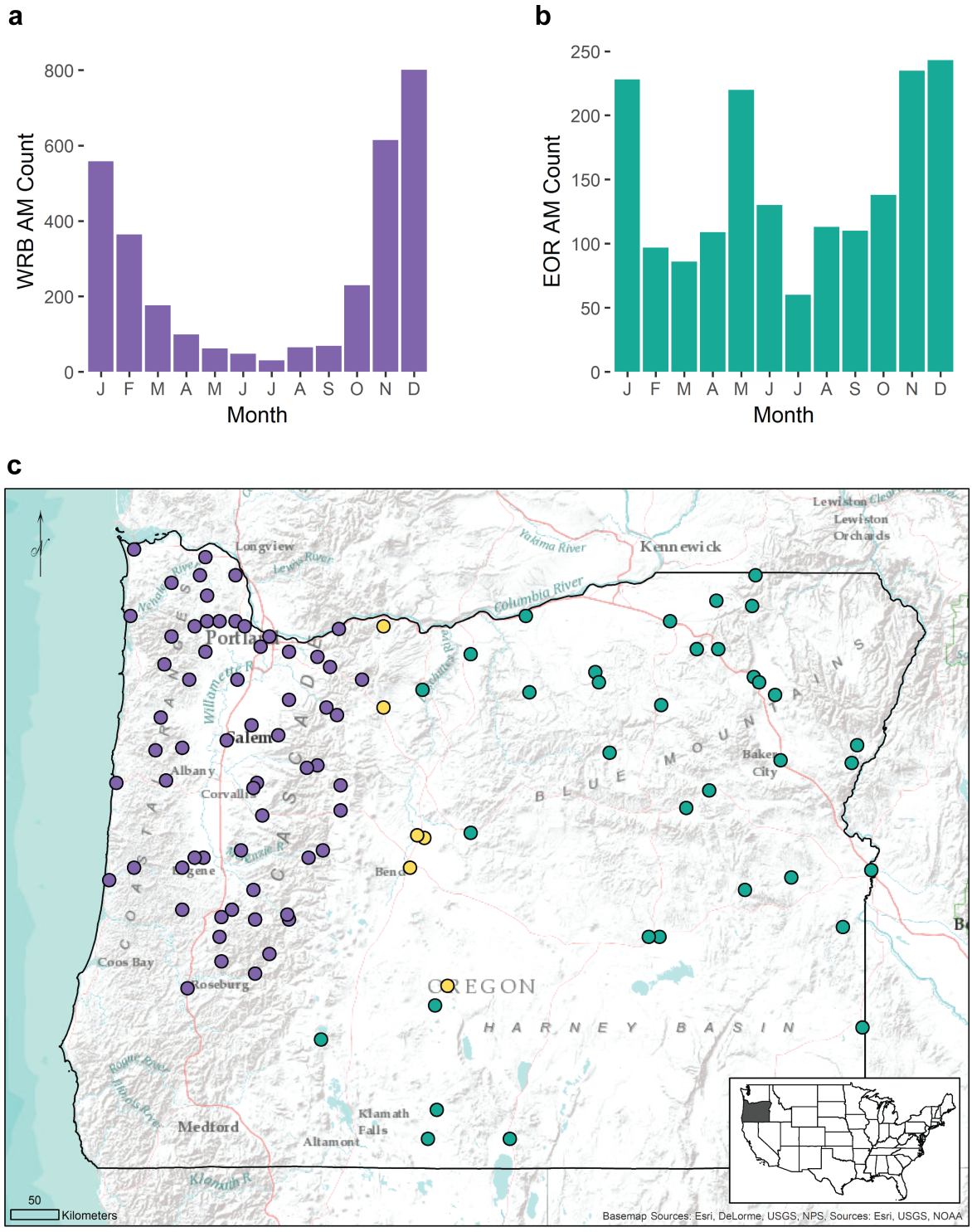

Figure 2.1: Study regions with location reference numbers, and Annual Maxima (AM) climatology where a) is the count of AM events by month for the Willamette River Basin (WRB) and b) is the count of AM events by month for the eastern Oregon (EOR) study region. Within the study region map, the purple markers indicate locations included exclusively within the WRB, while green markers indicate those within the EOR. The yellow markers are the locations that were included within both study regions.

it varies climatically from the WRB. In general, EOR is drier than western Oregon with approximately four times less precipitation falling east of the Cascade Range than to the west [Bond and Vecchi, 2003]. During the early summer months, areas within the EOR region often experience increases in precipitation due to thunderstorms which develop as cool marine air pushes inland east of the Cascade Range and interacts with warmer inland air [Harris and Hubbard, 1983, Melack et al., 1997, Mock, 1996]. As the summer months progress, decreases in precipitation are widespread as the Pacific subtropical high continues to increase in intensity and extent while the polar jet stream shifts northward, with a few localized exceptions due to thunderstorms [Mock, 1996].

The time series of Annual Maxima (AM) data for the WRB and EOR regions was produced for the Oregon Department of Transportation (ODOT) by Schaefer et al. [2008], which was conducted due to the lack of a National Oceanic and Atmospheric Administration (NOAA) precipitation atlas update for the region [Bonnin et al., 2006]. The data set is comprised of 24-hour annual precipitation maxima for 128 stations throughout Oregon, where annual is defined as the period between January 1st and December 31st [Schaefer et al., 2008]. The length of record for each station ranges from 10 to 66 years, with a combined 2,912 AM for the WRB, and 1,620 AM for EOR. We used the stations which fall within our specific study regions; 68 stations fall within the WRB region, while 41 stations fall within the bounds of EOR (Figure 2.1). Six of the stations (along the Columbia River Gorge and east of the Cascade Range crest) were included in both the WRB and EOR regions for additional model comparison. The remaining stations from the original data set fall within the Umpqua and Rogue River watersheds, which were not included in this analysis. Schaefer et al. [2008] performed quality checks on the station records for errors, incomplete records, and any anomalous precipitation amounts relative to neighboring gages. They also checked the station data for stationarity and temporal independence using a null hypothesis of zero slope and zero serial correlation, respectively; they could not reject the null hypothesis at a significance level of 0.05. Based on the dominance of larger scale winter storms across

the WRB, there is likely some spatial dependence between stations. However, the spatial dependence across the EOR region should be less since there are fewer stations spread over a larger region with several dominated by local convective storms.

The covariates we employed include the site-specific geographical information of longitude, latitude, elevation, and climatological information including monthly and annual precipitation, mean temperature, and mean dew point temperature from the PRISM Norm81m long-term (1981-2010) mean monthly gridded data set [Daly et al., 2008]. The covariates were selected based on the literature on the impacts of physical information (e.g., elevation, climatology) on local extreme precipitation [Oki et al., 1991, Javier et al., 2007, Papalexiou et al., 2018]. Temperature and dewpoint temperature were included since their interaction with precipitation extremes, primarily because of rainfall-temperature thermodynamic relations, have been recognized in previous publications [Trenberth and Shea, 2005, Zhao and Khalil, 1993, Adler et al., 2008].

The PRISM data set not only has the advantage of being extensively peer-reviewed, but also has a relatively fine spatial resolution across the contiguous United States (∼800m) [Daly et al., 2008]. From the PRISM data set we also derived the seasonal mean (November-March and April-October means) of the climatological variables monthly precipitation (P), monthly mean daily temperature (T), and monthly dew point temperature (T_d) for use in our models. Our choice of specific covariate data used for each of the models varies from simple (longitude and latitude; model XY) to more complex (longitude, latitude, elevation, monthly P, monthly T_d, and monthly T; model XYZPT6) (Table 2.1).

Table 2.1: Model Acronyms and Covariates Employed[a]

Acronym	Model Covariates
XY	Longitude, Latitude
XYZ	Lon., Lat., Elevation
XYZPT1	Lon., Lat., Elevation, P_A
XYZPT2	Lon., Lat., Elevation, P^*, T_d^*, T^*
XYZPT3	Lon., Lat., Elevation, P_A, T_{dA}, T_A
XYZPT4	Lon., Lat., Elevation, P^*, T_d^*, T^*, P^c, T_d^c, T^c
XYZPT5	Lon., Lat., Elevation, P_1,..., P_{12}, T_{dA}, T_A
XYZPT6	Lon., Lat., Elevation, P_1,..., P_{12},T_{d1},..., T_{d12},T_1,..., T_{12},

[a]Precipitation, dewpoint temperature, and mean daily temperature are denoted as P, T_d, and T, respectively. Numbered subscripts denote month (e.g., 1 for January, 12 for December). An asterisk denotes the mean across wet season months (November-March), while a superscript "c" denotes the mean across dry season months (May-April). Annual means (January-December) are denoted with a subscript "A".

2.4 Results

2.4.1 Model Selection

The selection of the best performing models for each region was based upon the comparison of the mean, median and spread of the CRPS and RMSE across sites (Figures 2.2 and S1). Additionally, I inspected individual location predicted CDFs (Figure 2.10) and mapped model performance to determine whether there was any noticeable difference between models (Figure 2.11). The results of the LOO-CV analysis suggest that from the eight models tested for each region, XYZPT2, XYZPT4, XYZPT5, and XYZPT6 were the top performing models for the WRB (Figure 2.2b), while XYZPT1 and XYZPT3 were the top for EOR (Figure 2.2a). I argue that these top performing models within a given region are equally good since their mean and median scores and their spatial distributions are similar. Therefore, the choice for the best model is the simplest model out of the top performing models for each region. For the WRB, the simplest top-performing model includes location, elevation, and mean

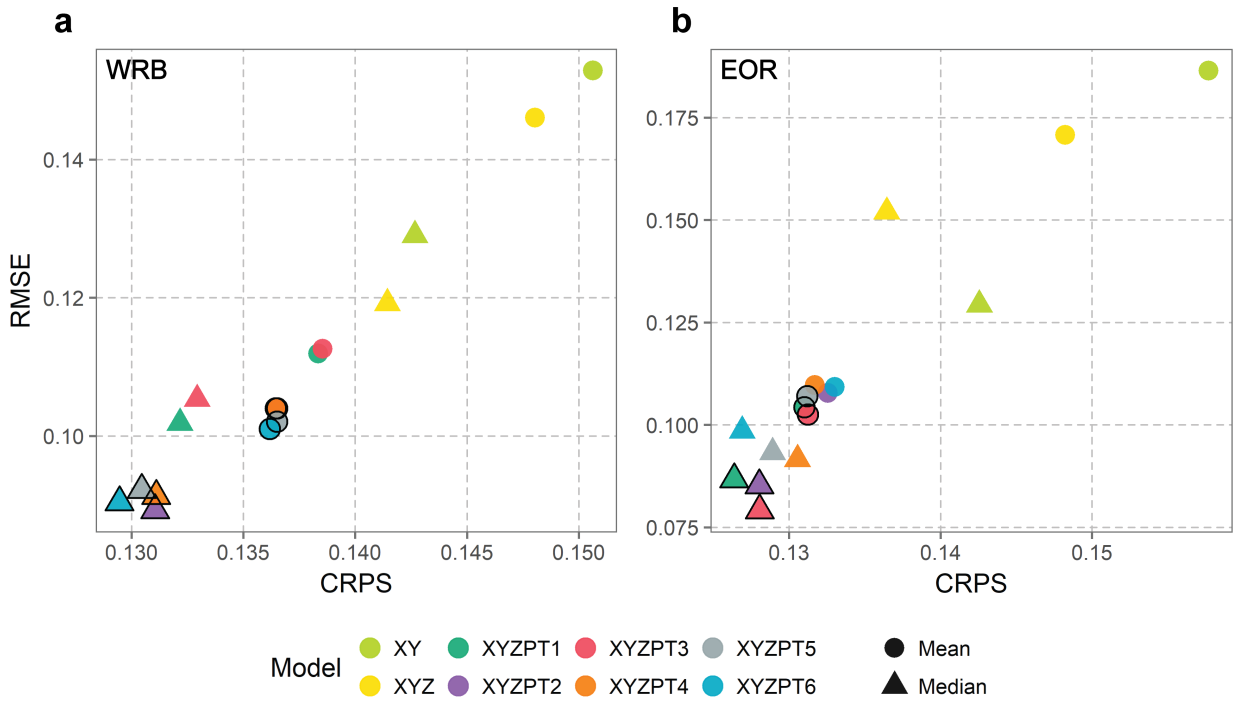

Figure 2.2: Comparison of mean and median CRPS and RMSE for a) the WRB region and b) the EOR region. The top performing 3 or 4 models are closely clustered where one may perform better with respect to CRPS, while another may have a slightly better RMSE. The top performing models across both mean and median results in a) are XYZPT2, XYZPT4, XYZPT5, and XYZPT6, while the top performing in b) are XYZPT1 and XYZPT3.

wet-season P, T, and T_d as covariates (model XYZPT2); while the simplest for the EOR contains location, elevation and mean annual P (model XYZPT1).

We also performed a spatial GEV analysis for each model to assess model fit, which is commonly used to fine-tune covariate selection when cross validation and/or BMA are not used. The GLM for each parameter contained the full set of covariates for each model. The Takeuchi information criterion (TIC)[Takeuchi, 1976] for each model was assessed relative to model complexity (Figure 2.3). The results confirm our selection of best model, and that the inclusion of climatic covariates greatly improves model fit. For the WRB, model XYZPT2 has a lower TIC relative to XYZPT1 and XYZPT3. For the EOR region, model XYZPT1 has a lower TIC relative to XYZPT2 and is close to the TIC result for the more complex XYZPT3. While XYZPT6 has the lowest TIC, we chose not to use it to avoid overfitting.

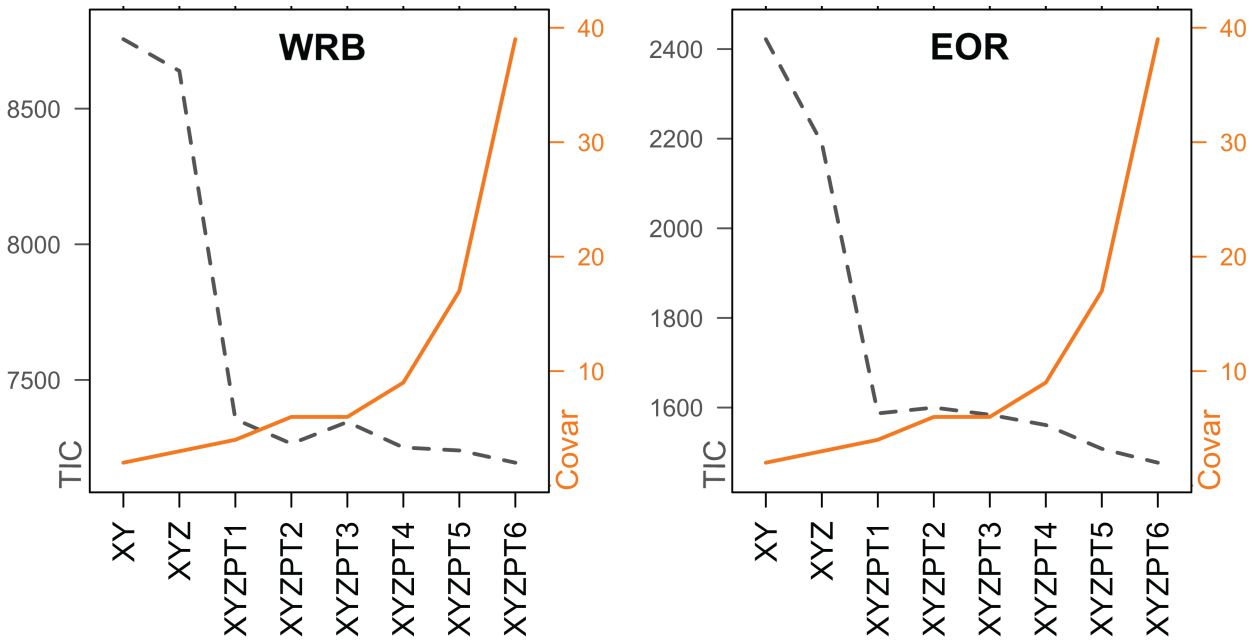

Figure 2.3: Spatial GEV model fit for both regions. Grey dashed line represents TIC, while the solid orange line represents the number of model covariates.

2.4.2 Posterior Inclusion Probability by Region

As noted previously, the methodology used here includes a BMA functionality that provides an estimate of the posterior inclusion probability (PIP) for the linear terms of each GEV parameter. While most model covariates have a non-negligible PIP, mean wet-season precipitation (November-March) has the greatest influence on the location parameter, μ, of the GEV distribution for both regions (Figure 2.4). Longitude (x), latitude (y), and elevation (z) have slightly greater μ PIP for the WRB models than for the EOR models, which could be due to the greater variability in elevation and mean precipitation across the relatively small WRB region.

Precipitation and longitude have the largest PIP for the inverse-scale parameter, κ, across the simpler models for both regions (Figure 2.4), with longitude appearing to be more important for the EOR models relative to the WRB models. Mean daily temperature (T) has a slightly higher κ PIP in the WRB models, relative to EOR, with wet-season T receiving a higher κ

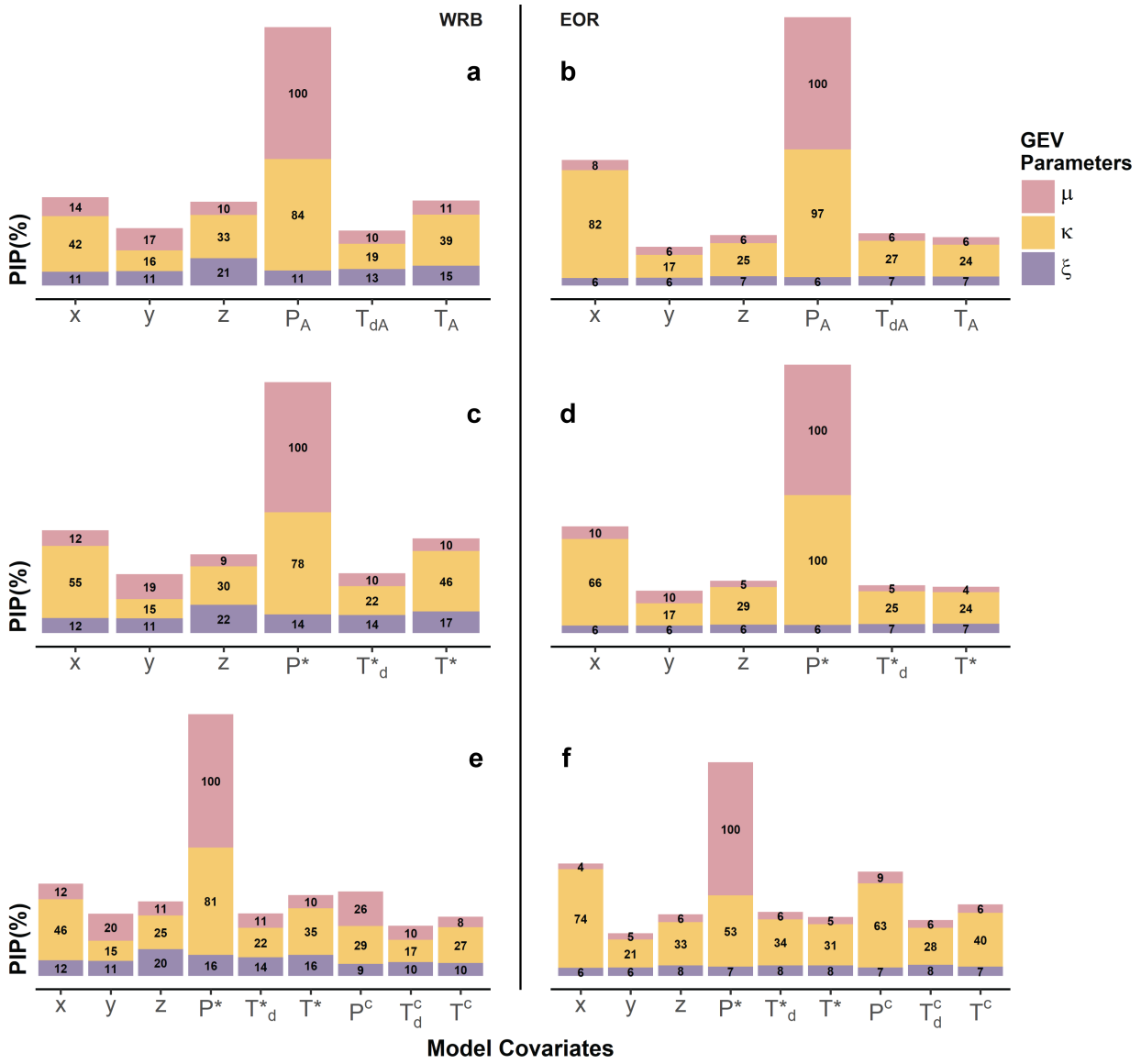

Figure 2.4: Posterior inclusion probability for the GEV location, inverse scale, and shape parameters (μ, κ, ξ) for the three simpler models. Model XYZPT3 for a) the WRB and b) EOR, model XYZPT2 for c) the WRB and d) EOR, and model XYZPT4 for e) the WRB and f) EOR. For all models and regions, the uppermost color (pink) represents μ, the middle color (orange) displays the results for κ, and the bottommost color (purple) shows the results for ξ.

PIP than dry-season T. The climatic difference between the regions can also be seen when P is separated into wet- and dry-seasons (Figure 2.4e, 2.4f), with the WRB showing a greater κ PIP for wet-season P and the EOR displaying similar PIPs for both seasons (dry-season P displaying a slightly higher κ PIP). The κ PIP results nicely echo the AM climatology of both regions, with precipitation in the WRB being driven by large synoptic systems originating from the Pacific during winter months, while precipitation in the EOR is generally driven by convective systems resulting in short duration, high intensity events in the early summer. Latitude consistently has one of the lowest κ PIP across models and regions.

For the WRB, elevation (z) appears to have the most influence on the shape parameter, ξ, of the simpler models (Figure 2.4a, 2.4c, 2.4e). However, this is not the case for the simpler EOR models where ξ does not depend on any single covariate for the region's top performing models (XYZPT1, and XYZPT3 shown in Figure 2.4b); it is only seen with model XYZPT6 (Figure 2.5b), which did not perform as well within the EOR region.

In the more complex models, XYZPT5 and XYZPT6, PIP results mostly reflect those of the simpler models, although in finer detail given that the covariates are on a monthly scale (Figure 2.5). Again, XYZPT5 and XYZPT6 where both among the top preforming stations for the WRB region, however, they were not among the top performing for the EOR region. In the WRB model XYZPT5 (Figure 2.5a), February precipitation (P_2) dominates μ PIP; while for the EOR XYZPT5, January and November precipitation (P_1 and P_{11}) dominate μ PIP (Figure 2.5b). For the WRB XYZPT6 (Figure 2.5c), February μ PIP remains the highest with December, January, and March μ PIP following close behind. For the EOR XYZPT6 (Figure 2.5d), January and November precipitation still stand out with the highest μ PIP.

Within these more complex models, the κ PIP results again reflect the differences in each region's primary storm mechanism. For both XYZPT5 and XYZPT6 in the WRB region, January precipitation is among the covariates with the highest κ PIP. In the WRB XYZPT6

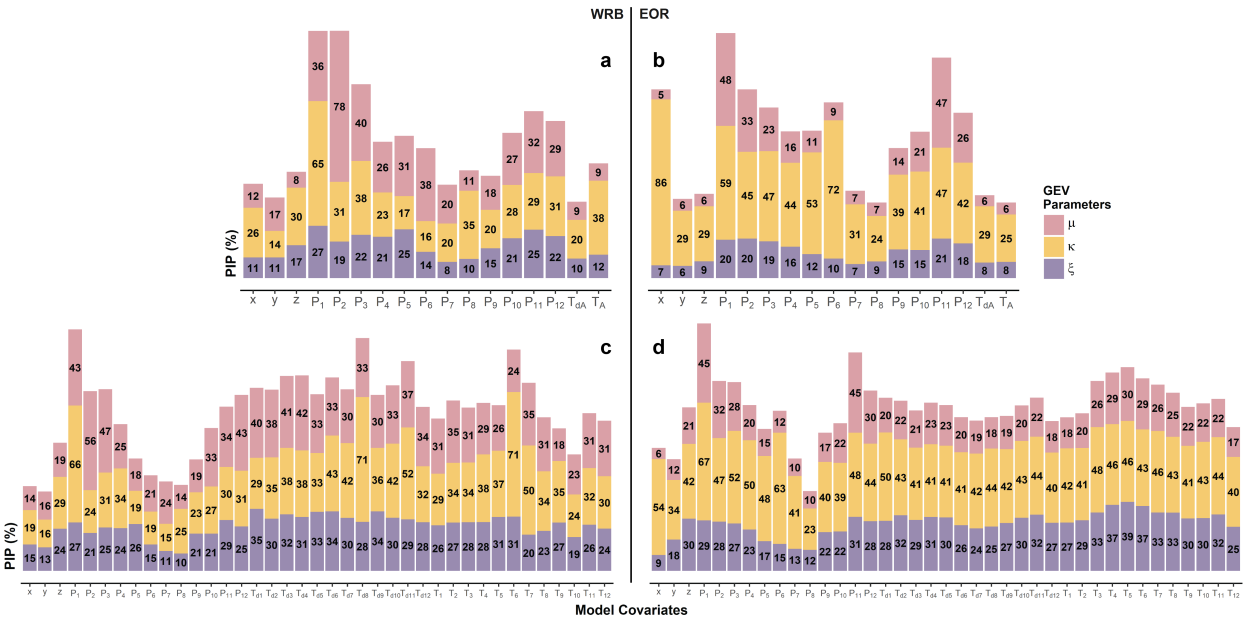

Figure 2.5: Posterior inclusion probability for the GEV parameters (μ, κ, ξ) for the two most complex models. Model XYZPT5 for a) the WRB and b) EOR, and model XYZPT6 for c) the WRB and d) EOR. For both models and regions, the uppermost color (pink) represents μ, the middle color (orange) displays the results for κ, and the bottommost color (purple) shows the results for ξ.

model, August dewpoint temperature ($T_{d,8}$) and June mean daily temperature (T_6) have the highest κ PIP, exceeding that of the January precipitation. In the EOR XYZPT5 model (Figure 2.5b), longitude and June precipitation have the highest κ PIP; while for the EOR XYZPT6 model (Figure 2.5d), January and June precipitation standout with the highest κ PIP. Latitude has one of the lowest κ PIP for both WRB models in Figure 2.5, which reflects the κ PIP results of the simpler WRB models in Figure 2.4. Both EOR models display a relatively higher κ PIP for latitude compared with the models in Figure 2.4.

Most noticeable of all, is the difference in the ξ PIP of the more complex models in comparison with those of the simpler models. While the simpler models had negligible to near-negligible ξ PIP, these more complex models display higher ξ PIP with more variability across covariates. For model XYZPT5 (Figure 2.5a, 2.5b), it generally appears that precipitation of wet-season months tends to have a higher ξ PIP for both regions; the exception to this being the May precipitation ξ PIP of the WRB XYZPT5 model. Model XYZPT6 (Figure 2.5c, 2.5d) mirrors

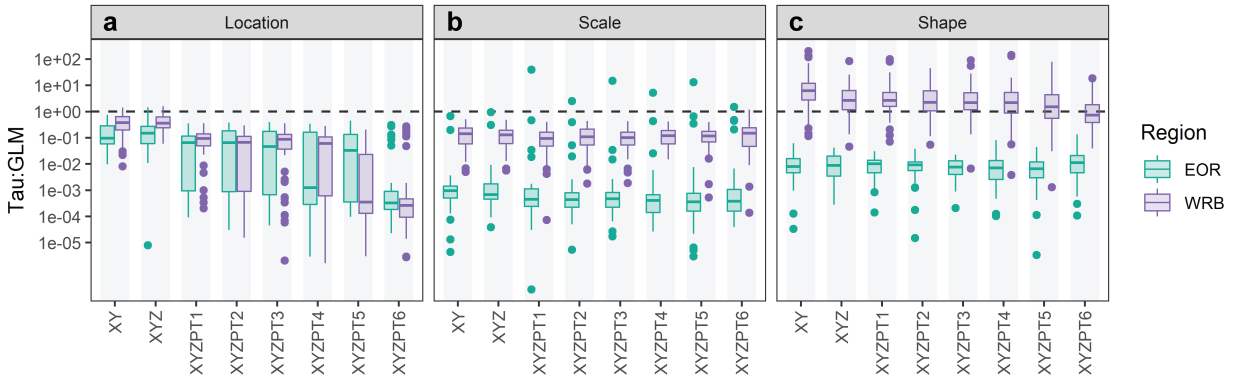

Figure 2.6: The contribution of the spatial random effects term relative to the general linear model (GLM) term for each GEV parameter and model. The dashed horizontal line is placed at one, representing a 1:1 ratio of the spatial random effects term to GLM.

the ξ PIP results for monthly P seen in XYZPT5 for the WRB region and has the same distribution but with higher PIPs for the EOR region. The EOR XYZPT6 model (Figure 2.5d), unlike the better performing EOR models, has a relatively high ξ PIP for elevation, T_d, and T.

The contribution of the spatial random effects (τ) term relative to the general linear model (GLM) component of each GEV parameter (Figure 2.6), when used in combination with PIP results, can provide additional insight into relevant model covariates. While the inclusion of climatic covariates decreases the τ term contribution for the location parameter of both regions, the inclusion of monthly T and T_d further greatly reduces τ across the majority of sites. This is demonstrated by the sizeable decrease in τ seen for model XYZPT6 relative to the other models (Figure 2.6a). For the WRB, comparison of models XYZPT5 and XYZPT6 reveals that winter and fall monthly P along with monthly T and T_d reduces the τ term contribution more than winter P only. For the EOR region, the inclusion of winter monthly P, monthly T and T_d, and elevation reduce the contribution of τ more than winter monthly P alone.

For the scale parameter (Figure 2.6b), most sites in the EOR region have a smaller τ term than sites in the WRB, with the exception of a few EOR outliers where the τ term is similar

in contribution or larger (southwestern-most site near Crater Lake) than the GLM term. Although the WRB sites have a higher contribution from the τ term relative to EOR, none of the sites have a τ term that contributes more than the GLM term. There is a slight reduction in the τ term contribution with the inclusion of climatic covariates for the scale parameter, but the change is less noticeable relative to the results for the location parameter. The inclusion of the monthly T and T_d of model XYZPT6 appears to increase some of the τ term contributions for the WRB. The main differences, when comparing PIPs for models XYZPT5 and XYZPT6 (Figure 2.5a, 2.5c), are a higher PIP for T_A relative to $T_{d,A}$ seen for the XYZPT5 model that is not seen for XYZPT6. Additionally, model XYZPT6 gave the highest PIPs to August T_d and June T, even higher than January P that had a relatively high PIP in both models. For the EOR, the τ term contributions of both models XYZPT5 and XYZPT6 are very similar with the exception of the outliers (Figure 2.6b). The τ term contribution of the EOR region's largest outlier's decreases by an order of magnitude with the inclusion of monthly T and T_d. The main differences, besides T and T_d, between the two models in PIP for the EOR region is the reduced PIP of longitude and the increased PIP of elevation for model XYZPT6 relative to XYZPT5 (Figure 2.5b, 2.5d).

The τ term contribution to the shape parameter for the EOR sites is much lower than that of the WRB sites (Figure 2.6c). For the majority of the WRB sites, the contribution of the τ term exceeds that of the GLM term, in some cases by a large proportion (y-axis in log scale). This could indicate that there are additional covariates not included in this study that influence the shape of the GEV distribution within the WRB. The main difference in shape parameter PIP results between model XYZPT6 and the other models, for both regions, is the large increase in the contribution of T and T_d. The XYZPT6 model had the lowest τ contribution of all the models for the WRB with a median contribution less than 1:1, indicating that including monthly T and T_d was beneficial. However, in the EOR region, the XYZPT6 model has a greater median τ term contribution to the shape parameter relative to all other models. This is the only potential indication of a term contribution link with

the EOR predictive performance results where XYZPT6 was among the worst models.

2.4.3 Model Performance at Stations within Region of Overlap

For the locations east of the Cascade Range, which were included in both regions (hereafter referred to as 'overlapping stations'), the AM temporal distribution of each station appears to correspond well with which region's models performed best at that location (Figure 2.7). This could be due to the different storm climatology; in the WRB winter storms dominate and most AM events occur during November-February, while in the EOR early summer (May-June) thunderstorms are also prominent. The WRB models performed better than the EOR models at stations 31 and 47 (Figure 2.7a-2.7b, also station 30 in Figure 2.13), which have more AM events occurring between December and January and resemble the AM temporal distribution for the pooled WRB data (Figure 2.1a). The EOR model performed better at stations 54 and 55 (Figure 2.7c-2.7d, also station 33 in Figure 2.13), which also have a relatively large number of AM falling between May and June (in addition to the expected winter storms of the Pacific Northwest region) and correspond with the AM temporal distribution for the pooled EOR data (Figure 2.1b). These results suggest that accounting for the dominate storm mechanisms that influence the AM temporal distribution within the pooled station data of the model may improve predictive performance.

Since dominant storm climatology appears to influence model performance among the overlapping stations, we also checked relative model performance at stations that were not included within the overlapping stations (Figure 2.8). Stations within each region were categorized as "WRB-like AM" if their January and December AM count was greater than their May and June AM count, and "EOR-like AM" if their May and June AM count was greater than or equal to their January and December AM count (Figures 2.15-2.16). Our results indicate that the median RMSE across EOR-like AM stations is lower (better median perfor-

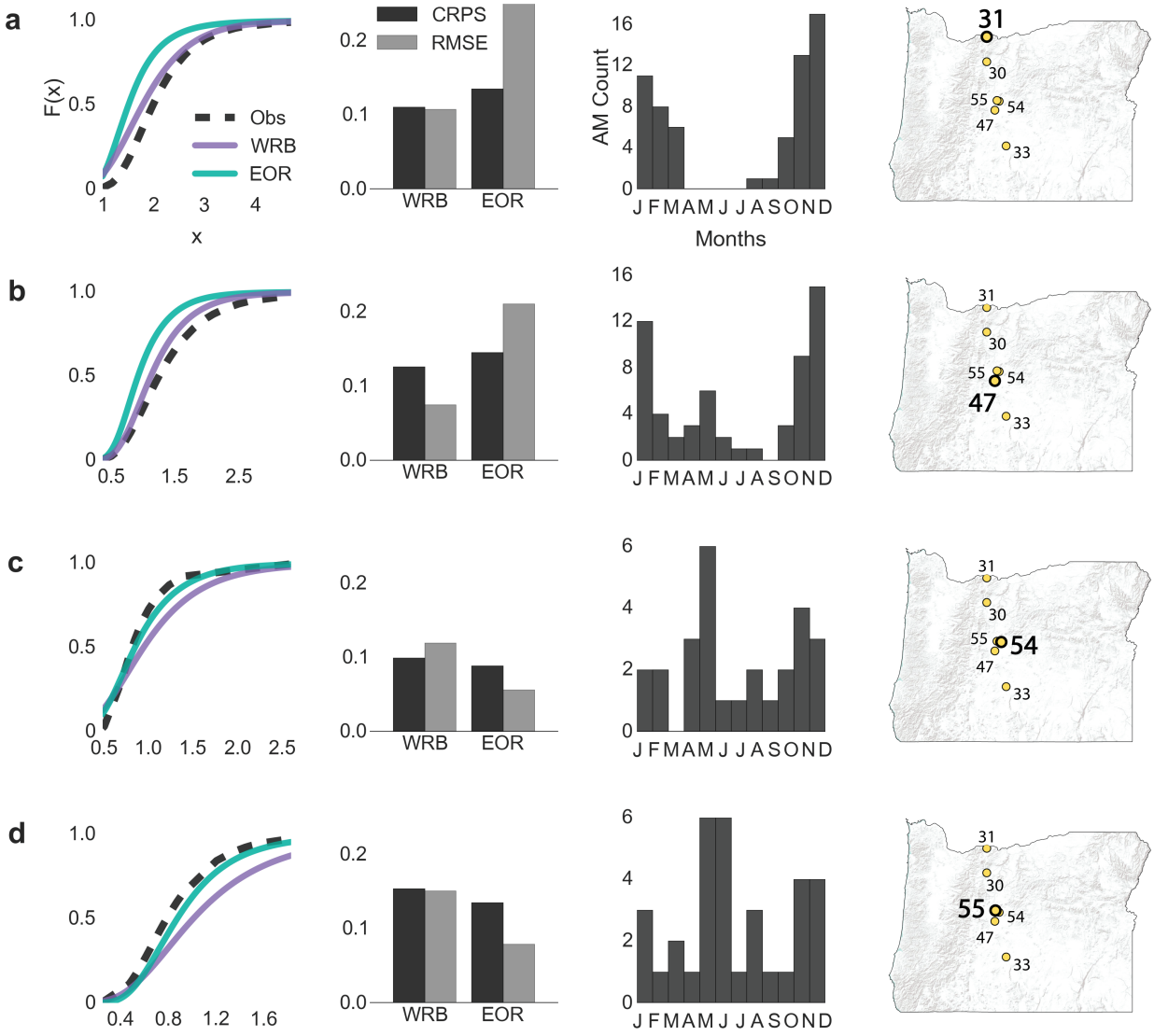

Figure 2.7: Comparison of the best model results at the overlapping stations. Each row of plots represents a single station, where row a) is station 31, row b) station 47, row c) station 54, and row c) station 55, as indicated by the map insets. Each includes, from left to right, the CDF of predicted versus observed annual maxima GEV distributions, CRPS and RMSE of each region's model, the location's AM climatology, and the location's spatial placement within the study region.

mance) than the median RMSE across WRB-like AM stations within the EOR region (Figure 2.8e). However, the CRPS results are not as conclusive (Figure 2.7a), which could be due to a bias in CRPS (Figures 2.17-2.18) introduced by normalizing by length of record. We were unable to duplicate this comparison within the WRB region since all the non-overlapping stations have WRB-like AM distributions (Figures 2.8c, 2.8g). Looking at the difference in performance between the EOR XYZPT2 model (best set of covariates for the WRB) and the EOR XYZPT1 model (best set of covariates for EOR) (Figure 2.12), we see that using the EOR model that makes use of the same set of covariates that worked best in the WRB region is not sufficient on its own to improve performance for the EOR locations which have a WRB-like AM temporal distribution. The predominance of region-based performance can also be seen when the CDF results of all climatic models (XYZPT1-XYZPT6) for both regions at the overlapping stations are plotted together (Figure 2.14), showing how the WRB models group together and are clearly different from the EOR model results despite using the same sets of covariates. Additional analysis of the relationship between spatial performance and covariate values was conducted (Figures 2.17-2.18), as well as a comparison of the contribution of the spatial random effects term of the best models at the overlapping sites (Figure 2.19); see Appendix A for more detail.

2.5 Conclusions

A limitation of existing precipitation frequency analysis methods is that integrating information on extremes across space (i.e., different observations) is not straightforward. Here, we addressed this through the application of a Bayesian hierarchical model (BHM) framework for the spatial analysis of 24-hour precipitation annual maxima (AM) data. The spatial BHM framework utilized in this study includes Bayesian model averaging (BMA) to account for model uncertainty related to the covariates employed, and also allows for analysis of co-

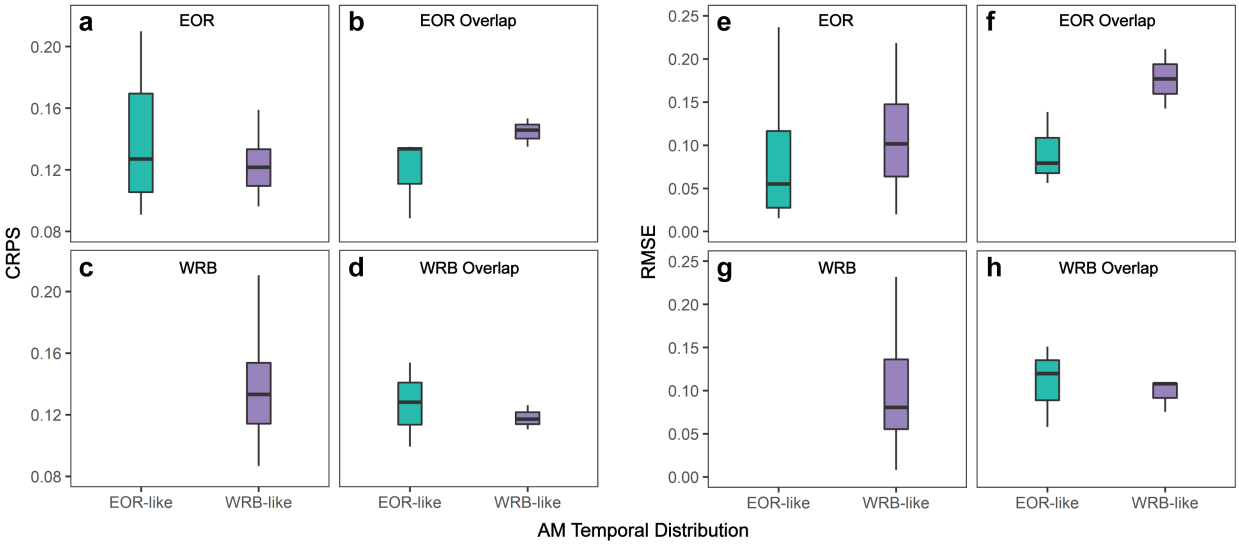

Figure 2.8: Comparison of station specific CRPS (a-d) and RMSE (e-h) versus AM temporal distribution by region. EOR (a and e) and WRB (c and g) display the quantiles of station-specific model performance when stations (excluding overlapping stations) are categorized by EOR-like or WRB-like AM temporal distributions. EOR Overlap (b and f) and WRB Overlap (d and h) display the same performance versus categorization for the overlapping stations only, using the EOR and WRB models' results, respectively.

variate posterior inclusion probability (PIP). To gain further insight into relevant covariates, we analyzed the contribution of the spatial random effects (τ) term to the linear models of the generalized extreme value (GEV) distribution parameters in combination with the PIP results. We explored a wide range of models using physically-based information pertaining to geographical and climatological factors that influence precipitation extremes across two regions in Oregon with different dominating rainfall generation mechanisms, and a region of overlap.

The top performing models for each region were determined by comparing mean and median model predictive performance of the LOO-CV results, wherein we compared site-specific predicted versus observed GEV distributions using continuous ranked probability score (CRPS) and root mean squared error (RMSE). Out of the top performing models for each region, one was chosen as the best model based on both performance metrics and model simplicity. Our choice of best model was also checked against a spatial GEV fit of the models. The

best model for the Willamette River Basin (WRB) included location, elevation, and mean wet-season precipitation, daily mean temperature, and dewpoint temperature; while the best model for the eastern Oregon (EOR) region included location, elevation, and mean annual precipitation. The improvement in model predictive performance with the inclusion of mean temperature and dewpoint temperature for the WRB is understandable given the variability in climate and topography of the WRB over a much smaller area relative to EOR, in addition to its proximity to the Pacific Ocean.

Including BMA may improve results over non-BMA models as demonstrated by Dyrrdal et al. [Dyrrdal et al., 2014], however we found that careful model selection remains an important component of tuning model performance. For example, the most complex model (XYZPT6) containing geographic and monthly climatic information (precipitation, P; dewpoint temperature, T_d; and mean daily temperature, T) was among the top performing models for the WRB region, while it performed among the worst in the EOR region despite the use of BMA. However, useful information can be gleaned from the posterior inclusion probability (PIP) results provided through BMA. Across the simpler models, mean wet-season P displayed the highest PIP for μ (GEV location parameter) within both the WRB and EOR. The κ (GEV inverse scale parameter) PIPs reflect the regional differences in storm climatology of the pooled data, with wet-season P and T, and longitude displaying higher κ PIP for the WRB region, and wet-season P, longitude, and dry-season P displaying higher κ PIP for the EOR region. Additionally, wet-season T stands out within the WRB κ PIP results, more so than dewpoint temperature. Elevation has a higher PIP for ξ (GEV shape parameter) within the WRB models, however, apart from model XYZPT6, this was not the case for the EOR models. PIP results of the more complex models generally reflect those of the simpler models, just in higher resolution and with higher ξ PIP across the climatic covariates for both regions. Additionally, the most complex model (XYZPT6) had the lowest overall τ term contribution relative to the general linear model (GLM) term for the GEV location parameter for both regions, indicating that the inclusion of monthly T and T_d information

improved location parameter estimates. However, inclusion of monthly T and T_d resulted in an increased contribution of the τ term for the scale parameter in both regions. For the shape parameter, inclusion of monthly T and T_d information reduced the median τ term contribution for the WRB, while it increased the τ term contribution for the EOR region.

Results from the overlapping stations indicate that the AM temporal distribution within the pooled calibration data may improve model predictive performance for locations with a similar AM temporal distribution, even more so than specific covariate selection. Although the stations in the region of overlap are well outside of the geographical WRB, the WRB model had better skill at the stations that have a similar AM temporal distribution as those within the WRB. The same can be seen for stations with a similar AM temporal distribution as the EOR region, the EOR model performs better at those stations relative to the WRB model. Most likely, this is linked to the storm climatology of the different regions; wherein the WRB is dominated by winter storms from the Pacific Ocean, while the EOR region experiences thunderstorms during the early warm-season and receives less precipitation during the cold-season than the WRB. Based on these results, we suggest exploring the inclusion of AM temporal distribution within the spatial BHM framework further, possibly through the inclusion of relevant covariates that can differentiate the dominate storm for each site.

2.6 Appendix A

This supporting information provides additional details regarding model predictive performance, region-based results at all overlapping stations, individual station annual maxima (AM) temporal distributions, and Pearson correlation coefficients of performance and station information for both regions.

Table 2.2: WRB Model Performance[a]

	WRB	CRPS			RMSE		
Acronym	Model Covariates	Mean	St.Dev.	Median	Mean	St.Dev.	Median
XY	Longitude, Latitude	0.151	0.048	0.143	0.153	0.101	0.129
XYZ	Lon., Lat., Elevation	0.148	0.046	0.141	0.146	0.097	0.119
XYZPT1	Lon., Lat., Elevation, P_A	0.138	0.038	0.132	0.112	0.072	0.102
XYZPT2	Lon., Lat., Elevation, P^*, T_d^*, T^*	0.137	0.037	0.131	0.104	0.066	0.089
XYZPT3	Lon., Lat., Elevation, P_A, T_{dA}, T_A	0.139	0.039	0.133	0.113	0.073	0.105
XYZPT4	Lon., Lat., Elevation, P^*, T_d^*, T^*, P^c, T_d^c, T^c	0.136	0.037	0.131	0.104	0.064	0.091
XYZPT5	Lon., Lat., Elevation, P_1,..., P_{12}, T_{dA}, T_A	0.137	0.039	0.130	0.102	0.065	0.092
XYZPT6	Lon., Lat., Elevation, P_1,..., P_{12}, T_{d1},..., T_{d12}, T_1,..., T_{12}	0.136	0.037	0.129	0.101	0.065	0.090

[a]Models considered for the WRB listed with each model's mean, standard deviation, and median CRPS and RMSE across stations. Subscripts and superscripts are as follows: $(\,)_A$ = mean annual; $(\,)_1$ = mean January; $(\,)_2$ = mean February; ...; $(\,)_{12}$ = mean December; $(\,)^*$ = mean [November, March], $(\,)^c$ = mean [April, October].

Table 2.3: EOR Model Performance[a]

	EOR	CRPS			RMSE		
Acronym	Model Covariates	Mean	St.Dev.	Median	Mean	St.Dev.	Median
XY	Latitude, Longitude	0.158	0.057	0.143	0.186	0.137	0.129
XYZ	Lat., Lon., Elevation	0.148	0.044	0.136	0.171	0.116	0.152
XYZPT1	Lat., Lon., Elevation, P_A	0.131	0.029	0.126	0.104	0.068	0.087
XYZPT2	Lat., Lon., Elevation, P^*, T_d^*, T^*	0.133	0.032	0.128	0.108	0.069	0.085
XYZPT3	Lat., Lon., Elevation, P_A, T_{dA}, T_A	0.131	0.030	0.128	0.102	0.070	0.079
XYZPT4	Lat., Lon., Elevation, P^*, T_d^*, T^*, P^c, T_d^c, T^c	0.132	0.031	0.131	0.110	0.066	0.092
XYZPT5	Lat., Lon., Elevation, P_1,..., P_{12}, T_{dA}, T_A	0.131	0.030	0.129	0.107	0.062	0.093
XYZPT6	Lat., Lon., Elevation, P_1,..., P_{12}, T_{d1},..., T_{d12}, T_1,..., T_{12}	0.133	0.033	0.127	0.109	0.063	0.099

[a]Models considered for the EOR listed with each model's mean, standard deviation, and median CRPS and RMSE across stations. Subscripts and superscripts are as follows: $(\,)_A$ = mean annual; $(\,)_1$ = mean January; $(\,)_2$ = mean February; ...; $(\,)_{12}$ = mean December; $(\,)^*$ = mean [November, March], $(\,)^c$ = mean [April, October].

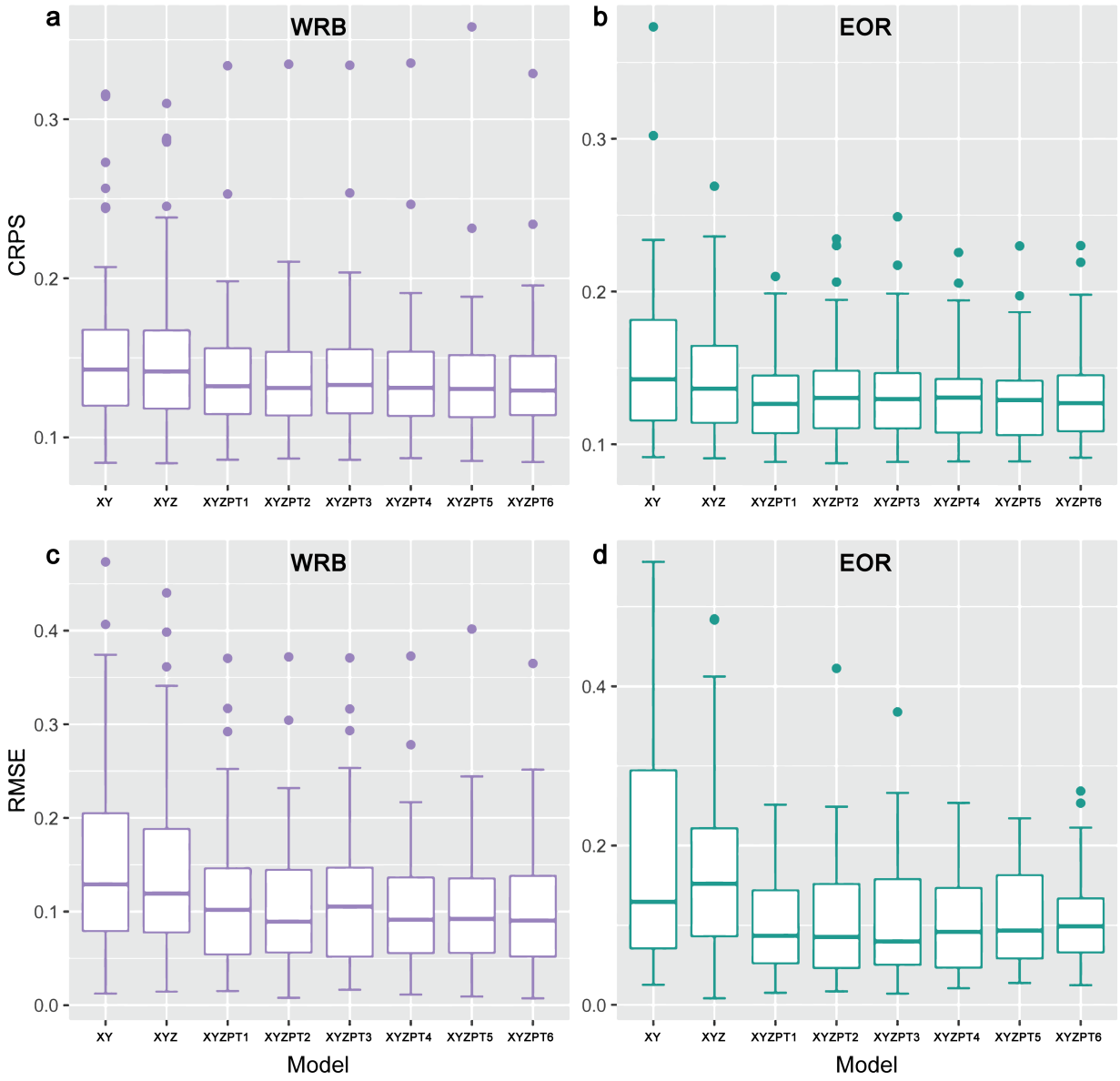

Figure 2.9: Distribution of station performance by model, where models are listed in order (left to right) by increasing complexity.

Table 2.4: Spatial GEV Model Fit

Model	TIC, WRB	TIC, EOR
XY	8756	2422
XYZ	8639	2190
XYZPT1	7355	1587
XYZPT2	7265	1600
XYZPT3	7345	1584
XYZPT4	7251	1561
XYZPT5	7240	1508
XYZPT6	7195	1477

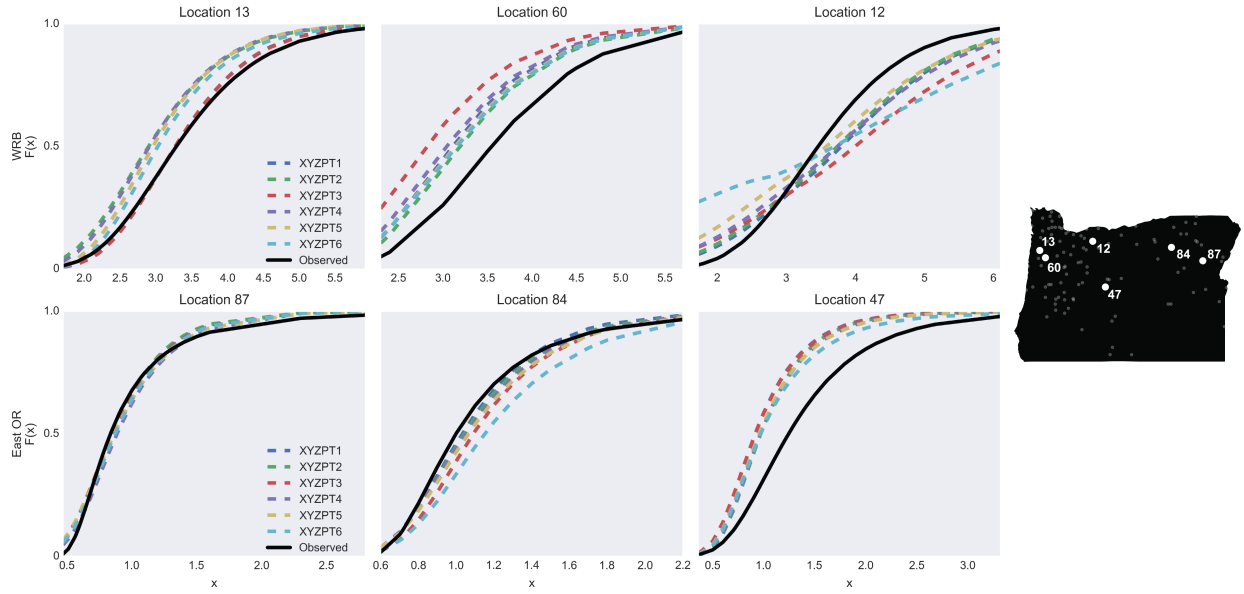

Figure 2.10: Examples of observed versus simulated distributions for the WRB and EOR models which include PRISM-based covariates. These CDFs are included to give examples of stations were predictive performance was good (sites 13, 87), moderate (sites 60, 84), and poor (sites 12, 47).

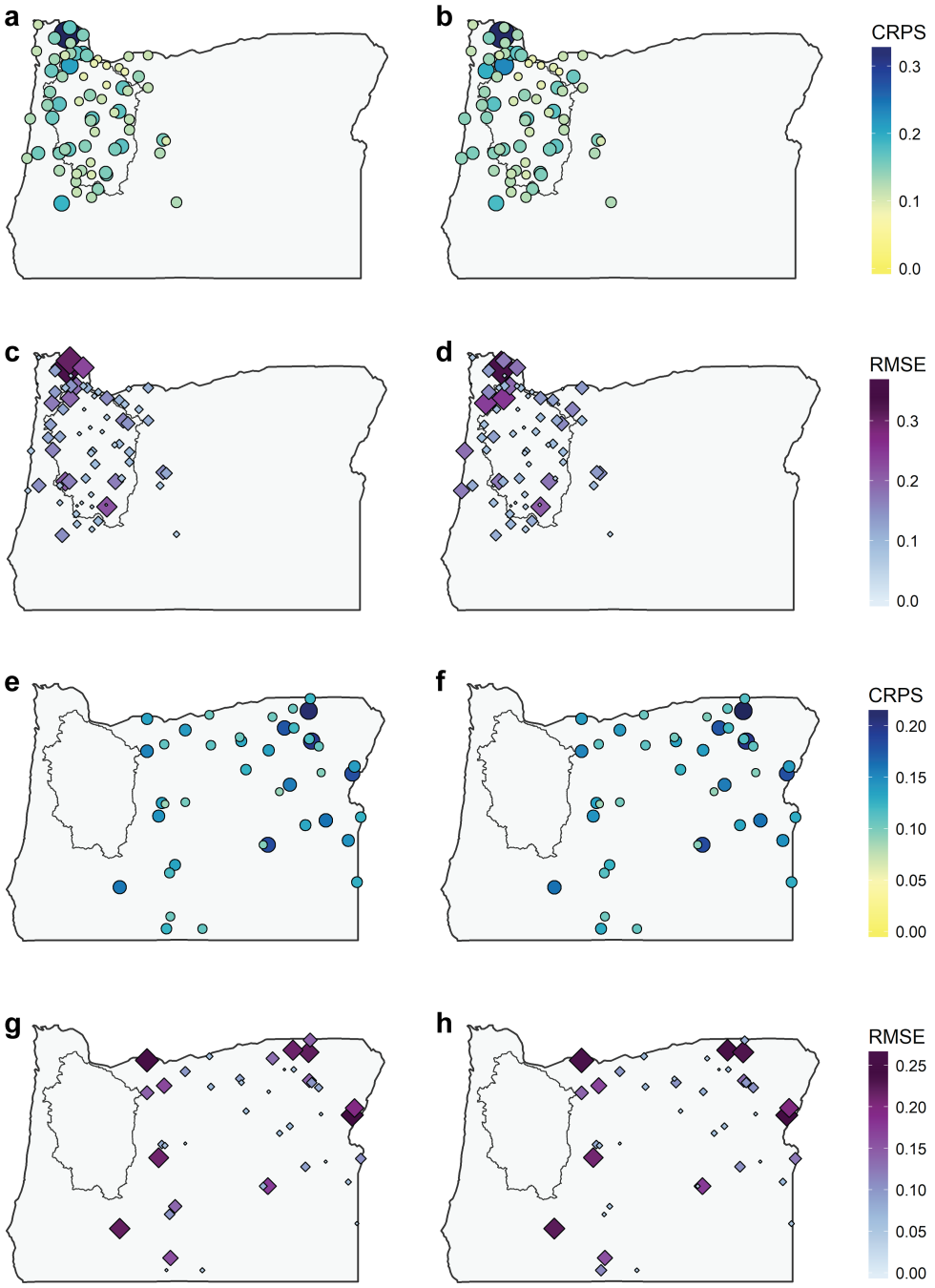

Figure 2.11: Maps of CRPS (circle markers) and RMSE (diamond markers) for the top models for each region (model complexity increases from left to right). The outline in the northwestern part of Oregon delineates the Willamette River watershed. Models displayed for the WRB are the simplest of the top performing XYZPT2 (a, c), and the most complex of the top performing XYZPT6 (b, d). Both top performing models are displayed for EOR; XYZPT1 (e, g) and XYZPT3 (f, h).

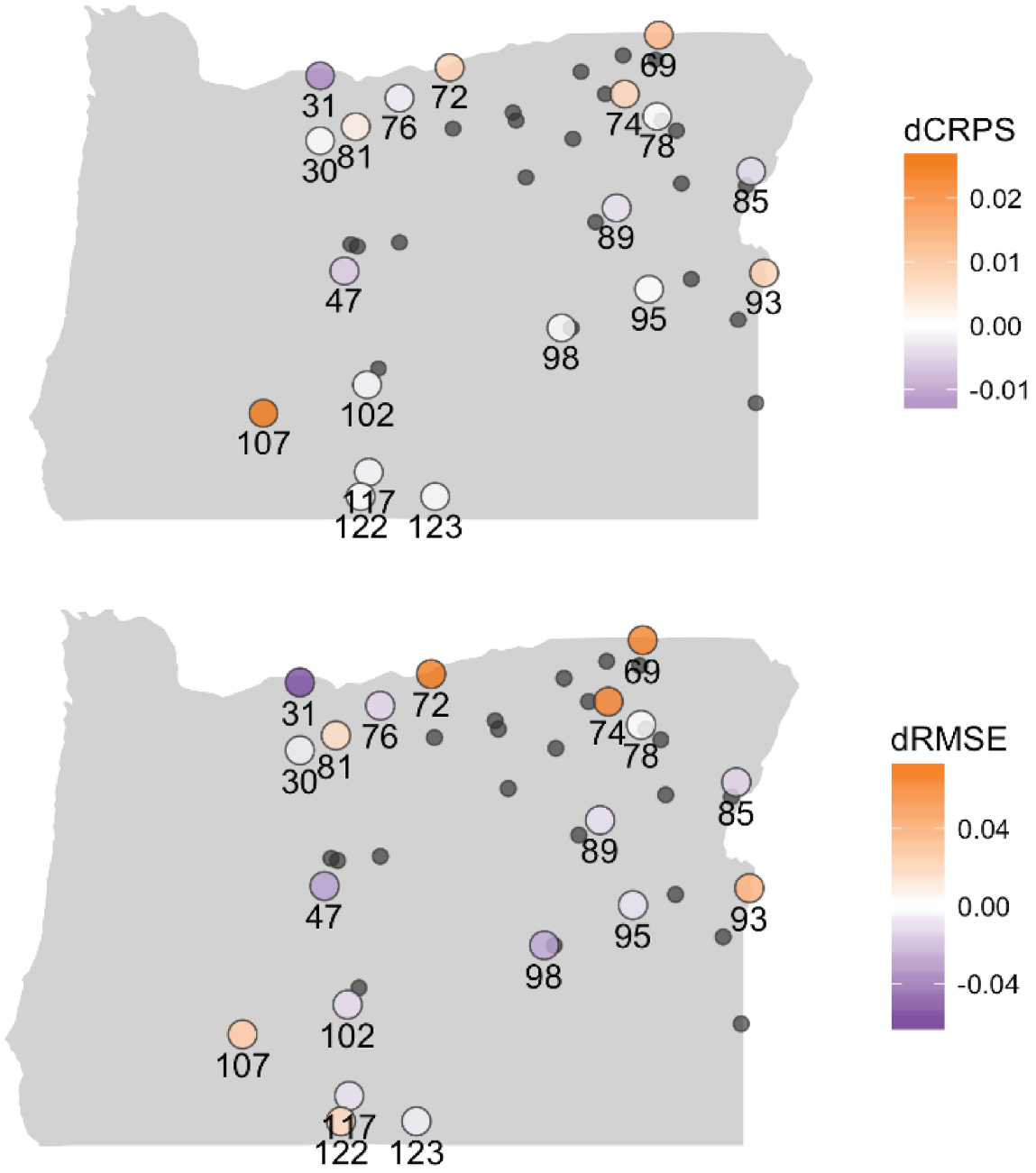

Figure 2.12: The difference in predictive performance between EOR models XYZPT2 and XYZPT1 at the EOR stations which have WRB-like AM. Using the best performing model for the WRB does not guarantee an improvement in performance for all EOR stations that have a WRB-like AM temporal distribution. A few show a slight improvement (purple), while the performance at others worsens (orange). More factors are involved than simply which set of covariates are used.

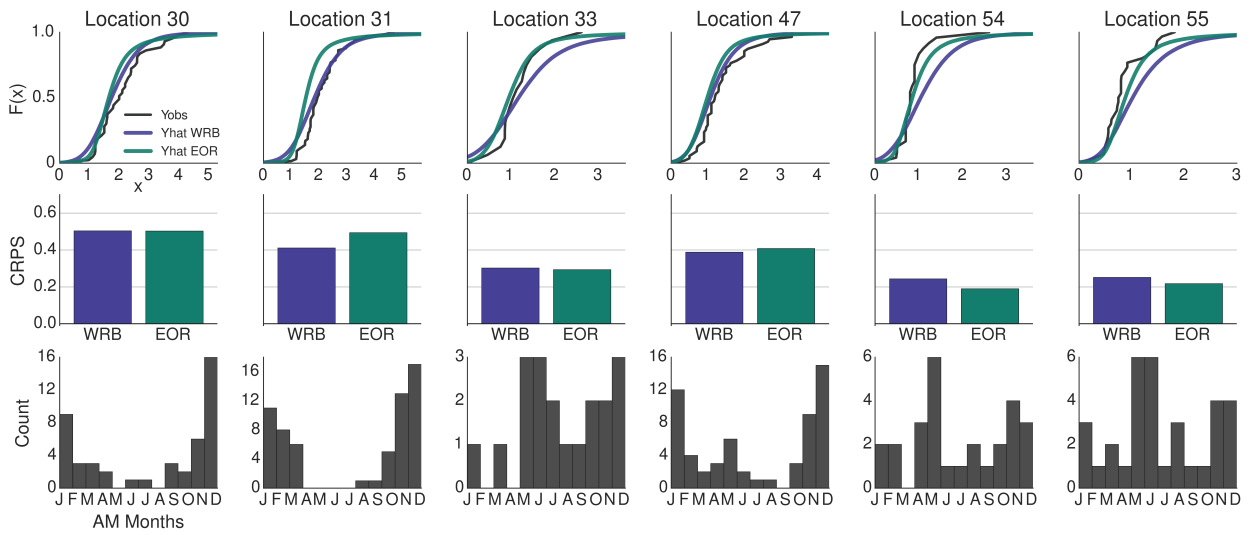

Figure 2.13: Performance at all overlapping stations. Example of how a small (hundredths) change in CRPS has a noticeable difference in CDF. Station 54's EOR result has a CRPS of 0.08 and the simulated CDF is similar to the observed. Whereas, the WRB result has a CRPS of 0.11 and performs poorly relative to the EOR model.

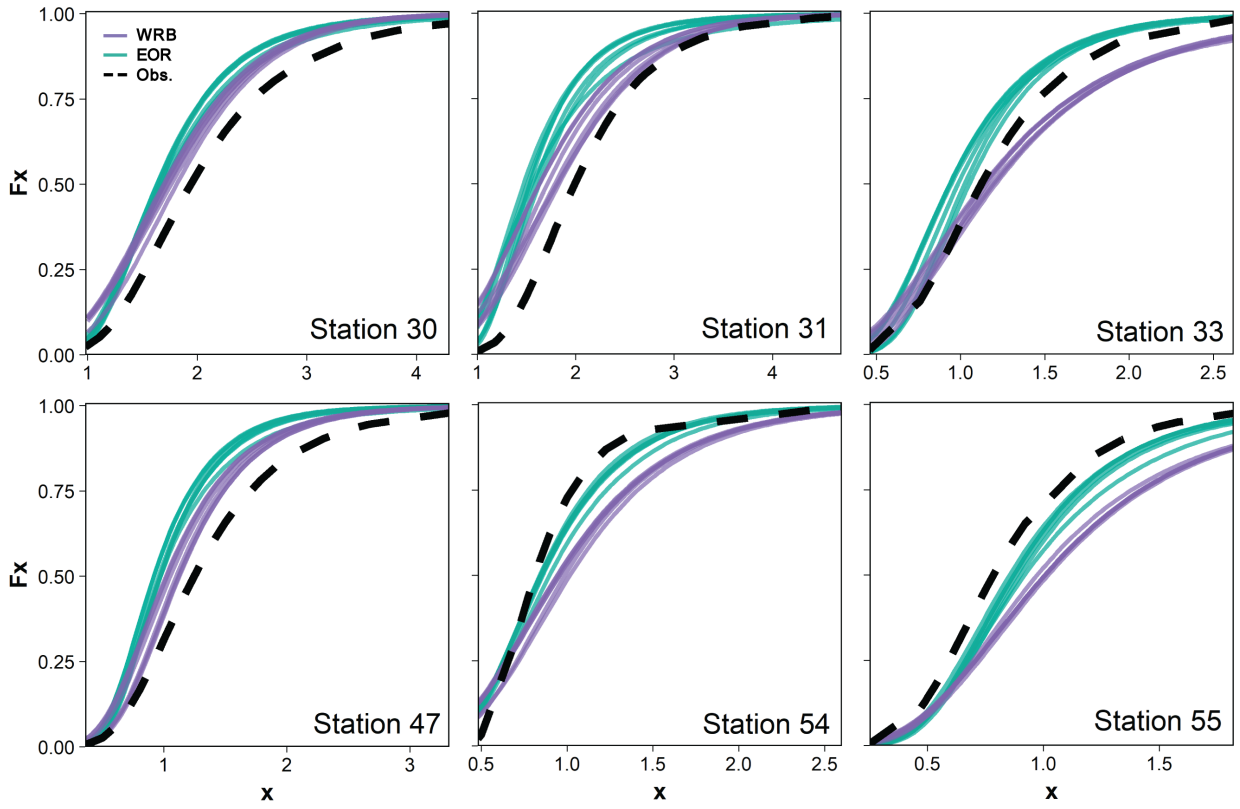

Figure 2.14: CDFs at the overlapping stations for models XYZPT1-XYZPT6 for both the WRB and EOR regions compared with CDF of observed. These models include both geographic and climatic information. The models for each region tend to group together, such that all the models (which include climatic information) from the region that performed best are generally better than those of the other region.

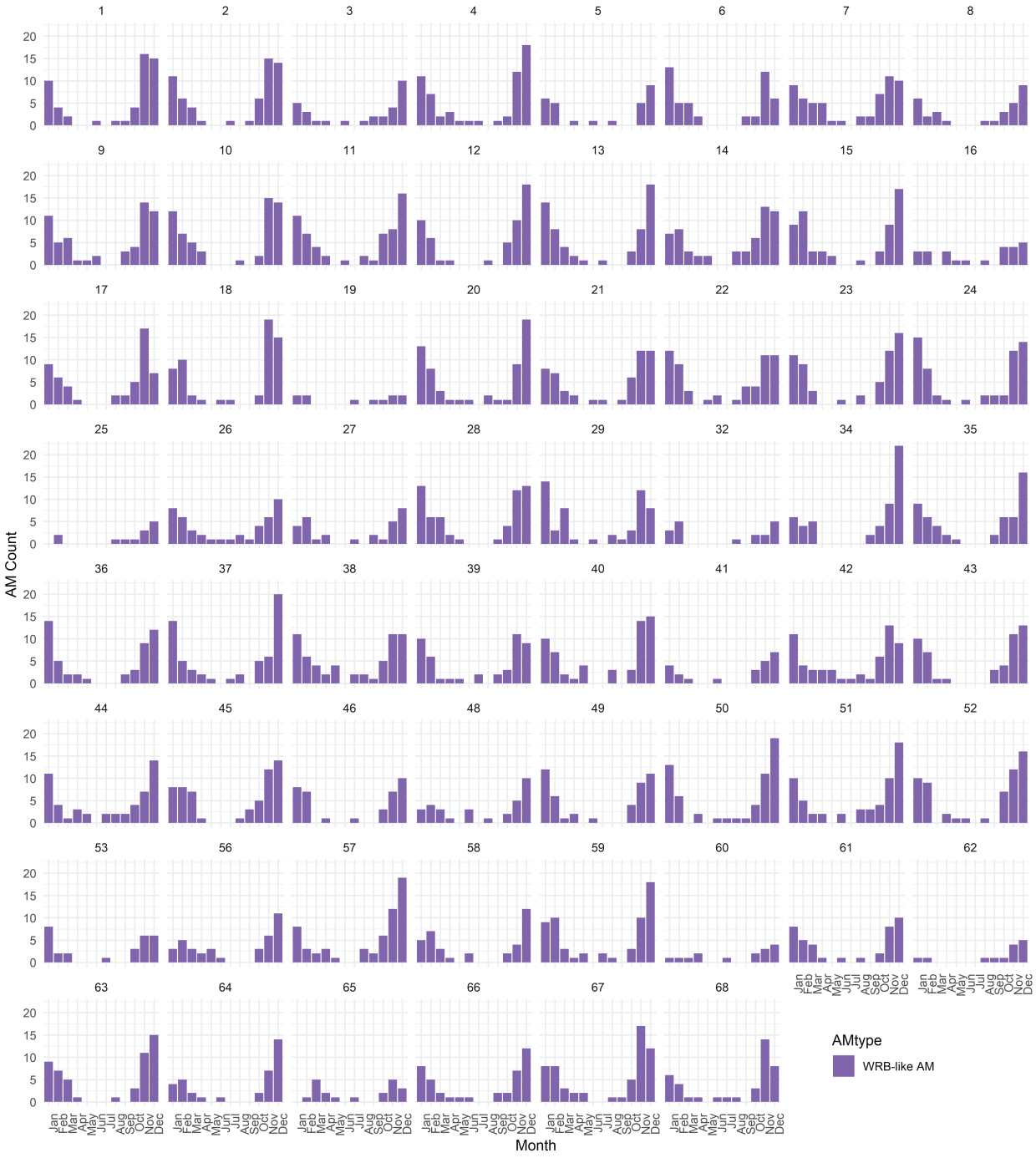

Figure 2.15: AM temporal distribution by station for the WRB study region, excluding the six overlapping stations. Fill color indicates AM type, Fill color indicates AM type, where purple indicate WRB-like AM. None of the non-overlap stations in the WRB have an EOR-like AM.

Figure 2.16: AM temporal distribution by station for the EOR study region, excluding the six overlapping stations. Fill color indicates AM type, where green represents EOR-like AM and purple indicates WRB-like AM.

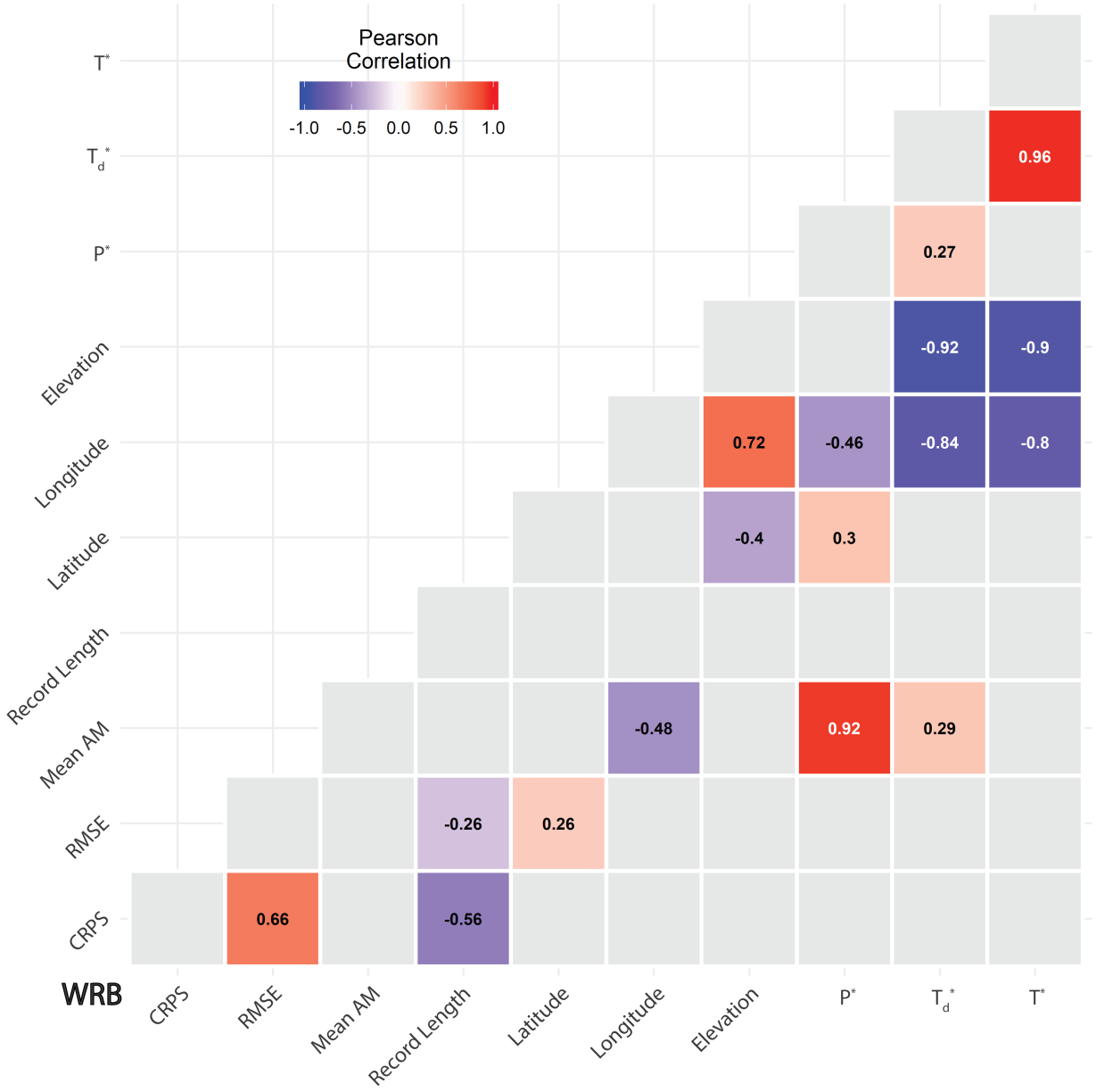

Figure 2.17: Statistically significant ($\alpha = 0.05$) Pearson correlation coefficients for the top WRB model's predictive performance and covariates, as well as mean AM and record length. The moderate negative correlation between CRPS and record length is due to normalizing CRPS by record length. The weak correlation between latitude and RMSE is most likely due to the stations at the northern end of the Coastal Mountains which display poorer model predictive performance across all models. The worst of the aforementioned stations has a relatively short record length and could be the reason for the equally weak negative correlation between RMSE and record length.

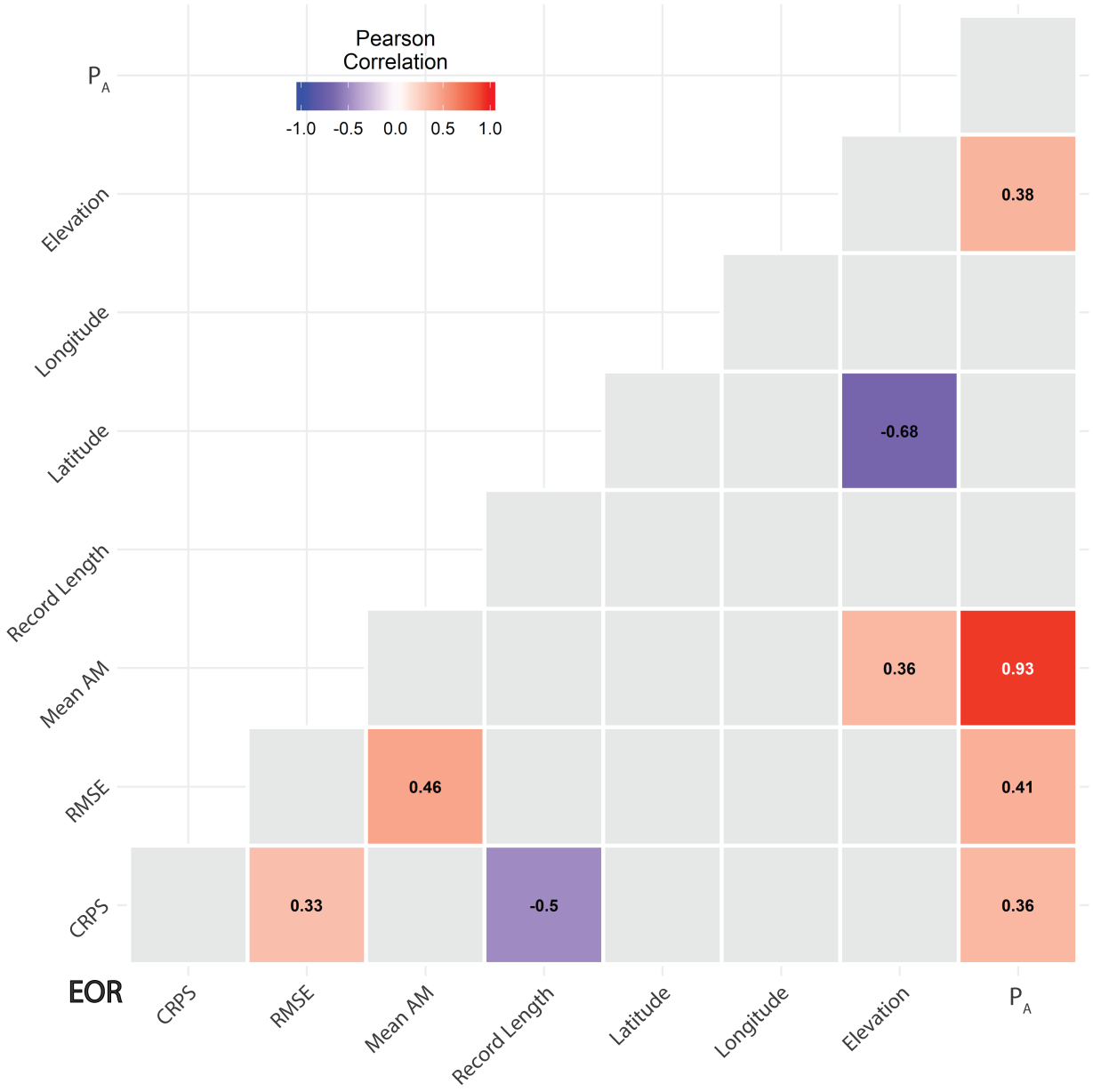

Figure 2.18: Statistically significant ($\alpha = 0.05$) Pearson correlation coefficients for the top EOR model's predictive performance and covariates, as well as mean AM and record length. The moderate negative correlation between CRPS and record length is due to normalizing CRPS by record length. The EOR region covers a large area that includes stations with WRB-like AM, this could be the reason for the weak correlations between performance, mean annual maximum, and annual precipitation.

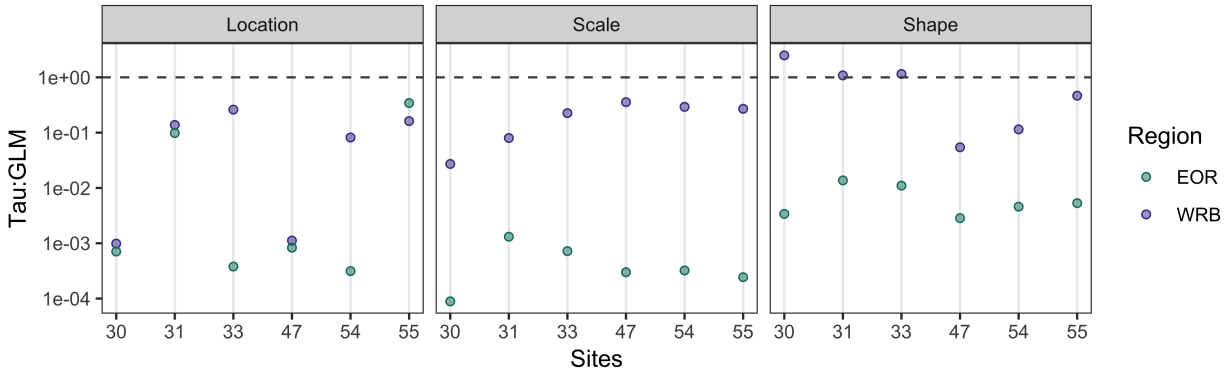

Figure 2.19: The relative contribution of the spatial random effects (τ) term at the overlapping stations for both regions' best models is shown above. There does not appear to be any indication that the contribution of the τ term of the WRB-based model versus the EOR-based model is linked with the difference in site-specific predictive performance.

Chapter 3

An Effective Trend Surface Fitting Framework for Spatial Analysis of Extreme Events

3.1 Introduction

The ability to estimate the magnitude and frequency of extreme events is an essential part of infrastructure planning and hazard mitigation [Gumbel, 1958, Luke et al., 2017, Stedinger and Griffis, 2008]. Given that many extreme climatic events are spatial processes, model development has been focused on addressing the challenge of integrating spatial information within extreme value analysis methods [Cooley, 2009, Davison et al., 2012].

Regional Frequency Analysis (RFA) methods are the industry standard for estimating the intensity, duration, and frequency of extreme events. RFA methods rely on geographic and climatological factors to assist in the delineation of subregions wherein the parameters of the underlying marginal distribution can be assumed to be acceptably homogeneous [Coles,

2001]. However, marginal parameters are often spatially heterogenous. Therefore, Latent Variable Models (LVM) (e.g., Bayesian Hierarchical Models) and Max-Stable Process (MSP) approaches have been developed that allow for the integration of geographical and climatic covariates within trend surfaces for distributing extremal model parameters in space [Cooley et al., 2007, Renard, 2011, Banerjee et al., 2014, Davison et al., 2012, Ribatet et al., 2012, Wikle et al., 1998].

A common challenge with utilizing these methods for spatial extreme value analysis is identifying the optimal set of spatial covariates [Blanchet and Davison, 2011, Davison et al., 2012, Ribatet, 2017]. Poor trend surface characterizations can complicate the dependence parameterization since these models often make use of a log-likelihood formulation [Blanchet and Davison, 2011, Ribatet, 2017]. For example, when working with a max-stable process model that uses a pairwise log-likelihood, there are 2^n possible models that involve subsets of n predictors [James et al., 2013]. If $n = 10/100$, then there are $1,024/1.267651e^{30}$ possible models to be considered for a single marginal parameter trend surface. Therefore, we introduce the addition of elastic-net regression during trend surface development to automate covariate selection and to reduce the computation time needed for the log-likelihood stage of spatial model development. While the methods in this study focus on using the generalized extreme value (GEV) family of distributions based on a block maxima approach, these improvements to trend surface modeling can be applied to models that utilize other distributions.

3.2 Methods

The linear trend surfaces used within the latent variable and max-stable process approaches are commonly of the form

$$\begin{aligned}
\mu(\mathbf{cov}_\mu) &= \eta_{\mu,0} + \eta_{\mu,1} cov_{\mu,1} + ... + \eta_{\mu,n_\mu} cov_{\mu,n_\mu} \\
\sigma(\mathbf{cov}_\sigma) &= \eta_{\sigma,0} + \eta_{\sigma,1} cov_{\sigma,1} + ... + \eta_{\sigma,n_\sigma} cov_{\sigma,n_\sigma} \\
\xi(\mathbf{cov}_\xi) &= \eta_{\xi,0} + \eta_{\xi,1} cov_{\xi,1} + ... + \eta_{\xi,n_\xi} cov_{\xi,n_\xi}
\end{aligned} \tag{3.1}$$

where $\eta_{\cdot,i}$, $cov_{\cdot,i}$, and n_μ, n_σ, n_ξ are the parameters, covariates, and number of non-zero covariates for the GEV distribution's location (μ), scale (σ), and shape (ξ) parameters, respectively. Our process for trend surface model selection involves two stages. First, the elastic-net regression is run using k-fold cross validation to select the best fitting general linear models for each GEV parameter independently (Eq. 3.1-3.3). For the second step, a sampling of the best fitting models for each parameter are selected based on the elastic-net results and then run in combination within a spatial GEV framework to determine the best trend surface for the region.

Elastic-net regularization is a hybrid of ridge and lasso regression methods that uses cyclical coordinate descent [Friedman et al., 2010]. The elastic-net penalty was originally introduced by Zou and Hastie [2005] as a compromise between ridge [Hoerl and Kennard, 1970, Tikhonov, 1943] and lasso [Tibshirani, 1996] regression. Given observations $y_i, i = 1, \ldots, n$, an $n \times m$ matrix of normalized covariates $\mathbf{X}$ and an assumed linear model

$$y_i = \eta_0 + \eta_1 x_{i,1} + ... + \eta_m x_{i,m}, \tag{3.2}$$

the elastic net minimizes

$$\frac{1}{2n}\sum_{i=1}^{n}(y_i - \eta_0 - \eta x_i^T)^2 + \lambda \sum_{j=1}^{m}\left[\frac{1}{2}(1-\alpha)\eta_j^2 + \alpha|\eta_j|\right], \tag{3.3}$$

where λ is a non-negative regularization parameter that is tuned to weight the overall strength of the penalty and $\alpha \in [0, 1]$ is specified to control the penalty term to vary from ridge regression at $\alpha = 0$ to lasso regression at $\alpha = 1$ [Friedman et al., 2010]. While ridge regression yields smooth solutions that include all the predictors, lasso regression results in automatic variable selection (i.e., sparse, much more easily interpretable solutions) [James et al., 2013]. As α increases from 0 to 1 for a fixed λ, the number of zero-valued η_j increases from 0 to the sparsity of the lasso [Friedman et al., 2010]. In this study, variable selection was desired in the interest of adherence with the principle of parsimony, therefore α was specified close to 1 for numerical stability [Friedman et al., 2010]. With α specified close to 1, the elastic net performs much like lasso regression while retaining ridge regression's capacity to collectively shrink the coefficients for any highly correlated covariables [Friedman et al., 2010, Hastie et al., 2009]. Exploiting extreme value theory, each independent elastic-net application used univariate at-site GEV estimates as the observations. Employing the 'glmnet' R package [Simon et al., 2011], k-fold cross validation (CV) was employed to ensure that the minimizing value for λ was properly located for each elastic-net application. The minimizing model (λ_{min}) is the one with the lowest mean squared error (MSE), while the best regularizing model λ_{reg} is defined as having the largest λ value within one standard error of λ_{min} [Friedman et al., 2010, Hastie et al., 2016, 2009].

For the second step of the trend surfaces modeling, spatial GEV models were fitted and evaluated using the 'SpatialExtremes' R package [Ribatet, 2020]. A sampling of the best performing trend surfaces (e.g., top ten) from the elastic-net CV for μ, σ, and ξ from the range $[\lambda_{min}, \lambda_{reg}] \cup (\lambda_{reg}, \lambda_{max})$, where λ_{max} corresponds with the intercept only model, were

selected and simultaneously fitted. For example, if there were ten top models for each GEV parameter and an intercept only model, then there would be $11^3 = 1331$ spatial GEV models to be fitted. The log-likelihood of the spatial GEV model used is given by

$$l(\eta_\mu, \eta_\sigma, \eta_\xi) = \sum_{i=1}^{n_{site}} \sum_{j=1}^{n_{obs}} \left\{ -log\sigma_i - \left(1+\xi_i \frac{y_{i,j}-\mu_i}{\sigma_i}\right)^{\frac{-1}{\xi_i}} - \left(1+\frac{1}{\xi_i}\right) log\left(1+\xi_i \frac{y_{i,j}-\mu_i}{\sigma_i}\right) \right\}, \quad (3.4)$$

where μ_i, σ_i, and ξ_i are the GEV parameters for the i^{th} site ($i = 1, ..., n_{site}$) with ξ_i assumed non-zero, and $y_{i,j}$ is the j^{th} observation for the i^{th} site [Ribatet, 2009]. The spatial GEV models were evaluated using information criterion scores (i.e., Takeuchi Information Criterion) [Takeuchi, 1976] and quantile-quantile comparisons of the spatial GEV model parameter estimates with their at-site counterparts [Blanchet and Davison, 2011, Ribatet, 2009].

3.3 Results

Two regions with distinct geographic and climatic drivers for the dominant storms observed within each region were selected for study (Fig. 3.1). These regions include northeastern Colorado (NECO) and the Texas-Louisiana (TXLA) Gulf Coast. The Front Range region of Colorado is dominated by localized thunderstorms during the summer months, while the Gulf Coast region is dominated by tropical storms and hurricanes. Observed daily precipitation data was retrieved from the NOAA Global Historical Climatology Network-Daily (GHCN-Daily) dataset [Menne et al., 2012a,b] for both NECO and TXLA. The 24-hr duration annual maxima (AM) time series were produced using sites with at least 40 years of data available with no more than 10% missing data in any given year. The covariates explored for both regions are based on the impacts of physical information (e.g., elevation, climatology) on local extreme precipitation [Oki et al., 1991, Javier et al., 2007, Papalexiou et al., 2018], and the rainfall-temperature thermodynamic relationship recognized in previous literature [Zhao

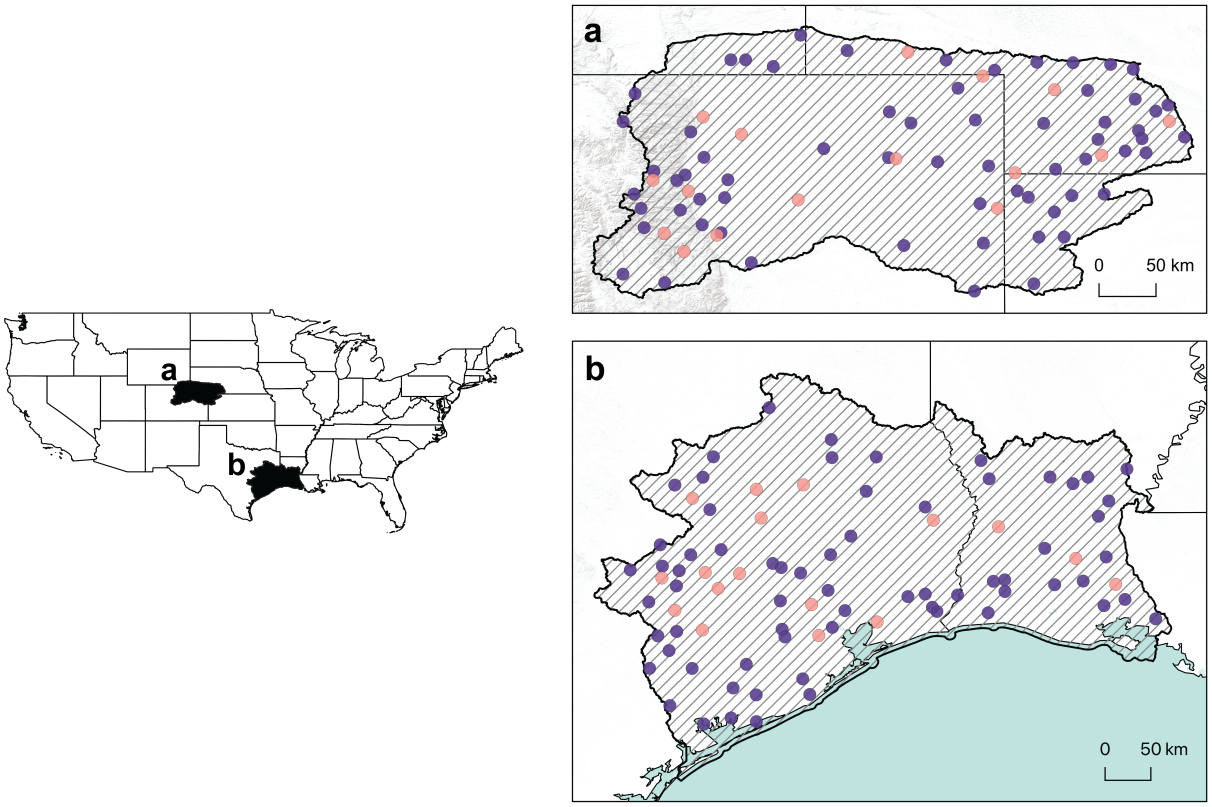

Figure 3.1: Study regions and sites associated with the observed AM data. The regions are (a) northeastern Colorado and (b) the Texas-Louisiana Gulf Coast. Purple markers indicate calibration sites, while orange markers indicate validation sites.

and Khalil, 1993, Trenberth and Shea, 2005, Adler et al., 2008]. The covariate data selected includes longitude, latitude, their product, elevation, and relevant monthly climatological information (i.e., precipitation, dewpoint temperature, maximum/minimum/mean temperature, and maximum and minimum vapor pressure deficit) from the PRISM Norm81m long-term (1981-2010) mean monthly gridded data sets at 30 arc second resolution [Daly et al., 2008]. These covariates and their squares constituted the entire set of covariables (190 in total) considered to build each trend surface within both study regions. Each respective elastic-net application was performed using 20 separate iterations of k-fold cross-validation (CV) for each GEV parameter with a k of 10 and an α of 0.95 for both regions. An of 0.95 was selected to achieve an α value that would favor the parsimonious lasso regression,

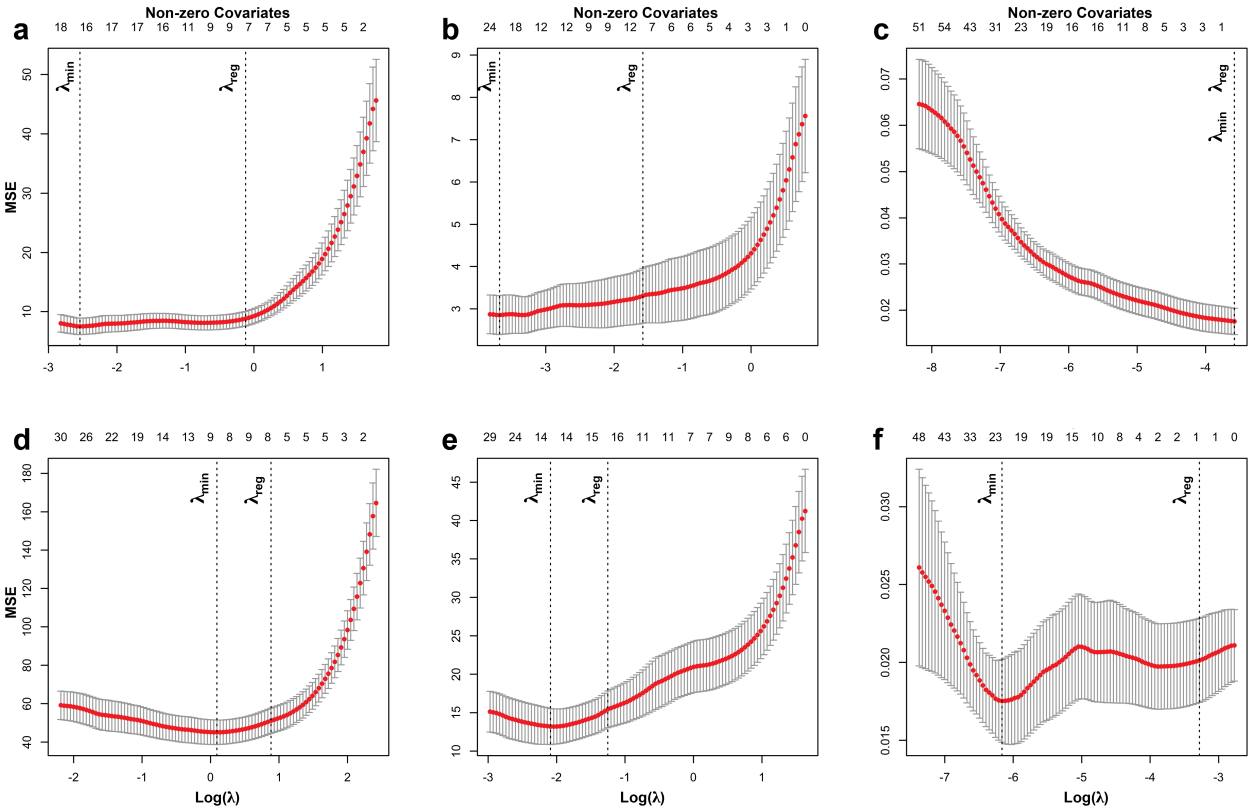

Figure 3.2: Elastic-net cross-validation (CV) summary plots for the NECO (top row) and TXLA (bottom row) that demonstrate the results for (a, d) $\mu(\mathbf{cov}_\mu)$), (b, e) $\sigma(\mathbf{cov}_\sigma)$), and (c, f) $\xi(\mathbf{cov}_\xi)$. The x-axis is the natural logarithm of λ, the y-axis is the mean squared error (MSE), the top of the plot indicates the number of non-zero covariates as λ varies, the red markers are the CV derived MSE with error bars indicating one standard error, and the dotted vertical lines indicate the locations of the CV identified λ-value that minimizes the MSE (λ_{min}) and the defined best regularizing model (λ_{reg}).

while still incorporating ridge regression's ability to reduce the coefficients for any highly correlated covariables [Friedman et al., 2010]. After narrowing down the models to the best performing run out of the 20 iterations, a sampling of the models was made over $[\lambda_{min}, \lambda_{reg}]$ along with the intercept. The results for each region's parameters are displayed in Figure 3.2 with the λ_{min} and λ_{reg} models indicated by dashed vertical lines.

In the second step of the trend surface modeling, the goal is to test all possible combinations of the sampled location, scale, and shape models to find the best single combined set within a spatial GEV framework. Table 3.1 details the non-zero covariates of the spatial GEV models with the lowest TIC by region that were selected from this iterative process. The QQ-plots

for the best of the top models for each regions' trend surfaces can be seen in Figure 3.3. The location and scale parameters fit relatively well at both the calibration and validation sites (Figure 3.3, columns 1-2). While the standard practice for the shape parameter is to set it to a fixed value, the variability in the shape parameter indicates this would not be the best option given the data within these regions (Figure 3.3, far right column). Of particular interest is that the increased number of covariates for the TXLA's model achieved an improved fit of the shape parameter's spatial variability without compromising the model's performance at the validation sites. Had we not introduced the elastic-net regression step within our trend surface modeling, we likely would not have chosen to use those covariates and would have settled for a worse fitting trend surface unknowingly. While some regions may require additional covariates to capture the spatial variability of the shape parameter, the results for the NECO region indicate that this is not the case for every region.

3.4 Conclusions

Due to the spatial nature of extreme climate events, the estimation of exceedance probabilities for infrastructure design and hazard mitigation depends on properly modeling the spatially varying marginal parameters. In a block maxima approach, the selection of trend surfaces to properly capture the spatially varying generalized extreme value (GEV) marginal parameters can be non-trivial when a large set of relevant covariates are available. I introduced elastic-net regularization as a simple and effective means by which to systematically identify optimal trend surfaces for the modeling of extreme events. The 190 covariates explored for both regions were selected based on the rainfall-temperature thermodynamic relationship and the impact of physical information (e.g., elevation, climatology) on local extreme precipitation. I demonstrated the method for modeling the trend surfaces using extreme 24-hr duration precipitation in two climatically distinct regions. This simple effec-

Table 3.1: The non-zero covariates for each region's selected trend surface models[a]

	$\mu(\mathbf{cov}_\mu)$	$\sigma(\mathbf{cov}_\sigma)$	$\xi(\mathbf{cov}_\xi)$
NECO	X, Y, P_{Mar}, P_{May}, P_{Jun}, P_{Oct}, P^2_{May}, P^2_{Jul}, P^2_{Aug}, P^2_{Dec}, $T_{D,Apr}$, $T_{D,May}$, $Min.T^2_{Oct}$, $Max.VPD_{Jul}$, $Min.VPD_{Jun}$, $Max.VPD^2_{Jul}$, $Min.VPD^2_{Mar}$, $Min.VPD^2_{Nov}$	Z, P_{Mar}, P^2_{May}, P^2_{Jul}, P^2_{Dec}, $T_{D,Nov}$, $Mean\,T^2_{Mar}$, $Min.VPD^2_{May}$, $Min.VPD^2_{Oct}$, $Max.VPD_{Aug}$, $Min.VPD^2_{Mar}$, $Min.VPD^2_{Dec}$	$Mean\,T^2_{Mar}$, $Min.VPD_{Dec}$
TXLA	Z, P_{May}, P_{Jul}, P^2_{Jan}, P^2_{Oct}, $T_{D,Jan}$, $Mean\,T_{Jul}$, $Min.VPD_{Jan}$, $Max.VPD^2_{Jul}$, $Max.VPD^2_{Sep}$, $Min.VPD^2_{Jun}$, $Min.VPD^2_{Jul}$	Z, P_{Sep}, P_{Nov}, P^2_{May}, P^2_{Oct}, $T_{D,Jul}$, $T^2_{D,Dec}$, $Max.T^2_{Jan}$, $Max.T^2_{Dec}$, $Min.VPD^2_{Jul}$	Z, P^2_{Apr}, P^2_{Oct}, $Mean\,T_{Aug}$, $Mean\,T^2_{Aug}$, $Max.VPD_{Dec}$, $Min.VPD_{Mar}$, $Min.VPD_{May}$, $Min.VPD_{Jul}$

[a]Covariates X, Y, Z are longitude, latitude, and elevation, respectively. Covariates in the table also include monthly precipitation (P), monthly mean and minimum temperature ($MeanT$, $Min.T$), monthly dewpoint temperature (T_D), and monthly minimum and maximum vapor pressure deficit ($Min.VPD$, $Max.VPD$).

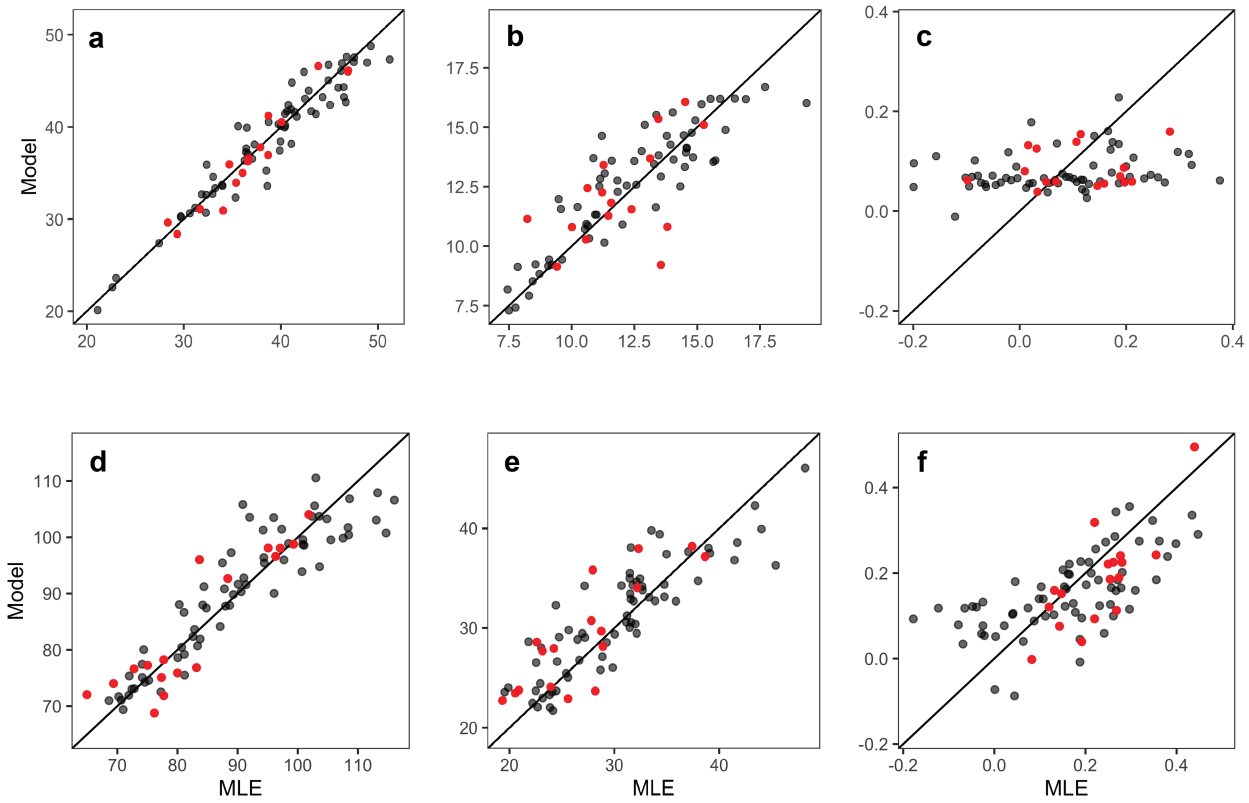

Figure 3.3: QQ-plots of the modeled trend surface versus MLE of AM data. Plots (a-c) are for the NECO region's (a) location, (b) scale, and (c) shape, while plots (d-f) are for the TXLA region's (d) location, (e) scale, and (f) shape. Black markers represent the calibration sites and red markers represent the validation sites.

tive approach for trend surface development is not specific to extreme precipitation analyses but can be applied to trend surfaces for other extreme event types and can be implemented within various modeling approaches. Further, spatial trend surfaces and more reliable analysis of spatial extremes can also improve downscaling and disaggregation schemes [Wilby and Wigley, 1997, Papalexiou et al., 2018].

Chapter 4

Areal Estimation of Extreme Precipitation Using Max-Stable Processes Across Climatically Different Regions

4.1 Introduction

Engineering hydrology needs credible mean areal estimates of extreme precipitation for planning analysis of critical infrastructure (e.g., roads, culverts, floodplain management). Of interest, is understanding to what extent the assumption of inter-site independence, which is currently used in practice, impacts areal-based exceedance results that are necessary for infrastructure design and management.

Precipitation is a spatial process and several methods have been developed to integrate spatial information into frequency analysis [Cooley, 2009]. Regional Frequency Analysis

(RFA) [Cunnane, 1988] is the most common methodology used to compute point estimates of extreme precipitation by practicing engineers. However, it is based on an index flood approach that is an engineered solution methodology that pools the data of neighboring stations, within homogeneous subregions, allowing for better quantile estimates of the frequency distribution than those based on at-site data alone [Hosking and Wallis, 1993, 2005]. Irrespective of the known difficulties with its implementation due to homogeneity requirements, it does not formally comply with extreme value theory, nor does it directly provide areal estimates. The additional step of using Areal Reduction Factors (ARFs) is required to transform point-based estimates to an areal averaged estimate [U.S. Weather Bureau, 1958].

In spatial extreme value analysis methods that make use of block maxima, the assumption is made that the distribution of the maxima at all locations in a region follow the Generalized Extreme Value (GEV) family of distributions where some (or all) of its parameters vary spatially, i.e. trend surfaces. This approach borrows strength spatially through the pooling of data, either over the whole region or within smaller subregions. Latent Variable Models (LVMs) provide an alternative to RFA that is able to handle some heterogeneity and incorporate geographic and climatalogical information within their models. While this approach is extremely useful for modeling point-wise return levels and exceedance probabilities, it does not allow for asymptotic dependence among neighboring locations. The simplifying assumption of spatial independence does not hold up well in regions dominated by large-scale storms and/or regions that contain dense sensor networks.

One draw-back in common between both RFA and LVMs is that they assume inter-site independence to simplify their likelihood formulation. However, this assumption can result in under- or over-estimation of exceedance probabilities in regions where either sensor networks are dense or large-scale storms dominate. The spectral representation of a Max-Stable Process (MSP) introduced by De Haan [1984] has resulted in the subsequent development of usable parametric models for spatial extreme value analysis that account for both the

regional processes and the spatial dependence between sites.

To transform RFA and LVM results from point-based to areal estimates requires the use of Areal Reduction Factors (ARFs). ARFs make simplifying assumptions that place restrictions on their usability (e.g., watershed size). In cases where the desire is to estimate areal exceedance probabilities, a method that accounts for dependence and produces a continuous estimate can be useful. Max-Stable Process (MSP) models provide estimates that are a continuous surface, meaning that areal-based estimates can be reached by averaging the results within the desired watershed or subbasin. While MSP models have come a long ways in their development, computational burdens of fitting a max stable process model do still remain. Therefore, incorporating new methods that incrementally assist in speeding up computation (like the one introduced in Chapter 3 of this dissertation) help to improve the broader adoption of MSP methods.

In this study, I present areal exceedance estimates of 24-hour extreme precipitation for two climatically different regions that include northeastern Colorado and the Texas-Louisiana Gulf Coast region. For each region I compare the MSP model results with the standard practice (i.e., RFA) method results that do not account for spatial dependence within the model. My results underscore the importance of correctly characterizing the dependence among the extreme data given the dominant storm generating mechanism of the region.

4.2 Data

For this study, I selected two regions from within the U.S. that have different geographic and climatic drivers for the dominant storms observed within each region (Figure 4.1). These regions include northeastern Colorado (NECO) and the Texas-Louisiana Gulf Coast (TXLA). The northeastern Colorado (NECO) region includes the Front Range toe the west and the

Great Plains to east. The region is dominated by localized convective storms that develop either from solar insolation or as the result of warm, moist subtropical air transported from the Gulf of Mexico meeting the cold, dry air of the Rockies [Greenland, 1989, McNulty, 1995]. The coastal Texas-Louisiana (TXLA) coastal region sits along the Gulf of Mexico, which is the predominant source of moisture for the region, in addition to the Atlantic Ocean [van der Wiel et al., 2017]. The region is dominated by thunderstorms, tropical cyclones, and hurricanes, occurring predominantly in the summer and fall seasons [NOAA Atlas 14, Keim and Faiers, 1996]. The Great Plains to the north are the main source of cold air [Hobbs et al., 1990].

I retrieved observed daily precipitation data from the NOAA Global Historical Climatology Network-Daily (GHCN-Daily) dataset [Menne et al., 2012a,b] for both regions. Sites within each region were checked first for duplicate records. Any duplicates station names were compared to confirm that they had the same geographical coordinates, or not. None of the sites used had duplicate stations, therefore no merging of records was necessary. Next the data was filtered for completeness by checking that the number of missing days at a given station did not exceed 10% of days within the year. To check for stationarity, I used the Mann-Kendall test with an $\alpha = 0.05$. Any sites that were non-stationary were removed. Anomalously high values (i.e., an order of magnitude greater then the next three highest values) were also removed since they are often due to a recording error or typo. For better comparison between my MSP estimates and the NOAA Atlas 14 estimates, I used only the sites with at least 40 years of data since record length impacts estimation of the GEV shape parameter, as demonstrated by Papalexiou and Koutsoyiannis [2013].

For the trend surface modeling, I used geographical information (i.e., longitude, latitude, elevation) and the extensively peer-reviewed climatological information from the PRISM Norm81m long-term (1981-2010) mean monthly gridded data sets (∼800m resolution)[Daly et al., 2008] and their squares. The PRISM data sets include the following: daily precip-

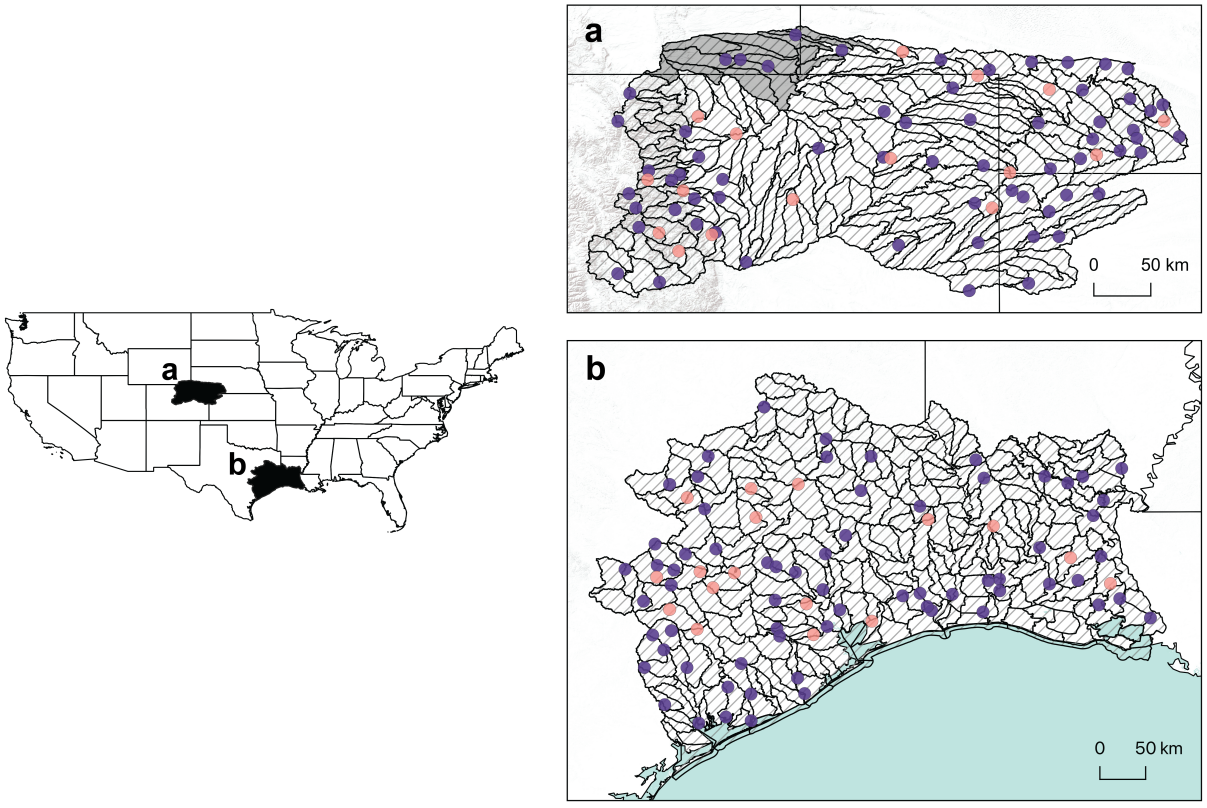

Figure 4.1: Maps of both the a) NECO and b) TXLA study regions. The watersheds (black lines) within the three study regions are delineated and station locations (markers) for the annual maxima precipitation data are displayed. Purple markers indicate calibration sites, while orange markers indicate validation sites. The watersheds in map a) that are shaded with gray do not have a complete NOAA Atlas-14 counterpart and were omitted from the results comparison.

itation; mean, minimum, and maximum daily temperature; mean dew point temperature; and minimum and maximum vapor pressure deficit. These covariates were selected given the impacts of physical processes on the local precipitation [Oki et al., 1991, Javier et al., 2007, Papalexiou et al., 2018] and the rainfall-temperature thermodynamic relationship recognized in previous literature Zhao and Khalil [1993], Trenberth and Shea [2005], Adler et al. [2008].

For the NOAA areal depth estimates, I retrieved ASCII grids from the NOAA Atlas 14 24-hour duration annual maximum precipitation frequency estimates for 2, 5, 10, 25, 50, and 100-year return periods [NOAA Atlas 14]. The ARF method I used to convert these point-based estimates to area averaged depths is based on the TP-29 method [U.S. Weather Bureau, 1958], which is detailed in the Methods section to follow. I used the U. S. Geological Survey (USGS) level 10 Watershed Boundary Dataset (WBD) for 2-digit Hydrologic Units 08, 10, and 12 which span the NECO and TXLA study regions [USGS, 2020a,b,c]. The level 10 watersheds satisfy the area restrictions imposed by the TP-29 ARF method.

4.3 Methods

Max-stable processes are the spatial analogue of multivariate extreme value models. A max-stable process Z is the limit process of point-wise maxima taken over an infinite number of independent replicates $\{X_i : i \in \mathbb{N}\}$ of a continuous stochastic process X defined on index set $\mathfrak{X}$. For suitable normalizing sequences $\{a_n(x) > 0\}$ and $\{b_n(x) \in \mathbb{R}\}$,

$$Z(x) = \lim_{n\to\infty} \frac{\max_{i=1,\ldots,n} X_i(x) - b_n(x)}{a_n(x)}, x \in \mathfrak{X} \tag{4.1}$$

where the limiting process Z is either degenerate or it is a max-stable process [De Haan, 1984, Ribatet and Sedki, 2013b]. By way of univariate extreme value theory, the cumulative distribution function of the pointwise distribution of Z are generalized extreme value (GEV)

distributions if Z is non-degenerate [de Haan and Ferreira, 2006], given by

$$Pr\{Z(x) \leq z\} = exp\Big\{ - \Big[1 + \xi\Big(\frac{z-\mu}{\sigma}\Big)^{-\frac{1}{\xi}}\Big]\Big\}, 1 + \xi\Big(\frac{z-\mu}{\sigma}\Big) > 0,\ x \in \mathfrak{X}. \tag{4.2}$$

where $\{\mu \in \mathbb{R}\}$, $\{\sigma > 0\}$, $\{\xi \in \mathbb{R}\}$ are the location, scale, and shape parameters of the GEV distribution, respectively [Fisher and Tippett, 1928]. In order to simplify calculations for fitting the spatial dependence, the GEV marginals can be transformed via standardization of $Z(x)$ to unit Fréchet marginals without loss of generality, which has the distribution function

$$Pr\{Z(x) \leq z\} = exp\Big(- \frac{1}{z}\Big),\ z > 0,\ x \in \mathfrak{X}. \tag{4.3}$$

Since the above naïve approach requires a very large n to ensure good approximations and its convergence is slow, a more efficient approach was introduced by De Haan [1984] that makes use of the spectral representation for Z. It states that there exists a family of non-negative continuous functions $\{f(x, y) : x, y \in \mathbb{R}^d\}$ such that

$$\int_{\mathbb{R}^d} f(x, y)dy = 1,\ \forall x \in \mathbb{R}^d,\ K \subset \mathfrak{X} \tag{4.4}$$

where $\int_{\mathbb{R}^d} \sup_{x \in K} f(x, y)dy < \infty$ and the max-stable process Z, with unit Fréchet margins, has the same distribution as

$$Z(x) = \max_{i=1,2,\ldots} \zeta_i f(x, U_i),\ x \in \mathbb{X}, \tag{4.5}$$

where $\{\zeta_i, U_i) : i \in \mathbb{N}\}$ are the points of a Poisson process on $(0, \infty) \times \mathbb{R}^d$ with intensity measure $d\Lambda(\zeta, u) = \zeta^{-2}d\zeta du$. Schlather [2002] storm profile model is a characterization of the spectral representation of Z that allows for the use of random functions, wherein there exists a non-negative stochastic process Y with continuous sample paths such that $E\{Y(x)\} = 1$

for all $x \in \mathbb{R}^d$ and for which

$$Z(x) = \max_{i=1,2,...} \zeta_i Y_i(x),\ x \in \mathbb{X}, \tag{4.6}$$

where Y_i are independent copies of Y, and $\{\zeta_i : i \in \mathbb{N}\}$ are the points of a Poisson process on $(0, \infty)$, and are sorted in decreasing order as $i \to \infty$, with intensity $d\Lambda(\zeta) = \zeta^{-2} d\zeta$. The joint distribution is

$$Pr\{Z(x_1) \leq z_1, ..., Z(x_k) \leq z_k\} = exp\Big[- \mathbb{E}\Big\{ \max_{j=1,...,k} \frac{Y(x_j)}{z_j} \Big\}\Big],\ k = 1, ..., K \tag{4.7}$$

for a finite set of locations $\{x_1, ..., x_k \in \mathfrak{X}\}$ and for fixed values $\{z_1, ..., z_k > 0\}$ for $K \in \mathbb{N}$ [Schlather, 2002]. Replacing either $f(x, U_i)$ of Equation 4.5 or $Y_i(x)$ of Equation 4.6 with a different probability density function leads to the current set of MSP families that include the Smith process [Smith, 1990], Schlather process [Schlather, 2002], and their respective generalizations; the Brown-Resnick process [Brown and Resnick, 1977, Kabluchko et al., 2009] and the extremal-t process [Opitz, 2013].

The extremal coefficient $\theta(h)$, which is incorporated into the bivariate density function formulation, is a measure of the strength of dependence between the margins and can be summarized as

$$\theta(h) = -zlogPr\big\{ Z(x+h) \leq z, Z(x) \leq z \big\} = \mathbb{E}\big[\max\{Y(x+h), Y(x)\} \big], \tag{4.8}$$

where $Pr\{Z(x+h) \leq z, Z(x) \leq z\} = exp\{-\theta(h)/z\}$ for $\{z > 0\}$ and for all spatial separations between pairs of locations $\{h \in \mathbb{R}^d\}$ [Schlather and Tawn, 2003]. The value of $\theta(h)$ ranges in value from $[1, d]$, where 1 is full dependence and d is the number of sites and indicates full independence (e.g., for pairwise comparison $d = 2$). However, values greater than d can occur and indicate a negative dependence between sites [Smith, 1990]. Since the variogram for a max-stable process often does not exist, the F-madogram is instead used for

assessing spatial dependence. The F-madogram can be defined as

$$\nu(h) = \frac{1}{2}\mathbb{E}|F\{Z(x+h)\} - F\{Z(x)\}|, \tag{4.9}$$

where F is the cumulative distribution function of $Z(x)$ [Cooley et al., 2006]. The relationship between the F-madogram and the extremal coefficient can be shown using the max-stability of Z and the relation $|x-y| = 2\max(x,y) - x - y$, which results in the equality

$$\theta(h) = \frac{1 + 2\nu_F(h)}{1 - 2\nu_F(h)}. \tag{4.10}$$

Since the likelihood formulation becomes intractable numerically as k increases (i.e., on the order of the k^{th} Bell number), the use of composite likelihoods that are linear combinations of individual log-likelihood components are the most common way to attain asymptotically unbiased estimating equations [Padoan et al., 2010]. The weighted pairwise composite log-likelihood function is given by

$$\ell_P(\psi; z) = \sum_{i=1}^{k-1} \sum_{j=i+1}^{k} \omega_{i,j} log f(z_i, z_j; \psi) \tag{4.11}$$

based on the data z at locations i and j, with weights set such that $\{\omega_{i,j} > 0\}$, $\sum_{i,j} \omega_{i,j} = 1$, and $f(\cdot, \cdot; \psi)$ is the bivariate density function with $k = 2$ [Padoan et al., 2010]. Similar to the usage of an ordinary maximum likelihood estimator, a maximum composite likelihood estimator (MCLE) can be used to provide an estimate of the parameter ψ, where

$$\hat{\psi}_P = \arg\max_{\psi \in \Psi} \ell_P(\psi; z) \tag{4.12}$$

satisfies

$$\sqrt{n}\big(\hat{\psi}_P - \psi_o\big) \to N\big\{0, \bar{I}(\psi)\big\},\ n \to \infty \tag{4.13}$$

$$\bar{I}(\psi) = H^{-1}(\psi_o)J(\psi_o)H^{-1}(\psi_o) \tag{4.14}$$

where $\bar{I}(\psi))$ is the sandwich information matrix with$H(\psi_o) = -\mathbb{E}[\nabla^2 \ell_P(\psi; z)]$ and $J(\psi_o) = Var[\nabla \ell_P(\psi; z)]$. Padoan et al. [2010] notes that while MCLE is asymptotically unbiased, it results in a loss of efficiency (related to $\bar{I}(\psi))$) relative to ordinary MLE methods.

The development of an MSP model is often performed as a two-stage procedure to overcome the computational burden of fitting both stages simultaneously [Ribatet, 2013]. The first stage accounts for spatial heterogeneity of the marginals through development of a trend surface model, while the second stage involves incorporating the spatial dependence through fitting a simple MSP model. In the first stage, a process-based spatial GEV analysis can be used to fit general linear models to each GEV parameter across the observed sites to build the trend surface model. For modeling the spatial dependence, the selection of the best fitting MSP model and covariance function is performed using unit Fréchet marginals. The models selected from these two steps are subsequently combined to inform a general MSP model wherein the marginal parameters and the dependence parameters are simultaneously fit.

The linear trend surfaces of a max-stable spatial process are of the form

$$\begin{aligned}
\mu(\mathbf{cov}_\mu) &= \eta_{\mu,0} + \eta_{\mu,1} cov_{\mu,1} + ... + \eta_{\mu,n_\mu} cov_{\mu,n_\mu} \\
\sigma(\mathbf{cov}_\sigma) &= \eta_{\sigma,0} + \eta_{\sigma,1} cov_{\sigma,1} + ... + \eta_{\sigma,n_\sigma} cov_{\sigma,n_\sigma} \\
\xi(\mathbf{cov}_\xi) &= \eta_{\xi,0} + \eta_{\xi,1} cov_{\xi,1} + ... + \eta_{\xi,n_\xi} cov_{\xi,n_\xi}
\end{aligned} \tag{4.15}$$

where $\eta_{\cdot,i}$, $cov_{\cdot,i}$, and n_μ, n_σ, n_ξ are the parameters, covariates, and number of non-zero co-

variates for the GEV distribution's location (μ), scale (σ), and shape (ξ) parameters, respectively. Our process for trend surface model selection involves two stages. For building the trend surface models, I used the site-specific geographical information of longitude, latitude, elevation, longitude*latitude, and their squares. I also included monthly climatological information from the PRISM Norm81m long-term (1981-2010) mean monthly gridded data sets ($\sim$800m resolution) [Daly et al., 2008] and their squares, which includes the following: precipitation; mean, minimum, and maximum daily temperature; mean dew point temperature; and minimum and maximum vapor pressure deficit.

I randomly separated the sites for each region into calibration (80%) and validation (20%) sets (Figure 4.1). At-site MLE fits of the observed AM were fitted to obtain GEV parameters for both calibration and validation sites. Using the calibration sites only, elastic-net regularization with repeated k-fold cross validation (CV) was run to select the best sets of general linear models for each GEV parameter individually given the set of covariates used from the PRISM data set, thus automating the covariate selection process (see Chapter 3 for more detail). The k-fold CV was repeated 20 times with a k of 10.

While it is possible to use the trend surfaces for determining quantile predictions at any new site in the domain, the spatial dependence has not yet been accounted for via selection of an appropriate max-stable model. As noted earlier, there are several MSP models to choose among that have different dependence structures. They all follow the spectral characterization of a MSP as introduced by De Haan [1984](Eq. 4.5) and later refined by Schlather [2002](Eq. 4.6), with variations among the models arising through the use of different probability density functions for either the $f(x, U_i)$ or for $Y_i(x)$. Therefore, selection of the best fitting MSP model is based on its ability to capture the spatial dependence structure of the extreme data. The Takeuchi Information Criteria (TIC)[Takeuchi, 1976] was used for assessing the fit of the MSP models due to its compatibility with the pairwise log-likelihood formulation used within these models.

The best fitting model for both regions based on the TIC results was the extremal-t model. Opitz [Opitz, 2013] presented the extremal-t model as the max-stable limit of a t random process which is a generalization of the extremal t distribution. The extremal-t model uses

$$Y_i(x) = c_\nu max\{0, \epsilon_i(x)\}^\nu, \tag{4.16}$$

with extremal-t process $c_\nu = \sqrt{\pi}2^{-0.5(\nu-2)}\Gamma[0.5(\nu+1)]^{-1}]$ and $\{\nu > 0\}$ degrees of freedom, where ϵ is a standard Gaussian process with correlation function ρ, and Γ is the Gamma function [Opitz, 2013, Ribatet and Sedki, 2013b]. Leading to a bivariate cumulative distribution used by the extremal-t model of

$$Pr\{Z(x_1) \leq z_1, Z(x_2) \leq z_2\} = exp\left[-\frac{T_\nu + 1}{z_1}\left\{-\frac{\rho(x_1 - x_2)}{b} + \frac{1}{b}\left(\frac{z_2}{z_1}\right)^{\frac{1}{\nu}}\right\} - \frac{T_\nu + 1}{z_2}\left\{-\frac{\rho(x_1 - x_2)}{b} + \frac{1}{b}\left(\frac{z_1}{z_2}\right)^{\frac{1}{\nu}}\right\}\right], \tag{4.17}$$

where T_v is the cumulative distribution function of the Student's t-distribution with $\nu > 0$ degrees of freedom and $b^2 = \{1 - \rho(x_1 - x_2)^2\}/(\nu + 1)$ [Ribatet and Sedki, 2013b].

For comparison with the results of the MSP model outlined above, I selected to use the NOAA Atlas-14 precipitation frequency estimates [NOAA Atlas 14] since they are derived using RFA methods that assume spatial independence, and they are widely used in practice within the U.S. However, the NOAA Atlas-14 precipitation frequency estimates are point-based. In order to compare these point-based estimates to the MSP areal depth estimates, conversion using areal reductions factors (ARFs) is required for each watershed. The ARF method I used is based on the approach outlined by Technical Paper No. 29 (TP-29) of the U.S. Weather Bureau [U.S. Weather Bureau, 1958]. Note that the TP-29 ARF method does not account for frequency, it only uses duration and area. The basic ARF formula is as

follows

$$ARF = \frac{P_a}{P_p} \tag{4.18}$$

where, for a given watershed and duration, P_a is the average precipitation depth, P_p is the average of the point-based precipitation estimates, and ARF is the areal reduction factor that varies with the duration and the area of the watershed [U.S. Weather Bureau, 1958]. For the ARF term, I used the simplification presented by Leclerc and Schaake [1972] as follows

$$ARF = 1 - exp(-1.1t^{0.25}) + exp(-1.1t^{0.25} - 0.01A) \tag{4.19}$$

where t is the duration in hours and A is the area of the watershed in square miles. For this study, t is 24 hours and the A was determined using the USGS WBD level 10 watersheds [USGS, 2020a,b,c] given that Eq. 4.19 only holds for a watershed size $\leq$ 1100 square miles. Given that the NOAA precipitation frequency grids are by return period, I then applied Eq. 4.19 to each watershed by return period. Meaning that for each watershed the average of the point-based estimates (P_p) for a given return period were multiplied by the ARF for that watershed to produce the corresponding areal depths (P_a). This is one noted downside of the TP-29 ARF method, namely, that the reduction factor ignores frequency [Asquith and Famiglietti, 2000, Olivera et al., 2008]. By omission, the TP-29 approach assumes that the storm sizes of higher frequency events match that of lower frequency events which could be inaccurate given the varying storm types within a region (e.g. thunderstorms versus hurricanes).

4.4 Results

Despite the often localized nature of thunderstorms in the NECO region, spatial dependence between pairs of sites does exist as demonstrated in Figure 4.2, which illustrates how the extremal coefficient $\theta(h)$ varies with distance h for both regions. While the NECO spatial dependence does drop off more quickly than the TXLA region, at shorter distances it is still present. Individual extremal coefficient plots for each region are shown in more detail within Figure 4.6 and include F-madogram results for the data.

Translating the concept of spatial dependence into physical terms, a large precipitation event over a region with a relatively dense sensor network would be observed at multiple gauged sites. Therefore, by accounting for spatial dependence the return level associated with a single storm event would be more rare than a method following the assumption of spatial independence, which would count each observation of the event across the network of gauges as separate events. Following this logic, the NECO return level results are to be expected for a region that does have spatial dependence among its data. Figure 4.3 summarizes the difference between the NOAA and MSP return level results for both regions. The MSP-based return levels are consistently lower than the NOAA RFA-based results at 5-year and higher return periods (Figure 4.3a). Therefore, for this region, a MSP analysis method likely is not necessary given the conservative estimates of the NOAA RFA results. These results are demonstrated in more detail in Figure 4.4, where return level results for a sampling of watersheds across both regions are displayed. To illustrate the difference between the RFA results and the MSP results from a return period perspective, the NECO watershed results in Figure 4.4d indicate that an event with an areal precipitation depth of approximately 3.5 inches has approximately a 25-year return period based on the RFA results (black line), while that same event has roughly a 50-year return period based on the MSP results (purple line).

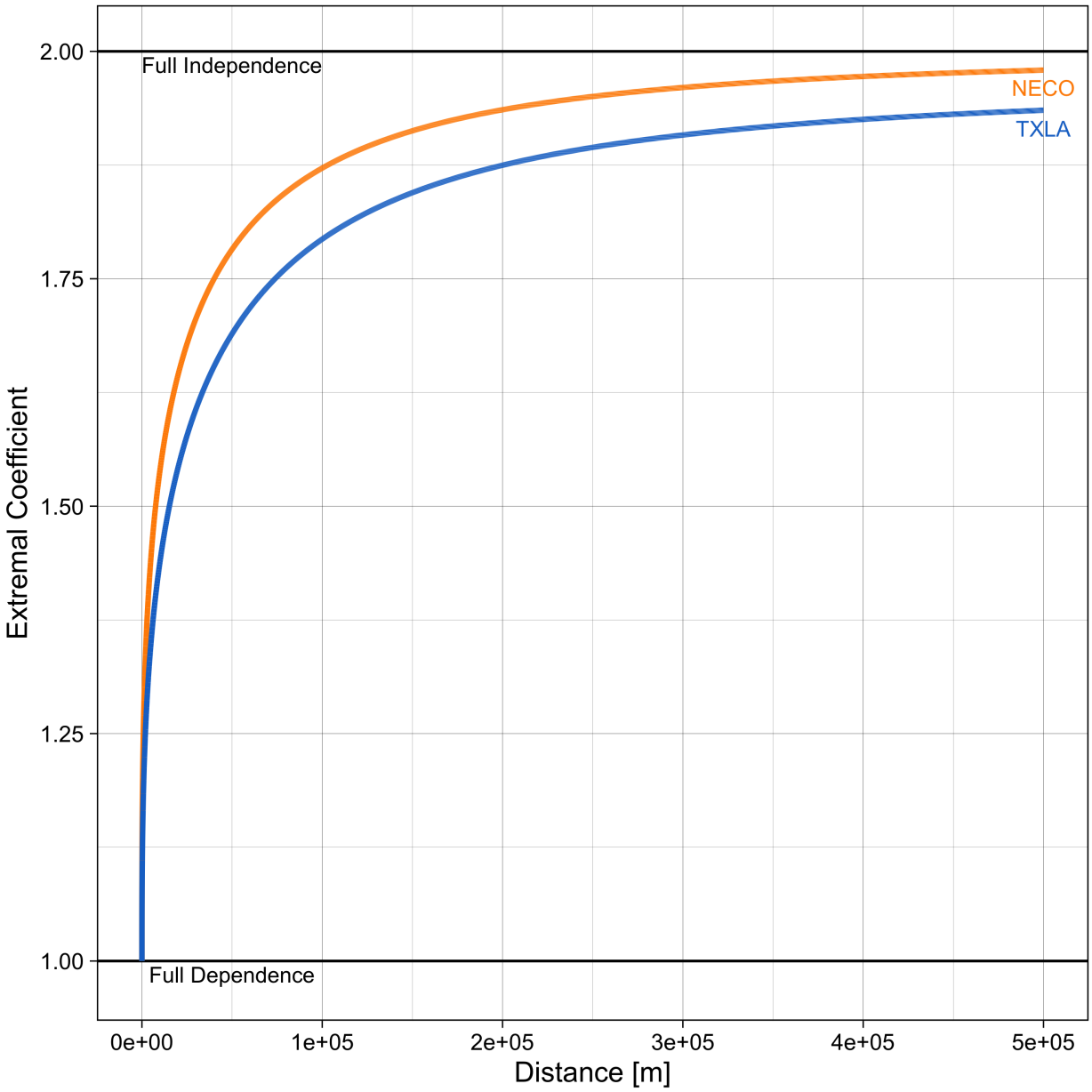

Figure 4.2: Extremal coefficient for both NECO (orange line) and TXLA (blue line) for comparison.

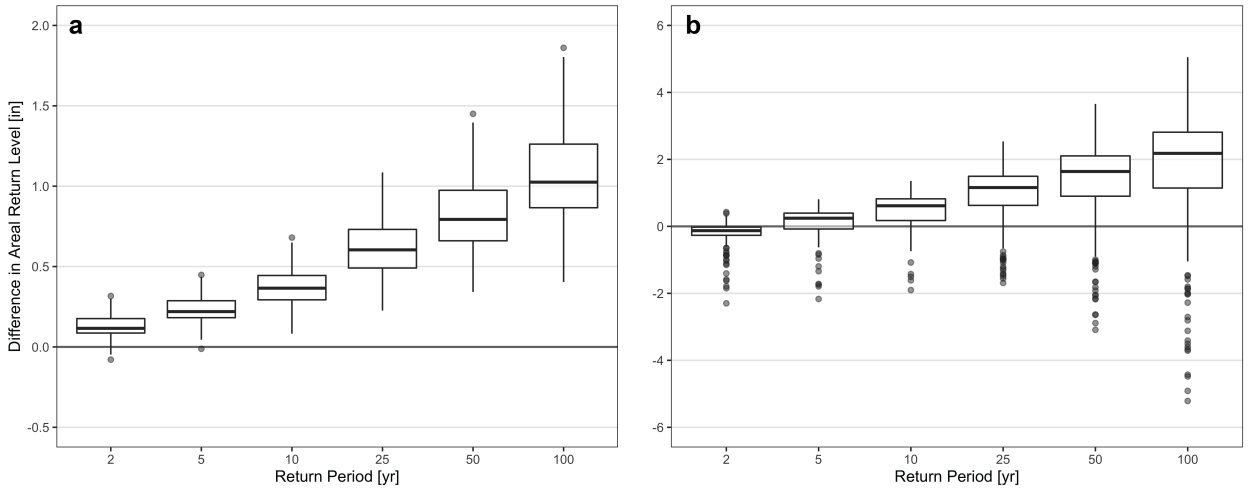

Figure 4.3: Return level differences between RFA estimates and MSP estimates for the a) NECO and b) TXLA regions. y-axis values > 0 indicate that the RFA values are greater than the MSP, while < 0 indicate the converse.

The median of the differences between the RFA results and the MSP results follow a similar increasing trend from 2-year through 100-year return periods in TXLA as seen in NECO (Figure 4.3b). However, there are several watersheds where the RFA results underestimate return levels relative to the MSP results (i.e., difference < 0) across all return periods. This could indicate that not accounting for the spatial dependence between sites leads to the underestimation of return levels within some areas of the TXLA region. Further, it could indicate that the RFA methods are not capturing the same spatial variability of the distribution parameters since there is also a noticeable increase in the return level differences of less frequent events at the 50 and 100-year return periods (see Chapter 3, Table 3.1 and Figure 3.3 for the TXLA trend surface covariates and fits). Figure 4.5 displays a sampling of watershed results for the region to provide more detail. The results displayed in Figures 4.5c,d,e are for watersheds where the RFA results underestimate return levels relative to the MSP results. Focusing specifically on Figures 4.5c,e the increasing difference between the two methods as the return levels increase indicates that the RFA methods are likely estimating smaller values for the shape parameter. While in these plots this may look like a small difference at first glance, note that the scale of the y-axis in the TXLA figures is larger than

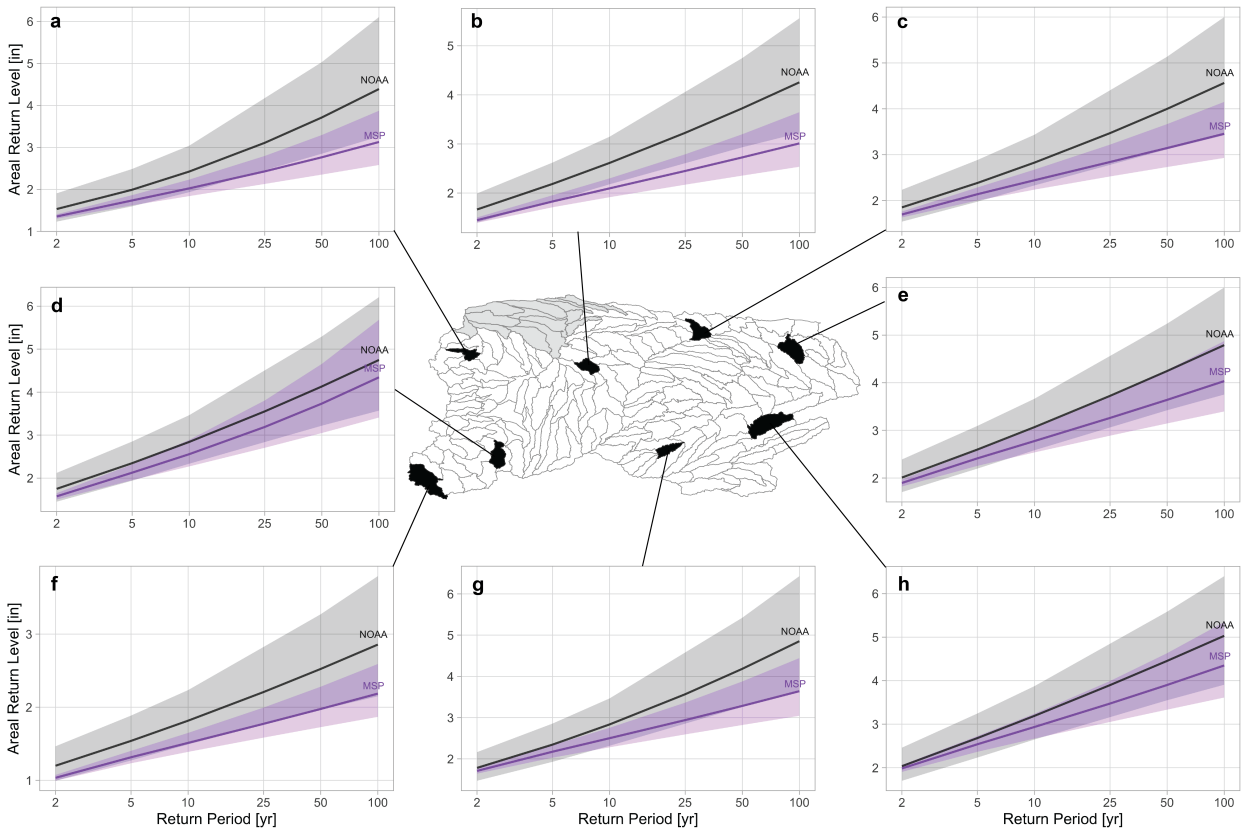

Figure 4.4: NECO areal return levels for a sampling of watersheds across the region. The purple line and ribbon display the MSP results and uncertainty, while the black line and ribbon are the NOAA results.

that of the NECO region. Therefore, the visually small differences in TXLA results indicate a difference of several inches in areal precipitation depths. Meanwhile, the watersheds in subplots a, b, and f of Figure 4.5 mirror the differences between models similar to those shown for the NECO region. The RFA and MSP results in Figures 4.5e,h show minimal difference.

Overall, there is much greater variability in the differences between the methods across the TXLA region than what is seen in the NECO region. Again, these two regions were selected to demonstrate differences in return level estimates when taking into account the spatial dependence within geographically and climatically different regions.

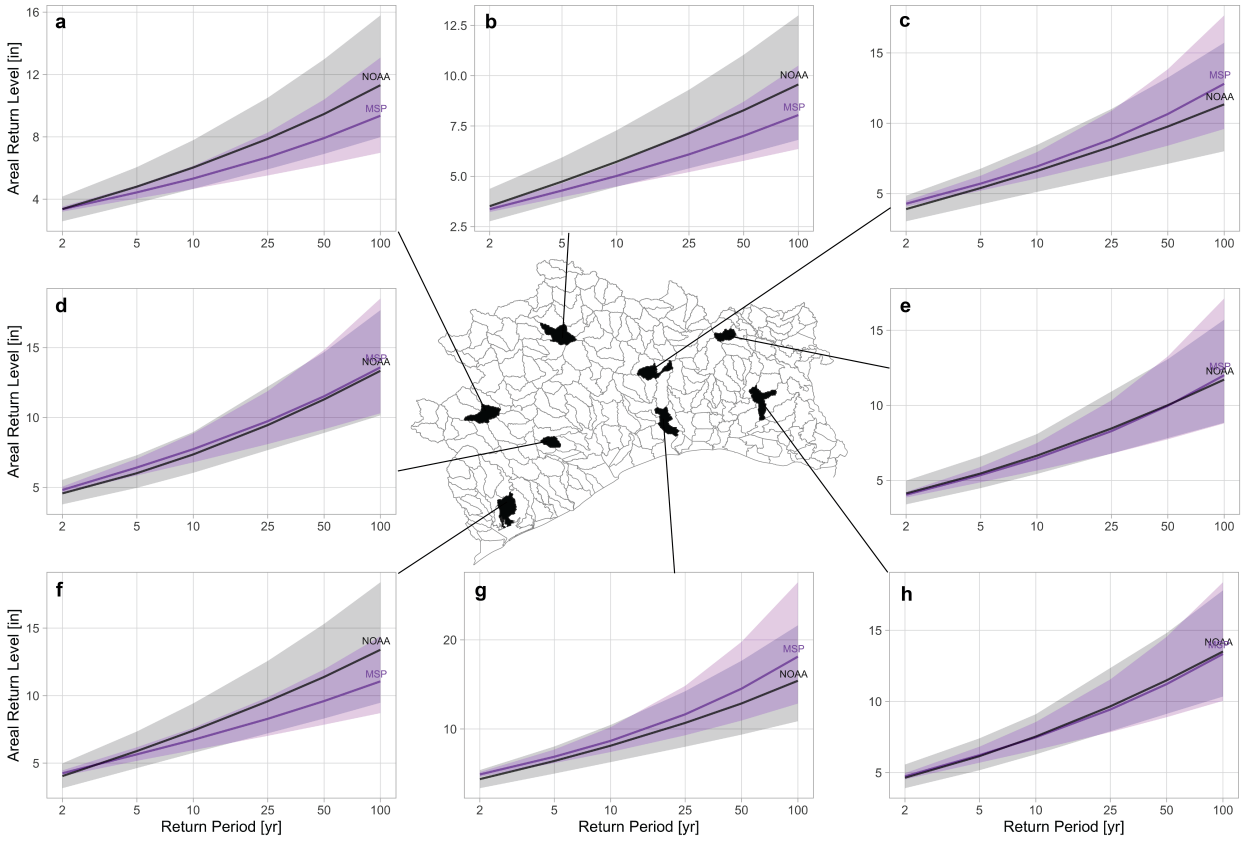

Figure 4.5: TXLA areal return levels for a sampling of watersheds across the region. The purple line and ribbon display the MSP results and uncertainty, while the black line and ribbon are the NOAA results.

4.5 Conclusions

Extreme precipitation is naturally a spatial process with physical drivers. Therefore, when modeling the frequency and intensity of extreme events, we need to account for both the spatial dependence of the extreme data and the drivers which vary depending on the geography and storm types that dominate a given region. While a Regional Frequency Analysis (RFA) may be a good approach within regions that are more homogeneous, have less dense station networks, and have more localized storms, other regions may benefit from accounting for spatial dependence. Namely, regions with dense station networks and that are dominated by large-scale storms. To minimize spatial dependence when using a model that does not account for it, the current practice is to filter the number of stations used to reduce the

chances of repeating the same storm reading multiple times and/or to expand the uncertainty bounds of the estimates to compensate for spatial dependence that is present. The former means that the estimates rely on fewer stations and less data, while the later leans heavily on large uncertainty bounds and assumes that they are sufficient.

Recognizing that simplifying assumptions can introduce under or over-estimation of exceedance probabilities, I explored the application of a Max-Stable Process (MSP) model that accounts for spatial dependence and allows for the inclusion of spatially varying geographic and climatic information. I compared the MSP model results with the NOAA Atlas 14 results that are estimated using RFA methods. To further compare the performance of these two methods, I compared their results from two regions with different dominant storm generating mechanisms. Northeastern Colorado (NECO) is a region where the Great Plains meet the Rockies and is dominated by localized thunderstorms during the warm summer months with occasional larger scale thunderstorms. The Texas-Louisiana (TXLA) Gulf Coast region is dominated by tropical moisture from the Gulf of Mexico and cold air from the Great Plains to the north that creates large thunderstorms, and the region is susceptible to hurricanes and tropical storms from the Atlantic Ocean.

I included several physically relevant covariates for modeling the spatial variability of each region's Generalized Extreme Value (GEV) parameters (i.e., trend surfaces). To automate the selection process and reduce computational burden, I employed elastic-net regression to select the most helpful set of covariates for each region's trend surfaces (discussed in Chapter 3). These trend surfaces where combined with the MSP model that also accounts for each region's spatial dependence. The end result is a continuous surface (spatial process) that facilitates the estimation of areal-based exceedance probabilities without the use of the areal reduction factors (ARFs) which RFA methods require for transforming point precipitation depths into areal depths.

The areal return level results displayed more variability in the differences between the RFA

and MSP methods across the TXLA region compared with what is seen in the NECO region. While the NECO MSP return levels were consistently lower than the RFA return levels, the TXLA region shows a mix of relative under and over-estimation with differences in return levels of several inches. Again, these two regions were selected to demonstrate differences in return level estimates when taking into account the spatial dependence within geographically and climatically different regions. These results indicate that capturing the spatial variability of the extreme distribution parameters in a high-dimensional space while also accounting for the spatial dependence could further benefit the estimates of areal exceedances for some regions. Therefore, consideration should be given to incorporating this kind of assessment into the methods used by practitioners to improve the selection of more conservative estimates for infrastructure design.

4.6 Appendix B

This supporting information provides additional details regarding the fit of the extremal coefficients, examples of max-stable process simulations with unit Frechet margins, and the trend surface rasters for both regions.

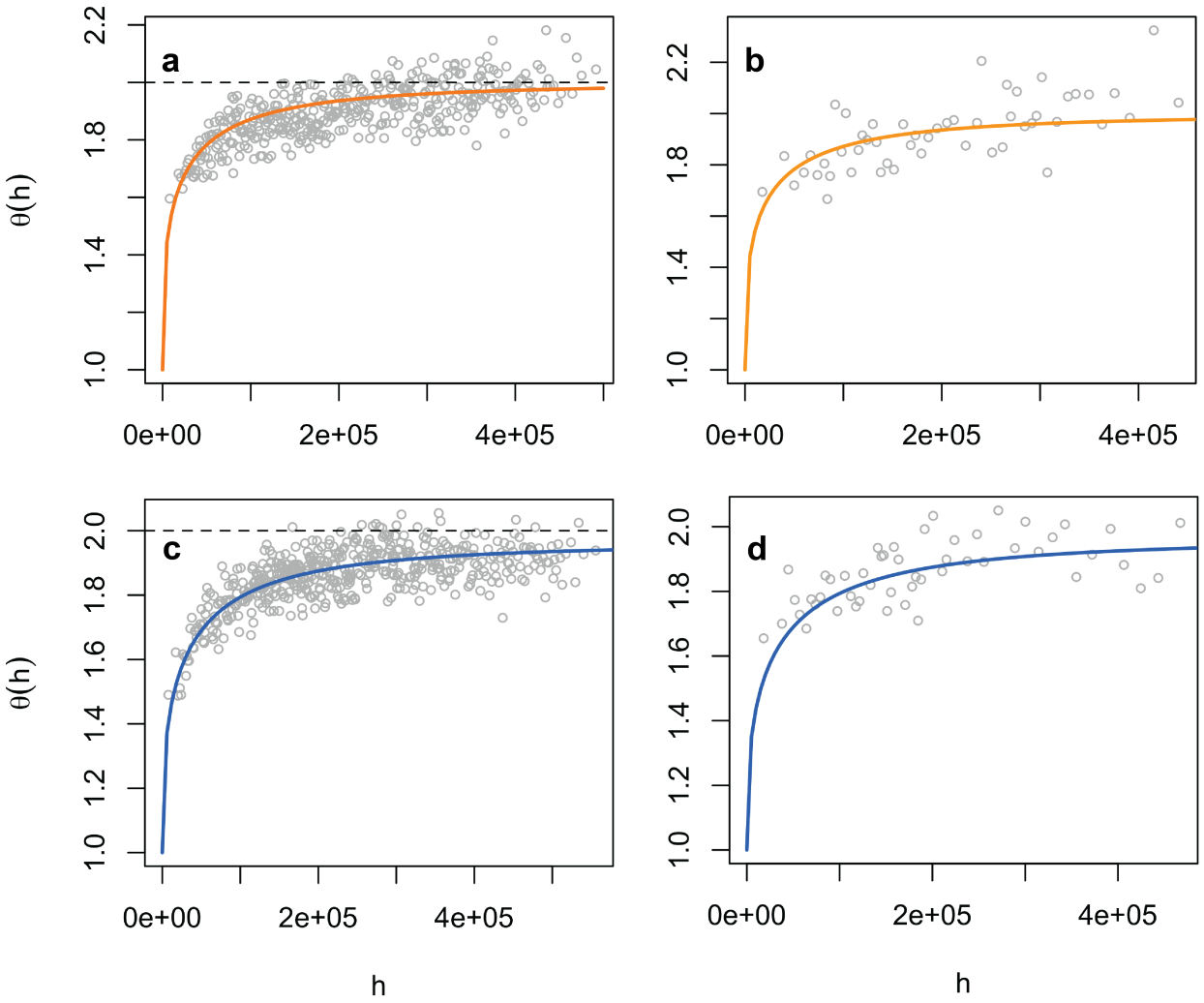

Figure 4.6: Extremal coefficient fit for a) NECO calibration sites, b) NECO validation sites, c) TXLA calibration sites, and d) TXLA validation sites. $\theta(h)$ is the extremal coefficient, h is the distance between pairs of sites in meters. Gray markers are the F-madogram of the sites.

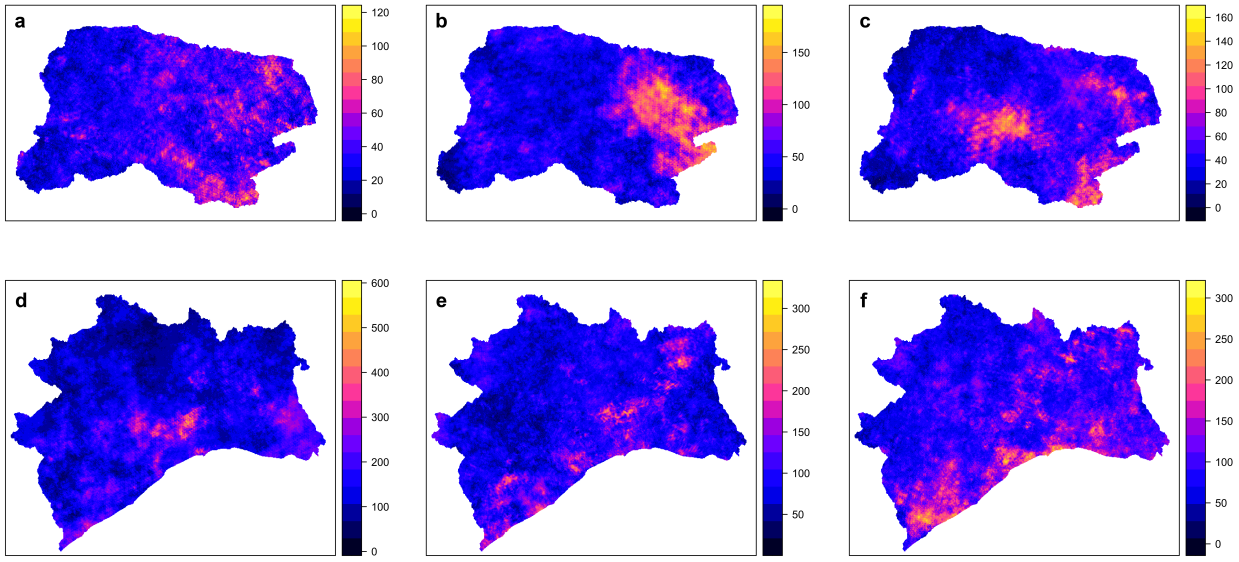

Figure 4.7: Examples of the max-stable process simulations with unit Fréchet margins for NECO (a-c) and TXLA (d-f). For each region 500 of these simulations were generated. Each simulation takes hours to complete.

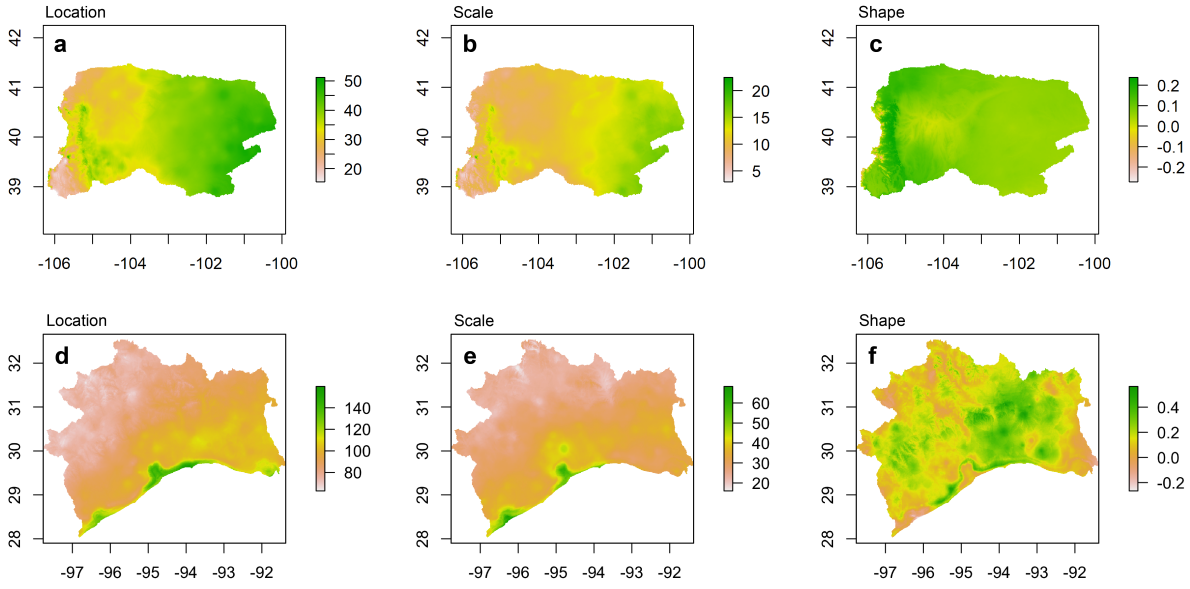

Figure 4.8: Trend surfaces for NECO (a-c) and TXLA (d-f).

Chapter 5

Conclusion

The ability to estimate the intensity and frequency of extreme precipitation is an essential part of infrastructure planning and flood prediction. Understanding the risks associated with spatial extremes at present and estimating their future occurrences, requires more complicated, rigorous, and robust methods. Extreme precipitation events are highly variable across space and time, and current methods for analyzing spatial extremes often involve significant simplifying assumptions. Additionally, these extreme events are infrequent and data records are often inadequate for estimating the rarest of these events considering that their recurrence interval extends beyond the length of record. Estimates of extreme precipitation are often required in regions where gauge data is sparse and storm events are localized making extreme events difficult to predict. Even in regions that do have relatively dense observational networks and large-scale storms, integrating the spatial data for extremes and their drivers is not straightforward. Given these challenges, methods for estimating exceedance probabilities that enable the proper modeling of spatially varying extreme marginal parameters and account for spatial dependence between sites need to be explored and refined.

Given that miscalculating the spatial variability of extreme distribution parameters in a

high-dimensional space can lead to under or over-estimation of exceedance probabilities, in Chapter 2 I explored the benefit of incorporating additional climatic covariates relevant to the physical drivers for modeling 24-hour annual maximum precipitation beyond what have been used within previous studies. Based on my results, I would recommend exploring the inclusion of additional climatic covariates, such as mean temperature and dew point temperature, for regions with a heterogeneous climate and topography to improve model predictive performance. In addition to these covariate results, my results within the overlapping region indicate that predictive performance improves when the dominant extreme storm type of the pooled data for the model matches that of the prediction sites despite differences in their mean annual precipitation.

Based on the computational load of running a full Bayesian hierarchical model with Bayesian model averaging repeatedly with leave-one-out cross validation from Chapter 2, I introduced the application of elastic-net regularization with k-fold validation in Chapter 3 to reduce the time and effort required to narrow down the topmost relevant covariates for trend surface development out of a relatively large set. This automated approach to covariate selection provided a noticeable improvement in computational time and helped to reduce the bias of manually selecting covariates based on assumptions.

The trend surfaces that I developed in Chapter 3, were used within the Max-Stable Process (MSP) models of Chapter 4. After exploring the improvements in predictive performance due to incorporating additional covariates in the previous chapters, in Chapter 4 I explored the impact of also accounting for spatial dependence by comparing the MSP results with regional frequency analysis results. Again, two distinct climate regions with different dominate storms mechanisms where used as study regions. My results indicate that capturing the spatial variability of the distribution parameters in a high-dimensional space while also accounting for the spatial dependence could further benefit the estimates of areal exceedances for some regions.

The results presented in this dissertation highlight the need for the inclusion of additional physically-informed covariates and improved methods for covariate selection that not only improve estimation of extreme precipitation but also improve the computation time and automate the process to reduce the bias that traditional manual selection introduces. Consideration should be given to incorporating assessments of relevant covariates and spatial dependence within the methods used by practitioners to ensure the selection of conservative estimates for infrastructure design.

Bibliography

Kjersti Aas, Claudia Czado, Arnoldo Frigessi, and Henrik Bakken. Pair-copula constructions of multiple dependence. *Insurance: Mathematics and Economics*, 44(2):182–198, April 2009. ISSN 0167-6687. doi: 10.1016/j.insmatheco.2007.02.001.

Robert F. Adler, Guojun Gu, Jian-Jian Wang, George J. Huffman, Scott Curtis, and David Bolvin. Relationships between global precipitation and surface temperature on interannual and longer timescales (1979–2006). *Journal of Geophysical Research: Atmospheres*, 113 (D22), 2008. ISSN 2156-2202. doi: 10.1029/2008JD010536.

Amir AghaKouchak, András Bárdossy, and Emad Habib. Copula-based uncertainty modelling: application to multisensor precipitation estimates. 24:2111–2124, 2010. ISSN 1099-1085. doi: 10.1002/hyp.7632.

Kuk-Hyun Ahn, Richard Palmer, and Scott Steinschneider. A hierarchical bayesian model for regionalized seasonal forecasts: Application to low flows in the northeastern united states. *Water Resources Research*, 53(1):503–521, 2017. ISSN 1944-7973. doi: 10.1002/2016WR019605.

W. H Asquith and J. S Famiglietti. Precipitation areal-reduction factor estimation using an annual-maxima centered approach. *Journal of Hydrology*, 230(1):55–69, Apr 2000. ISSN 0022-1694. doi: 10.1016/S0022-1694(00)00170-0.

Sudipto Banerjee, Bradley P. Carlin, Alan E. Gelfand, Bradley P. Carlin, and Alan E. Gelfand. *Hierarchical Modeling and Analysis for Spatial Data*. Chapman and Hall/CRC, Sep 2014. ISBN 978-0-429-13717-4.

A Bardossy and G G S Pegram. Copula based multisite model for daily precipitation simulation. *Hydrol. Earth Syst. Sci.*, page 16, 2009.

V. Barnett. The Ordering of Multivariate Data. *Journal of the Royal Statistical Society. Series A (General)*, 139(3):318–355, 1976. ISSN 0035-9238. doi: 10.2307/2344839. Publisher: [Royal Statistical Society, Wiley].

Tim Bedford and Roger M. Cooke. Probability Density Decomposition for Conditionally Dependent Random Variables Modeled by Vines. *Annals of Mathematics and Artificial Intelligence*, 32(1):245–268, August 2001. ISSN 1573-7470. doi: 10.1023/A:1016725902970.

Tim Bedford and Roger M. Cooke. Vines: A New Graphical Model for Dependent Random Variables. *The Annals of Statistics*, 30(4):1031–1068, 2002. ISSN 0090-5364. Publisher: Institute of Mathematical Statistics.

Jan Beirlant, Yuri Goegebeur, Johan Segers, and Jozef L. Teugels. *Statistics of Extremes: Theory and Applications*. John Wiley & Sons, March 2006. ISBN 978-0-470-01237-6. Google-Books-ID: jqmRwfG6aloC.

Martin Beniston. Trends in joint quantiles of temperature and precipitation in Europe since 1901 and projected for 2100. *Geophysical Research Letters*, 36(7), 2009. ISSN 1944-8007. doi: 10.1029/2008GL037119.

Juliette Blanchet and Anthony C. Davison. Spatial modeling of extreme snow depth. *The Annals of Applied Statistics*, 5(3):1699–1725, Sep 2011. ISSN 1932-6157, 1941-7330. doi: 10.1214/11-AOAS464.

Nicholas A. Bond and Gabriel A. Vecchi. The influence of the madden–julian oscillation on precipitation in oregon and washington. *Weather and Forecasting*, 18(4):600–613, Aug 2003. ISSN 0882-8156. doi: 10.1175/1520-0434(2003)018⟨0600:TIOTMO⟩2.0.CO;2.

GM Bonnin, D Martin, B Lin, T Parzybok, M Yekta, and D Riley. Precipitation-frequency atlas of the united states: Noaa atlas 14, volume 1, version 4. *NOAA, National Weather Service, Silver Spring, Maryland*, 2006.

Paola Bortot and Carlo Gaetan. Multivariate Extremes. In *Wiley StatsRef: Statistics Reference Online*. American Cancer Society, 2014. ISBN 978-1-118-44511-2. doi: 10.1002/9781118445112.stat07511.

C. Bracken, B. Rajagopalan, L. Cheng, W. Kleiber, and S. Gangopadhyay. Spatial Bayesian hierarchical modeling of precipitation extremes over a large domain. *Water Resources Research*, 52(8):6643–6655, August 2016. ISSN 1944-7973. doi: 10.1002/2016WR018768.

Eike Christian Brechmann and Ulf Schepsmeier. Modeling Dependence with C- and D-Vine Copulas: The *R* Package **CDVine**. *Journal of Statistical Software*, 52(3), 2013. ISSN 1548-7660. doi: 10.18637/jss.v052.i03.

Bruce M. Brown and Sidney I. Resnick. Extreme values of independent stochastic processes. *Journal of Applied Probability*, 14(4):732–739, Dec 1977. ISSN 0021-9002, 1475-6072. doi: 10.2307/3213346.

Donald H. Burn. Evaluation of regional flood frequency analysis with a region of influence approach. *Water Resources Research*, 26(10):2257–2265, 1990. ISSN 1944-7973. doi: 10.1029/WR026i010p02257.

András Bárdossy. Copula-based geostatistical models for groundwater quality parameters. *Water Resources Research*, 42(11), 2006. ISSN 1944-7973. doi: 10.1029/2005WR004754.

Linyin Cheng and Amir AghaKouchak. Nonstationary precipitation intensity-duration-frequency curves for infrastructure design in a changing climate. *Scientific Reports*, 4: 7093–7093, 2014. doi: 10.1038/srep07093.

Linyin Cheng, Amir AghaKouchak, Eric Gilleland, and Richard W. Katz. Non-stationary extreme value analysis in a changing climate. *Climatic Change*, 127(2):353–369, Sep 2014a. ISSN 0165-0009, 1573-1480. doi: 10.1007/s10584-014-1254-5.

Linyin Cheng, Eric Gilleland, Matthew J. Heaton, and Amir AghaKouchak. Empirical bayes estimation for the conditional extreme value model. *Stat*, 3(1):391–406, 2014b. ISSN 2049-1573. doi: 10.1002/sta4.71.

Felicia Chiang, Omid Mazdiyasni, and Amir AghaKouchak. Amplified warming of droughts in southern United States in observations and model simulations. *Science Advances*, 4 (8):eaat2380, August 2018. ISSN 2375-2548. doi: 10.1126/sciadv.aat2380. Publisher: American Association for the Advancement of Science Section: Research Article.

Coles. *An Introduction to Statistical Modeling of Extreme Values*. Statistics. Springer, London, 2001. ISBN 978-1-4471-3675-0.

Stuart Coles and Francesco Pauli. Models and inference for uncertainty in extremal dependence. *Biometrika*, 89(1):183–196, March 2002. ISSN 0006-3444. doi: 10.1093/biomet/89.1.183. Publisher: Oxford Academic.

Stuart Coles, Janet Heffernan, and Jonathan Tawn. Dependence Measures for Extreme Value Analyses. *Extremes*, 2(4):339–365, December 1999. ISSN 1572-915X. doi: 10.1023/A:1009963131610.

Stuart G. Coles and Jonathan A. Tawn. Modelling Extreme Multivariate Events. *Journal of the Royal Statistical Society. Series B (Methodological)*, 53(2):377–392, 1991. ISSN 0035-9246. Publisher: [Royal Statistical Society, Wiley].

Stuart G. Coles and Jonathan A. Tawn. A bayesian analysis of extreme rainfall data. *Applied Statistics*, 45(4):463, 1996. ISSN 00359254. doi: 10.2307/2986068.

Dan Cooley, Philippe Naveau, and Paul Poncet. *Variograms for spatial max-stable random fields*, volume 187, page 373–390. Springer New York, 2006. ISBN 978-0-387-31741-0. doi: 10.1007/0-387-36062-X_17.

Daniel Cooley. Extreme value analysis and the study of climate change. *Climatic Change*, 97(1–2):77, Aug 2009. ISSN 0165-0009, 1573-1480. doi: 10.1007/s10584-009-9627-x.

Daniel Cooley, Douglas Nychka, and Philippe Naveau. Bayesian spatial modeling of extreme precipitation return levels. *Journal of the American Statistical Association*, 102(479): 824–840, Sep 2007. ISSN 0162-1459. doi: 10.1198/016214506000000780.

Anaïs Couasnon, Antonia Sebastian, and Oswaldo Morales-Nápoles. A copula-based bayesian network for modeling compound flood hazard from riverine and coastal interactions at the catchment scale: An application to the houston ship channel, texas. *Water*, 10(9):1190, 2018a.

Anaïs Couasnon, Antonia Sebastian, and Oswaldo Morales-Nápoles. A copula-based bayesian network for modeling compound flood hazard from riverine and coastal interactions at the catchment scale: An application to the houston ship channel, texas. *Water*, 10(99):1190, Sep 2018b. doi: 10.3390/w10091190.

Conleth Cunnane. Methods and merits of regional flood frequency analysis. *Journal of Hydrology*, 100(1):269–290, Jul 1988. ISSN 0022-1694. doi: 10.1016/0022-1694(88)90188-6.

Claudia Czado, Ulf Schepsmeier, and Aleksey Min. Maximum likelihood estimation of mixed C-vines with application to exchange rates. *Statistical Modelling*, 12(3):229–255, June 2012. ISSN 1471-082X. doi: 10.1177/1471082X1101200302. Publisher: SAGE Publications India.

Tate Dalrymple. *Flood-frequency analyses, Manual of Hydrology: Part 3.* Number 1543-A in Water Supply Paper. 1960.

Christopher Daly, Ronald P. Neilson, and Donald L. Phillips. A statistical-topographic model for mapping climatological precipitation over mountainous terrain. *Journal of Applied Meteorology*, 33(2):140–158, Feb 1994. ISSN 0894-8763. doi: 10.1175/1520-0450(1994)033⟨0140:ASTMFM⟩2.0.CO;2.

Christopher Daly, George Taylor, and Wayne Gibson. The prism approach to mapping precipitation and temperature. In *10th Conference on Applied Climatology, American Meteorological Society, 20-23 October, Reno NV*, page 10–12, 1997.

Christopher Daly, Michael Halbleib, Joseph I. Smith, Wayne P. Gibson, Matthew K. Doggett, George H. Taylor, Jan Curtis, and Phillip P. Pasteris. Physiographically sensitive mapping of climatological temperature and precipitation across the conterminous united states. *International Journal of Climatology*, 28(15):2031–2064, Dec 2008. ISSN 1097-0088. doi: 10.1002/joc.1688.

A. C. Davison and R. L. Smith. Models for exceedances over high thresholds. *Journal of the Royal Statistical Society: Series B (Methodological)*, 52(3):393–425, 1990. ISSN 2517-6161. doi: 10.1111/j.2517-6161.1990.tb01796.x.

A. C. Davison, S. A. Padoan, and M. Ribatet. Statistical modeling of spatial extremes. *Statistical Science*, 27(2):161–186, May 2012. ISSN 0883-4237, 2168-8745. doi: 10.1214/11-STS376. Zbl: 1330.86021.

A.C. Davison and R. Huser. Statistics of extremes. *Annual Review of Statistics and Its Application*, 2(1):203–235, 2015. doi: 10.1146/annurev-statistics-010814-020133.

L. De Haan. A spectral representation for max-stable processes. *The Annals of Probability*, 12(4):1194–1204, 1984. ISSN 0091-1798.

Laurens de Haan and Ana Ferreira. *Extreme value theory: an introduction.* Springer series in operations research. Springer, 2006. ISBN 978-0-387-23946-0.

Dipak K. Dey and Jun Yan. *Extreme Value Modeling and Risk Analysis: Methods and Applications*. CRC Press, Jan 2016. ISBN 978-1-4987-0131-0. Google-Books-ID: PYhUCwAAQBAJ.

Gerrit Draisma, Holger Drees, Ana Ferreira, and Laurens De Haan. Bivariate tail estimation: dependence in asymptotic independence. *Bernoulli*, 10(2):251–280, April 2004. ISSN 1350-7265. doi: 10.3150/bj/1082380219. Publisher: Bernoulli Society for Mathematical Statistics and Probability.

Anita Verpe Dyrrdal, Alex Lenkoski, Thordis L. Thorarinsdottir, and Frode Stordal. Bayesian hierarchical modeling of extreme hourly precipitation in norway. *Environmetrics*, 26(2):89–106, Aug 2014. ISSN 1099-095X. doi: 10.1002/env.2301.

David R. Easterling, Gerald A. Meehl, Camille Parmesan, Stanley A. Changnon, Thomas R. Karl, and Linda O. Mearns. Climate Extremes: Observations, Modeling, and Impacts. *Science*, 289(5487):2068–2074, September 2000. ISSN 0036-8075, 1095-9203. doi: 10.1126/science.289.5487.2068. Publisher: American Association for the Advancement of Science Section: Review.

Theodoros Economou, David B. Stephenson, and Christopher A. T. Ferro. Spatio-temporal modelling of extreme storms. *The Annals of Applied Statistics*, 8(4):2223–2246, Dec 2014. ISSN 1932-6157. doi: 10.1214/14-AOAS766.

John F. England Jr., Timothy A. Cohn, Beth A. Faber, Jery R. Stedinger, Wilbert O. Thomas Jr., Andrea G. Veilleux, Julie E. Kiang, and Robert R. Mason. *Guidelines for Determining Flood Flow Frequency*. Number 17C in Bulletin 17C. 2015.

E. M. Fischer and R. Knutti. Robust projections of combined humidity and temperature extremes. *Nature Climate Change*, 3(2):126–130, February 2013. ISSN 1758-6798. doi: 10.1038/nclimate1682. Number: 2 Publisher: Nature Publishing Group.

R. A. Fisher and L. H. C. Tippett. Limiting forms of the frequency distribution of the largest or smallest member of a sample. *Mathematical Proceedings of the Cambridge Philosophical Society*, 24(2):180–190, Apr 1928. ISSN 1469-8064, 0305-0041. doi: 10.1017/S0305004100015681.

H. J. Fowler and C. G. Kilsby. A regional frequency analysis of united kingdom extreme rainfall from 1961 to 2000. *International Journal of Climatology*, 23(11):1313–1334, Sep 2003. ISSN 1097-0088. doi: 10.1002/joc.943.

Jerome Friedman, Trevor Hastie, and Rob Tibshirani. Regularization paths for generalized linear models via coordinate descent. *Journal of statistical software*, 33(1):1–22, 2010. ISSN 1548-7660.

Souparno Ghosh and Bani K. Mallick. A hierarchical bayesian spatio-temporal model for extreme precipitation events. *Environmetrics*, 22(2):192–204, Mar 2011. ISSN 1099-095X. doi: 10.1002/env.1043.

Walter R Gilks. Introducing markov chain monte carlo. *Markov chain Monte Carlo in practice*, 1996.

Karin L. Gleason, Jay H. Lawrimore, David H. Levinson, Thomas R. Karl, and David J. Karoly. A Revised U.S. Climate Extremes Index. *Journal of Climate*, 21(10):2124–2137, May 2008. ISSN 0894-8755. doi: 10.1175/2007JCLI1883.1. Publisher: American Meteorological Society.

Tilmann Gneiting and Adrian E. Raftery. Strictly proper scoring rules, prediction, and estimation. *Journal of the American Statistical Association*, 102(477):359–378, Mar 2007. ISSN 0162-1459. doi: 10.1198/016214506000001437.

David Greenland. The climate of niwot ridge, front range, colorado, u.s.a. *Arctic and Alpine Research*, 21(4):380–391, Nov 1989. ISSN 0004-0851. doi: 10.1080/00040851.1989.12002751.

J. Arthur Greenwood, J. Maciunas Landwehr, N. C. Matalas, and J. R. Wallis. Probability weighted moments: Definition and relation to parameters of several distributions expressable in inverse form. *Water Resources Research*, 15:1049–1054, 1979. ISSN 1944-7973. doi: 10.1029/WR015i005p01049.

Patrick L Grover, Donald H Burn, and Juraj M Cunderlik. A comparison of index flood estimation procedures for ungauged catchments. *Canadian Journal of Civil Engineering*, 29(5):734–741, Oct 2002. ISSN 0315-1468, 1208-6029. doi: 10.1139/l02-065.

Gordon Gudendorf and Johan Segers. Extreme-Value Copulas. In Piotr Jaworski, Fabrizio Durante, Wolfgang Karl Härdle, and Tomasz Rychlik, editors, *Copula Theory and Its Applications*, Lecture Notes in Statistics, pages 127–145, Berlin, Heidelberg, 2010. Springer. ISBN 978-3-642-12465-5. doi: 10.1007/978-3-642-12465-5_6.

E. J. Gumbel. Probability-interpretation of the observed return-periods of floods. *Eos, Transactions American Geophysical Union*, 22(3):836–850, Jul 1941. ISSN 2324-9250. doi: 10.1029/TR022i003p00836.

E. J. Gumbel. *Statistics of Extremes*. Columbia University Press, Mar 1958. ISBN 978-0-231-89131-8.

John Handmer, Yasushi Honda, Zbigniew W Kundzewicz, Nigel Arnell, Gerardo Benito, Jerry Hatfield, Ismail Fadl Mohamed, Pascal Peduzzi, Shaohong Wu, Boris Sherstyukov, et al. Changes in impacts of climate extremes: human systems and ecosystems. In *Managing the risks of extreme events and disasters to advance climate change adaptation special report of the intergovernmental panel on climate change*, pages 231–290. Intergovernmental Panel on Climate Change, 2012.

Anca Hanea, Oswaldo Morales Napoles, and Dan Ababei. Non-parametric bayesian networks: Improving theory and reviewing applications. *Reliability Engineering & System Safety*, 144:265–284, 2015.

Zengchao Hao, Amir AghaKouchak, and Thomas J. Phillips. Changes in concurrent monthly precipitation and temperature extremes. *Environmental Research Letters*, 8(3):034014, August 2013. ISSN 1748-9326. doi: 10.1088/1748-9326/8/3/034014. Publisher: IOP Publishing.

D.D. Harris and L.E. Hubbard. *Magnitude and Frequency of Floods in Eastern Oregon*. Number 82–4078. 1983.

Trevor Hastie, Sami Tibshirani, and Harry Friedman. *The Elements of Statistical Learning: Data Mining, Inference, and Prediction*. Springer-Verlag, 2nd edition edition, 2009.

Trevor Hastie, Junyang Qian, and Kenneth Tay. An introduction to 'glmnet', 2016.

Peter J Hawkes. Joint probability analysis for estimation of extremes. *Journal of Hydraulic Research*, 46(S2):246–256, 2008.

Janet Heffernan and Sidney Resnick. Hidden regular variation and the rank transform. *Advances in Applied Probability*, 37(2):393–414, June 2005. ISSN 0001-8678, 1475-6064. doi: 10.1239/aap/1118858631. Publisher: Cambridge University Press.

Janet E. Heffernan and Sidney I. Resnick. Limit laws for random vectors with an extreme component. *Annals of Applied Probability*, 17(2):537–571, April 2007. ISSN 1050-5164, 2168-8737. doi: 10.1214/105051606000000835. Publisher: Institute of Mathematical Statistics.

Janet E. Heffernan and Jonathan A. Tawn. A conditional approach for multivariate extreme values (with discussion). *Journal of the Royal Statistical Society: Series B (Statistical Methodology)*, 66(3):497–546, 2004. ISSN 1467-9868. doi: 10.1111/j.1467-9868.2004.02050.x.

Hans Hersbach. Decomposition of the continuous ranked probability score for ensemble prediction systems. *Weather and Forecasting*, 15(5):559–570, Oct 2000. ISSN 0882-8156. doi: 10.1175/1520-0434(2000)015⟨0559:DOTCRP⟩2.0.CO;2.

Peter V. Hobbs, John D. Locatelli, and Jonathan E. Martin. Cold fronts aloft and the forecasting of precipitation and severe weather east of the rocky mountains. *Weather and Forecasting*, 5(4):613–626, Dec 1990. ISSN 0882-8156. doi: 10.1175/1520-0434(1990)005⟨0613:CFAATF⟩2.0.CO;2.

Arthur E. Hoerl and Robert W. Kennard. Ridge regression: Biased estimation for nonorthogonal problems. *Technometrics*, 12(1):55–67, 1970. ISSN 0040-1706. doi: 10.2307/1267351.

J. R. M. Hosking. L-moments: Analysis and estimation of distributions using linear combinations of order statistics. *Journal of the Royal Statistical Society: Series B (Methodological)*, 52(1):105–124, 1990. ISSN 2517-6161. doi: 10.1111/j.2517-6161.1990.tb01775.x.

J. R. M. Hosking and J. R. Wallis. The effect of intersite dependence on regional flood frequency analysis. *Water Resources Research*, 24(4):588–600, Apr 1988. ISSN 1944-7973. doi: 10.1029/WR024i004p00588.

J. R. M. Hosking and J. R. Wallis. Some statistics useful in regional frequency analysis. *Water Resources Research*, 29(2):271–281, Feb 1993. ISSN 1944-7973. doi: 10.1029/92WR01980.

J. R. M. Hosking and James R. Wallis. *Regional Frequency Analysis: An Approach Based on L-Moments*. Cambridge University Press, Sep 2005. ISBN 978-0-521-01940-8. Google-Books-ID: gurAnfB4nvUC.

R. Huser and A. C. Davison. Space—time modelling of extreme events. *Journal of the Royal Statistical Society. Series B (Statistical Methodology)*, 76(2):439–461, 2014. ISSN 1369-7412. Publisher: Royal Statistical Society, Wiley.

Fredline Ilorme and Veronica Webster Griffis. A novel procedure for delineation of hydrologically homogeneous regions and the classification of ungauged sites for design flood estimation. *Journal of Hydrology*, 492:151–162, Jun 2013. ISSN 0022-1694. doi: 10.1016/j.jhydrol.2013.03.045.

WS Jäger and O Morales Nápoles. A vine-copula model for time series of significant wave heights and mean zero-crossing periods in the north sea. *ASCE-ASME Journal of Risk and Uncertainty in Engineering Systems, Part A: Civil Engineering*, 3(4):04017014, 2017.

Gareth James, Daniela Witten, Trevor Hastie, and Robert Tibshirani. *An Introduction to Statistical Learning: with Applications in R*, volume 112. Springer, 2013.

Julie Rose N. Javier, James A. Smith, John England, Mary Lynn Baeck, Matthias Steiner, and Alexandros A. Ntelekos. Climatology of extreme rainfall and flooding from orographic thunderstorm systems in the upper arkansas river basin. 43, 2007. ISSN 1944-7973. doi: 10.1029/2006WR005093.

A. F. Jenkinson. The frequency distribution of the annual maximum (or minimum) values of meteorological elements. *Quarterly Journal of the Royal Meteorological Society*, 81(348): 158–171, Apr 1955. ISSN 1477-870X. doi: 10.1002/qj.49708134804.

Harry Joe. Families of m-Variate Distributions with Given Margins and m(m-1)/2 Bivariate Dependence Parameters. *Lecture Notes-Monograph Series*, 28:120–141, 1996. ISSN 0749-2170. Publisher: Institute of Mathematical Statistics.

Harry Joe. *Multivariate Models and Multivariate Dependence Concepts*. CRC Press, May 1997. ISBN 978-0-412-07331-1. Google-Books-ID: iJbRZL2QzMAC.

Harry Joe, Richard L. Smith, and Ishay Weissman. Bivariate Threshold Methods for Extremes. *Journal of the Royal Statistical Society. Series B (Methodological)*, 54(1):171–183, 1992. ISSN 0035-9246. Publisher: [Royal Statistical Society, Wiley].

Mario Leon Juncosa. The asymptotic behavior of the minimum in a sequence of random variables. *Duke Mathematical Journal*, 16(4):609–618, 1949.

Zakhar Kabluchko, Martin Schlather, and Laurens de Haan. Stationary max-stable fields associated to negative definite functions. *Annals of Probability*, 37(5):2042–2065, September 2009. ISSN 0091-1798, 2168-894X. doi: 10.1214/09-AOP455. Publisher: Institute of Mathematical Statistics.

Shih-Chieh Kao and Rao S. Govindaraju. Trivariate statistical analysis of extreme rainfall events via the Plackett family of copulas. *Water Resources Research*, 44(2), 2008. ISSN 1944-7973. doi: 10.1029/2007WR006261.

Thomas R. Karl, Richard W. Knight, David R. Easterling, and Robert G. Quayle. Indices of Climate Change for the United States. *Bulletin of the American Meteorological Society*, 77(2):279–292, February 1996. ISSN 0003-0007. doi: 10.1175/1520-0477(1996)077⟨0279:IOCCFT⟩2.0.CO;2. Publisher: American Meteorological Society.

Richard W Katz. Statistics of extremes in climate change. *Climatic change*, 100(1):71–76, 2010.

Richard W Katz, Marc B Parlange, and Philippe Naveau. Statistics of extremes in hydrology. *Advances in Water Resources*, 25(8):1287–1304, August 2002. ISSN 0309-1708. doi: 10.1016/S0309-1708(02)00056-8.

Caroline Keef, Ioannis Papastathopoulos, and Jonathan A. Tawn. Estimation of the conditional distribution of a multivariate variable given that one of its components is large: Additional constraints for the Heffernan and Tawn model. *Journal of Multivariate Analysis*, 115:396–404, March 2013. ISSN 0047-259X. doi: 10.1016/j.jmva.2012.10.012.

Barry D. Keim and Gregory E. Faiers. Heavy rainfall distributions by season in louisiana: Synoptic interpretations and quantile estimates1. *JAWRA Journal of the American Water Resources Association*, 32(1):117–124, 1996. ISSN 1752-1688. doi: 10.1111/j.1752-1688.1996.tb03439.x.

A. N. Kolmogorov. *Grundbegriffe der wahrscheinlichkeitsrechnung*. Springer-Verlag, 1933 edition.

Samuel Kotz, N. Balakrishnan, and Norman L. Johnson. *Continuous Multivariate Distributions, Volume 1: Models and Applications*. John Wiley & Sons, April 2004. ISBN 978-0-471-65403-2.

D. Kurowicka and R. M. Cooke. Sampling algorithms for generating joint uniform distributions using the vine-copula method. *Computational Statistics & Data Analysis*, 51(6):2889–2906, March 2007. ISSN 0167-9473. doi: 10.1016/j.csda.2006.11.043.

Hyun-Han Kwon, Casey Brown, and Upmanu Lall. Climate informed flood frequency analysis and prediction in montana using hierarchical bayesian modeling. *Geophysical Research Letters*, 35(5):L05404, Mar 2008. ISSN 1944-8007. doi: 10.1029/2007GL032220.

M Lang, TBMJ Ouarda, and B Bobée. Towards operational guidelines for over-threshold modeling. *Journal of hydrology*, 225(3-4):103–117, 1999.

M. R. Leadbetter. On a basis for 'peaks over threshold' modeling. *Statistics Probability Letters*, 12(4):357–362, Oct 1991. ISSN 0167-7152. doi: 10.1016/0167-7152(91)90107-3.

Guy Leclerc and John C Schaake. Derivation of hydrologic frequency curves. 1972.

Anthony W. Ledford and Jonathan A. Tawn. Statistics for near independence in multivariate extreme values. *Biometrika*, 83(1):169–187, March 1996. ISSN 0006-3444. doi: 10.1093/biomet/83.1.169. Publisher: Oxford Academic.

Anthony W. Ledford and Jonathan A. Tawn. Modelling Dependence within Joint Tail Regions. *Journal of the Royal Statistical Society: Series B (Statistical Methodology)*, 59 (2):475–499, 1997. ISSN 1467-9868. doi: 10.1111/1467-9868.00080.

Karl K. Lee and John C. Risley. *Estimates for Ground-Water Recharge, Base Flow, and Stream Reach Gains and Losses in the Willamette River Basin, Oregon*. Number 01–4215. 2002.

Alex Lenkoski. *spatial.gev.bma: Hierarchical spatial generalized extreme value (GEV) modeling with Bayesian Model Averaging (BMA)*. May 2014.

Michael Leonard, Seth Westra, Aloke Phatak, Martin Lambert, Bart van den Hurk, Kathleen McInnes, James Risbey, Sandra Schuster, Doerte Jakob, and Mark Stafford-Smith. A compound event framework for understanding extreme impacts. *WIREs Climate Change*, 5(1):113–128, 2014. doi: https://doi.org/10.1002/wcc.252.

Zhiyong Liu, Linyin Cheng, Zengchao Hao, Jingjing Li, Andrea Thorstensen, and Hongkai Gao. A Framework for Exploring Joint Effects of Conditional Factors on Compound Floods. *Water Resources Research*, 54(4):2681–2696, 2018. ISSN 1944-7973. doi: 10.1002/2017WR021662.

Charlotte A. Love, Brian E. Skahill, John F. England, Gregory Karlovits, Angela Duren, and Amir AghaKouchak. Integrating climatic and physical information in a bayesian hierarchical model of extreme daily precipitation. *Water*, 12(88):2211, Aug 2020. doi: 10.3390/w12082211.

Adam Luke, Jasper A. Vrugt, Amir AghaKouchak, Richard Matthew, and Brett F. Sanders. Predicting nonstationary flood frequencies: Evidence supports an updated stationarity thesis in the united states. *Water Resources Research*, 53(7):5469–5494, 2017. ISSN 1944-7973. doi: 10.1002/2016WR019676.

Shahrbanou Madadgar and Hamid Moradkhani. Improved bayesian multimodeling: Integration of copulas and bayesian model averaging. *Water Resources Research*, 50(12): 9586–9603, Dec 2014. ISSN 1944-7973. doi: 10.1002/2014WR015965.

Douglas Maraun, Henning W. Rust, and Timothy J. Osborn. Synoptic airflow and uk daily precipitation extremes. *Extremes*, 13(2):133–153, Jan 2010. ISSN 1386-1999, 1572-915X. doi: 10.1007/s10687-010-0102-x.

Krishanu Maulik and Sidney Resnick. Characterizations and Examples of Hidden Regular Variation. *Extremes*, 7(1):31–67, March 2004. ISSN 1572-915X. doi: 10.1007/s10687-004-4728-4.

Omid Mazdiyasni and Amir AghaKouchak. Substantial increase in concurrent droughts and heatwaves in the United States. *Proceedings of the National Academy of Sciences*, 112(37): 11484–11489, September 2015. ISSN 0027-8424, 1091-6490. doi: 10.1073/pnas.1422945112. Publisher: National Academy of Sciences Section: Physical Sciences.

Omid Mazdiyasni, Amir AghaKouchak, Steven J. Davis, Shahrbanou Madadgar, Ali Mehran, Elisa Ragno, Mojtaba Sadegh, Ashmita Sengupta, Subimal Ghosh, C. T. Dhanya, and Mohsen Niknejad. Increasing probability of mortality during Indian heat waves. *Science Advances*, 3(6):e1700066, June 2017. ISSN 2375-2548. doi: 10.1126/sciadv.1700066. Publisher: American Association for the Advancement of Science Section: Research Article.

Richard P. McNulty. Severe and convective weather: A central region forecasting challenge. 10:187–202, Jun 1995. ISSN 0882-8156. doi: 10.1175/1520-0434(1995)010⟨0187:SACWAC⟩2.0.CO;2.

John M. Melack, Jeff Dozier, Charles R. Goldman, David Greenland, Alexander M. Milner, and Robert J. Naiman. Effects of climate change on inland waters of the pacific coastal mountains and western great basin of north america. *Hydrological Processes*, 11 (8):971–992, 1997. ISSN 1099-1085. doi: 10.1002/(SICI)1099-1085(19970630)11:8⟨971::AID-HYP514⟩3.0.CO;2-Y.

Kerrie L. Mengersen, Pierre Pudlo, and Christian P. Robert. Bayesian computation via empirical likelihood. 110:1321–1326, Jan 2013. ISSN 0027-8424, 1091-6490. doi: 10.1073/pnas.1208827110.

Matthew J. Menne, Imke Durre, Bryant Korzeniewski, Shelley McNeill, Kristy Thomas, Xungang Yin, Steven Anthony, Ron Ray, Russell S. Vose, Byron E. Gleason, and Tamara G. Houston. Global historical climatology network - daily (ghcn-daily), version 3, 2012a.

Matthew J. Menne, Imke Durre, Russell S. Vose, Byron E. Gleason, and Tamara G. Houston. An overview of the global historical climatology network-daily database. *Journal of Atmospheric and Oceanic Technology*, 29(7):897–910, Jul 2012b. ISSN 0739-0572, 1520-0426. doi: 10.1175/JTECH-D-11-00103.1.

Cary J. Mock. Climatic controls and spatial variations of precipitation in the western united states. *Journal of Climate*, 9(5):1111–1125, May 1996. ISSN 0894-8755. doi: 10.1175/1520-0442(1996)009⟨1111:CCASVO⟩2.0.CO;2.

Oswaldo Morales-Nápoles, David Joaquín Delgado-Hernández, David De-León-Escobedo, and Juan Carlos Arteaga-Arcos. A continuous bayesian network for earth dams' risk assessment: methodology and quantification. *Structure and Infrastructure Engineering*, 10(5):589–603, 2014.

S Nadarajah. A polynomial model for bivariate extreme value distributions. *Statistics & Probability Letters*, 42(1):15–25, March 1999. ISSN 0167-7152. doi: 10.1016/S0167-7152(98)00179-5.

M. R. Najafi and H. Moradkhani. A hierarchical bayesian approach for the analysis of climate change impact on runoff extremes. *Hydrological Processes*, 28(26):6292–6308, Dec 2014. ISSN 1099-1085. doi: 10.1002/hyp.10113.

M. R. Najafi and Hamid Moradkhani. Analysis of runoff extremes using spatial hierarchical bayesian modeling. *Water Resources Research*, 49(10):6656–6670, Oct 2013. ISSN 1944-7973. doi: 10.1002/wrcr.20381.

NOAA Atlas 14. Precipitation-frequency atlas of the united states. URL `https://www.weather.gov/owp/hdsc_currentpf`.

T. Oki, K. Musiake, and T. Koike. Spatial rainfall distribution at a storm event in mountainous regions, estimated by orography and wind direction. 27:359–369, 1991. ISSN 1944-7973. doi: 10.1029/90WR02427.

Francisco Olivera, Janghwoan Choi, Dongkyun Kim, and Ming-Han Li. Estimation of average rainfall areal reduction factors in texas using nexrad data. *Journal of Hydrologic Engineering*, 13(6):438–448, Jun 2008. ISSN 1084-0699, 1943-5584. doi: 10.1061/(ASCE)1084-0699(2008)13:6(438).

T. Opitz. Extremal t processes: Elliptical domain of attraction and a spectral representation. 122:409–413, Nov 2013. ISSN 0047-259X. doi: 10.1016/j.jmva.2013.08.008.

Sean M. O'Brien and David B. Dunson. Bayesian multivariate logistic regression. *Biometrics*, 60(3):739–746, 2004. ISSN 1541-0420. doi: 10.1111/j.0006-341X.2004.00224.x.

S. A. Padoan, M. Ribatet, and S. A. Sisson. Likelihood-based inference for max-stable processes. *Journal of the American Statistical Association*, 105(489):263–277, Mar 2010. ISSN 0162-1459. doi: 10.1198/jasa.2009.tm08577.

Simon Michael Papalexiou and Demetris Koutsoyiannis. Battle of extreme value distributions: A global survey on extreme daily rainfall. *Water Resources Research*, 49(1):187–201, 2013. ISSN 1944-7973. doi: 10.1029/2012WR012557.

Simon Michael Papalexiou, Yannis Markonis, Federico Lombardo, Amir AghaKouchak, and Efi Foufoula-Georgiou. Precise temporal disaggregation preserving marginals and correlations (dipmac) for stationary and nonstationary processes. *Water Resources Research*, 54(10):7435–7458, 2018. ISSN 1944-7973. doi: 10.1029/2018WR022726.

James Pickands. Multivariate extreme value distribution. *Proceedings 43th, Session of International Statistical Institution, 1981*, 1981.

P. Prescott and A. T. Walden. Maximum likelihood estimation of the parameters of the generalized extreme-value distribution. *Biometrika*, 67(3):723–724, Jan 1980. ISSN 0006-3444. doi: 10.1093/biomet/67.3.723.

Nicolas Raillard, Pierre Ailliot, and Jianfeng Yao. Modeling extreme values of processes observed at irregular time steps: Application to significant wave height. *The Annals of Applied Statistics*, 8(1):622–647, Mar 2014. ISSN 1932-6157, 1941-7330. doi: 10.1214/13-AOAS711.

Alexandra Ramos and Anthony Ledford. A new class of models for bivariate joint tails. *Journal of the Royal Statistical Society: Series B (Statistical Methodology)*, 71(1):219–241, 2009. ISSN 1467-9868. doi: 10.1111/j.1467-9868.2008.00684.x.

Kelly T. Redmond and Roy W. Koch. Surface climate and streamflow variability in the western united states and their relationship to large-scale circulation indices. *Water Resources Research*, 27(9):2381–2399, 1991. ISSN 1944-7973. doi: 10.1029/91WR00690.

Brian J. Reich and Benjamin A. Shaby. *A finite-dimensional construction of a max-stable process for spatial extremes*. Number 2633 in Technical Reports. 2011.

Brian J. Reich, Benjamin A. Shaby, and Daniel Cooley. A hierarchical model for serially-dependent extremes: A study of heat waves in the western us. *Journal of Agricultural, Biological, and Environmental Statistics*, 19(1):119–135, Mar 2014. ISSN 1537-2693. doi: 10.1007/s13253-013-0161-y.

B. Renard and M. Lang. Use of a gaussian copula for multivariate extreme value analysis: Some case studies in hydrology. *Advances in Water Resources*, 30(4):897–912, Apr 2007. ISSN 0309-1708. doi: 10.1016/j.advwatres.2006.08.001.

Benjamin Renard. A bayesian hierarchical approach to regional frequency analysis. *Water Resources Research*, 7:W11513, 2011. doi: 10.1029/2010WR010089.

Sidney Resnick. Hidden Regular Variation, Second Order Regular Variation and Asymptotic Independence. *Extremes*, 5(4):303–336, December 2002. ISSN 1572-915X. doi: 10.1023/A:1025148622954.

Mathieu Ribatet. A user's guide to the spatialextremes package. 2009.

Mathieu Ribatet. Spatial extremes: Max-stable processes at work. *Journal of the French Society of Statistics*, 154(2):156–177, Sep 2013. ISSN 2102-6238.

Mathieu Ribatet. *Modelling spatial extremes using max-stable processes*, page 369–391. Cambridge University Press, Jan 2017. doi: 10.1017/9781316339251.014.

Mathieu Ribatet. *SpatialExtremes: Modelling Spatial Extremes*, 2020. URL `https://CRAN.R-project.org/package=SpatialExtremes`. R package version 2.0-9.

Mathieu Ribatet and Mohammed Sedki. Extreme value copulas and max-stable processes. *Journal de la société française de statistique*, 154(1):138–150, 2013a.

Mathieu Ribatet and Mohammed Sedki. Extreme value copulas and max-stable processes. *Journal de la Societe Française de Statistique*, 154(1):138–150, 2013b.

Mathieu Ribatet, Daniel Cooley, and Anthony C. Davison. Bayesian inference from composite likelihoods, with an application to spatial extremes. *Statistica Sinica*, 22(2):813–845, 2012. ISSN 1017-0405.

Mathieu Ribatet, Clement Dombry, and Marco Oesting. *Spatial Extremes and Max-Stable Processes*. Chapman and Hall/CRC, 2016. ISBN 978-0-429-16119-3.

Joacim Rocklöv and Bertil Forsberg. Comparing approaches for studying the effects of climate extremes – a case study of hospital admissions in Sweden during an extremely warm summer. *Global Health Action*, 2(1):2034, November 2009. ISSN 1654-9716. doi: 10.3402/gha.v2i0.2034.

Mojtaba Sadegh, Elisa Ragno, and Amir AghaKouchak. Multivariate Copula Analysis Toolbox (MvCAT): Describing dependence and underlying uncertainty using a Bayesian framework. *Water Resources Research*, 53(6):5166–5183, 2017. ISSN 1944-7973. doi: 10.1002/2016WR020242.

G. Salvadori and C. De Michele. Multivariate multiparameter extreme value models and return periods: A copula approach. *Water Resources Research*, 46(10), 2010. ISSN 1944-7973. doi: 10.1029/2009WR009040.

Gianfausto Salvadori, Carlo De Michele, Nathabandu T. Kottegoda, and Renzo Rosso. *Extremes in Nature: An Approach Using Copulas*. Springer Science & Business Media, June 2007. ISBN 978-1-4020-4415-1. Google-Books-ID: c9JJGZTt7UcC.

Huiyan Sang and Alan E. Gelfand. Hierarchical modeling for extreme values observed over space and time. *Environmental and Ecological Statistics*, 16(3):407–426, Jan 2008. ISSN 1352-8505, 1573-3009. doi: 10.1007/s10651-007-0078-0.

M. G. Schaefer. Regional analyses of precipitation annual maxima in washington state. *Water Resources Research*, 26(1):119–131, Jan 1990. ISSN 1944-7973. doi: 10.1029/WR026i001p00119.

M. G. Schaefer, B. L. Barker, G. H. Taylor, and J. R. Wallis. Regional precipitation-frequency analysis and spatial mapping of 24-hour precipitation for oregon. Jan 2008.

Doris Schirmacher and Ernesto Schirmacher. Multivariate dependence modeling using pair-copulas. Technical report, Technical report, 2008.

Martin Schlather. Models for Stationary Max-Stable Random Fields. *Extremes; New York*, 5(1):33–44, March 2002. ISSN 13861999.

Martin Schlather and Jonathan A. Tawn. A dependence measure for multivariate and spatial extreme values: Properties and inference. *Biometrika*, 90(1):139–156, Mar 2003. ISSN 0006-3444. doi: 10.1093/biomet/90.1.139.

Richard M. Shane and Walter R. Lynn. Mathematical model for flood risk evaluation. *Journal of the Hydraulics Division*, 90(6):1–20, Nov 1964. doi: 10.1061/JYCEAJ.0001127.

Noah Simon, Jerome Friedman, Trevor Hastie, and Rob Tibshirani. Regularization paths for cox's proportional hazards model via coordinate descent. *Journal of Statistical Software*, 39(5):1–13, 2011. URL `http://www.jstatsoft.org/v39/i05/`.

M Sklar. Fonctions de repartition an dimensions et leurs marges. *Publ. inst. statist. univ. Paris*, 8:229–231, 1959.

R. L. Smith. Max-Stable Processes and Spatial Extremes. Technical report, University of Surrey, Guildford GU2 5XH, England, October 1990.

R. G. Steadman. The Assessment of Sultriness. Part I: A Temperature-Humidity Index Based on Human Physiology and Clothing Science. *Journal of Applied Meteorology*, 18 (7):861–873, July 1979. ISSN 0021-8952. doi: 10.1175/1520-0450(1979)018⟨0861:TAOSPI⟩2.0.CO;2. Publisher: American Meteorological Society.

Robert G. Steadman. A Universal Scale of Apparent Temperature. *Journal of Climate and Applied Meteorology*, 23(12):1674–1687, December 1984. ISSN 0733-3021. doi: 10.1175/1520-0450(1984)023⟨1674:AUSOAT⟩2.0.CO;2. Publisher: American Meteorological Society.

Jery R. Stedinger and Veronica W. Griffis. Flood frequency analysis in the united states: Time to update. *Journal of Hydrologic Engineering*, 13(4):199–204, Apr 2008. doi: http://dx.doi.org/10.1061/(ASCE)1084-0699(2008)13:4(199)#sthash.pT4lIs2M.dpuf.

JR Stedinger, RM Vogel, E Foufoula-Georgiou, and DR Maidment. Handbook of hydrology. *McGraw-Hill, Inc., New York, USA*, 1993.

Scott Steinschneider and Upmanu Lall. A hierarchical bayesian regional model for nonstationary precipitation extremes in northern california conditioned on tropical moisture exports. *Water Resources Research*, 51(3):1472–1492, Mar 2015. ISSN 1944-7973. doi: 10.1002/2014WR016664.

Alec G. Stephenson, Eric A. Lehmann, and Aloke Phatak. A max-stable process model for rainfall extremes at different accumulation durations. *Weather and Climate Extremes*, 13: 44–53, Sep 2016. ISSN 2212-0947. doi: 10.1016/j.wace.2016.07.002.

Kei Takeuchi. The distribution of information statistics and the criterion of goodness of fit of models. *Mathematical Science*, 153:12–18, 1976.

Jonathan A. Tawn. Bivariate extreme value theory: Models and estimation. *Biometrika*, 75 (3):397–415, September 1988. ISSN 0006-3444. doi: 10.1093/biomet/75.3.397. Publisher: Oxford Academic.

Robert Tibshirani. Regression shrinkage and selection via the lasso. *Journal of the Royal Statistical Society: Series B (Methodological)*, 58(1):267–288, 1996. ISSN 2517-6161. doi: 10.1111/j.2517-6161.1996.tb02080.x.

Andrey Nikolayevich Tikhonov. On the stability of inverse problems. In *Dokl. Akad. Nauk SSSR*, volume 39, pages 195–198, 1943.

P. Todorovic and E. Zelenhasic. A stochastic model for flood analysis. 6:1641–1648, Dec 1970. ISSN 1944-7973. doi: 10.1029/WR006i006p01641.

Faranak Tootoonchi, Mojtaba Sadegh, Jan Olaf Haerter, Olle Räty, Thomas Grabs, and Claudia Teutschbein. Copulas for hydroclimatic analysis: A practice-oriented overview. *WIREs Water*, n/a(n/a):e1579, 2021. ISSN 2049-1948. doi: 10.1002/wat2.1579.

Kevin E. Trenberth and Dennis J. Shea. Relationships between precipitation and surface temperature. *Geophysical Research Letters*, 32(14), 2005. ISSN 1944-8007. doi: 10.1029/2005GL022760.

Efthymios G. Tsionas. Bayesian multivariate poisson regression. *Communications in Statistics - Theory and Methods*, 30(2):243–255, Mar 2001. ISSN 0361-0926. doi: 10.1081/STA-100002028.

U.S. Weather Bureau. *Rainfall Intesity-Frequency Regime - Part 2: Southeastern United States*. Number 29. Mar 1958. Prepared for the U. S. Department of Agriculture.

USGS. Usgs watershed boundary dataset (wbd) for 2-digit hydrologic unit - 08, 2020a. URL `https://www.sciencebase.gov/catalog/item/5a1632b4e4b09fc93dd171e8`.

USGS. Usgs watershed boundary dataset (wbd) for 2-digit hydrologic unit - 10, 2020b. URL `https://www.sciencebase.gov/catalog/item/5a1632b6e4b09fc93dd171fb`.

USGS. Usgs watershed boundary dataset (wbd) for 2-digit hydrologic unit - 12, 2020c. URL `https://www.sciencebase.gov/catalog/item/5a1632b7e4b09fc93dd17202`.

Karin van der Wiel, Sarah B. Kapnick, Geert Jan van Oldenborgh, Kirien Whan, Sjoukje Philip, Gabriel A. Vecchi, Roop K. Singh, Julie Arrighi, and Heidi Cullen. Rapid attribution of the august 2016 flood-inducing extreme precipitation in south louisiana to climate change. *Hydrology and Earth System Sciences*, 21(2):897–921, Feb 2017. ISSN 1027-5606. doi: 10.5194/hess-21-897-2017.

S. Vandenberghe, N. E. C. Verhoest, C. Onof, and B. De Baets. A comparative copula-based bivariate frequency analysis of observed and simulated storm events: A case study on Bartlett-Lewis modeled rainfall. *Water Resources Research*, 47(7), 2011. ISSN 1944-7973. doi: 10.1029/2009WR008388.

Seth Westra and Scott A. Sisson. Detection of non-stationarity in precipitation extremes using a max-stable process model. *Journal of Hydrology*, 406(1):119–128, August 2011. ISSN 0022-1694. doi: 10.1016/j.jhydrol.2011.06.014.

CHRISTOPHER K. Wikle, L. Mark Berliner, and Noel Cressie. Hierarchical bayesian space-time models. *Environmental and Ecological Statistics*, 5(2):117–154, Jun 1998. ISSN 1573-3009. doi: 10.1023/A:1009662704779.

R.L. Wilby and T.M.L. Wigley. Downscaling general circulation model output: a review of methods and limitations. *Progress in Physical Geography: Earth and Environment*, 21(4):530–548, Dec 1997. ISSN 0309-1333. doi: 10.1177/030913339702100403.

Weining Zhao and M. a. K. Khalil. The relationship between precipitation and temperature over the contiguous united states. *Journal of Climate*, 6(6):1232–1236, Jun 1993. ISSN 0894-8755, 1520-0442. doi: 10.1175/1520-0442(1993)006⟨1232:TRBPAT⟩2.0.CO;2.

Feifei Zheng, Seth Westra, Michael Leonard, and Scott A Sisson. Modeling dependence between extreme rainfall and storm surge to estimate coastal flooding risk. *Water Resources Research*, 50(3):2050–2071, 2014.

Hui Zou and Trevor Hastie. Regularization and variable selection via the elastic net. *Journal of the Royal Statistical Society: Series B (Statistical Methodology)*, 67(2):301–320, 2005. ISSN 1467-9868. doi: 10.1111/j.1467-9868.2005.00503.x.